CEMENT BASED SMART NANOCOMPOSITES CONTAINING METAL OXIDES, GRAPHENE OXIDES AND POLYMERS FOR BUILDING APPLICATIONS

A Thesis submitted to the

UPES

For the Award of

Doctor of Philosophy

In

Civil Engineering

By

A. N. SHANKAR

August 2024

SUPERVISOR

Dr. Prasanta Mandal

DEPARTMENT OF HSE & CIVIL ENGINEERING
SCHOOL OF ADVANCED ENGINEERING
UPES
DEHRADUN-248007: UTTARAKHAND

CEMENT BASED SMART NANOCOMPOSITES CONTAINING METAL OXIDES, GRAPHENE OXIDES AND POLYMERS FOR BUILDING APPLICATIONS

A Thesis submitted to the

UPES

For the Award of

Doctor of Philosophy

In

Civil Engineering

By

A. N. SHANKAR

(Registration No. 500072293)

August 2024

SUPERVISOR

Dr. Prasanta Mandal

Professor, Civil Engineering, UPES

DEPARTMENT OF HSE & CIVIL ENGINEERING
SCHOOL OF ADVANCED ENGINEERING
UPES
DEHRADUN-248007: UTTARAKHAND

Dedicated To
My
Parents, Wife and Daughters

DECLARATION

I declare that the thesis entitled "**Cement Based Smart Nanocomposites Containing Metal Oxides, Graphene Oxides and Polymers for Building Applications**" has been prepared by me under the guidance of Dr. Prasanta Mandal, Professor, Department of Physics, Applied Science Cluster, UPES. No part of this thesis has formed the basis for the award of any degree or fellowship previously.

A. N. SHANKAR
(Registration No. 500072293)
Department Of HSE& Civil Engineering
School of Advanced Engineering [SOAE],
UPES
Dehradun-248007, Uttarakhand

CERTIFICATE

I certify that A. N. SHANKAR has prepared his thesis entitled "**Cement Based Smart Nanocomposites Containing Metal Oxides, Graphene Oxides and Polymers for Building Applications**", for the award of PhD degree of the University of Petroleum & Energy Studies, under my guidance. He has carried out the work at School of Advanced Engineering, UPES.

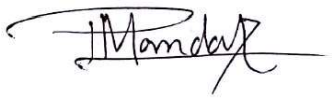

Dr. Prasanta Mandal
Professor
Department of Physics, Applied Science Cluster
School of Advanced Engineering,

UPES

Dehradun -248007, Uttarakhand

Date:

Abstract

Ordinary Portland Cement (OPC) based nanocomposites containing metal oxides, graphene oxides and polymers have been of great interests due to their potentials in civil construction and smart applications in photocatalytic activities, antimicrobial effect, corrosion resistance etc. Developing such cement nanocomposites with optimal content has been quite challenging that not only retain their basic mechanical strength but also exhibit smart properties. Present thesis work deals with the development of OPC based nanocomposites containing TiO_2 (titanium dioxide), SiO_2 (silicon dioxide), Fe_2O_3 (iron oxide), GO (graphene oxide), RGO (reduced graphene oxide) and PVA (polyvinyl alcohol). Mechanical, structural and spectroscopic investigations are carried out systematically to understand cement hydration and formation of C-S-H (calcium silicate hydrate) gel. Three different types of cementitious materials are prepared containing: (a) Fe_2O_3, TiO_2, SiO_2 and Cu (copper) nanoparticles, (b) GO and RGO along with Fe_2O_3, and (c) PVA along with GO and Fe_2O_3 at different wt% ranging from 0.05% to 5%. The standard test cube samples are cured at standard curing time of 3 days, 7 days, 14 days and 28 days. At each stage of curing mechanical and structural changes are monitored by studying compressive strength measurements and X-ray diffraction, respectively. It has been found that addition of minor quantity (0.05% to 5%) of these functional nanomaterials improves mechanical strength by ~10-30%. Addition beyond this wt% leads to the reduction of mechanical strength which is attributed to the formation of nanoparticle agglomeration and form separate nanoparticle phase. In the first type of cement nanocomposite (category as in (a)), highest improvement in mechanical strength is seen to be ~ 33% (compressive strength) and ~20% (flexural strength) for the optimal content of 3wt% Fe_2O_3. Further addition of GO or RGO by small wt% (~0.1%) to optimized OPC-Fe_2O_3 cement paste (category as in (b)) and 0.1wt% PVA to OPC-Fe_2O_3-GO shows a slightly less improvement in the compressive strength. This improvement is attributed to the accelerated reaction of C-S-H gel formation as supported by X-ray diffraction structural studies and Fourier transform infrared (FTIR) analysis which show the presence of gel phase (β-phase). The developed nanocomposites are considered for the study of photocatalytic and antimicrobial smart properties. Photocatalytic dye degradation is investigated using UV-Vis spectroscopy. Excellent dye degradation is observed for the nanocomposites containing TiO_2, Fe_2O_3 and Cu nanoparticles with highest dye degradation rate for nanocomposite containing Fe_2O_3 which is about 2.5 times faster than that of reference OPC. Antimicrobial studies on

OPC-Fe_2O_3-GO and OPC-Fe_2O_3-GO-PVA shows higher restricted colonial growth of *E-coli* compared to reference OPC by about 20% and 18%, respectively. The present findings have important implications in future developments of OPC based cementitious nanocomposites for civil construction and smart applications.

Acknowledgements

Foremost, I would like to express my heart felt thanks to my supervisor, Dr. Prasanta Mandal for introducing me to the intriguing subject of cementitious composites containing nanomaterials and functional nanomaterials, and for his great enthusiasm and inspiration in explaining the present research topic clearly and simply. His valuable guidance, consistent interactions and encouragement and support throughout my course of this study helped me in shaping the thesis in its present form. I am extremely indebted to Dr. Prasanta Mandal for his critical evaluation, suggestions and comments on the experimental observations and results, which helped me establishing the overall direction of research and critical understanding.

I wish to express my special thanks to Prof Manish Kumar and Prof. Nihal Anwar Siddiqui, Prof J. K. Pandey for their critical evaluation on the research work, consistent encouragement and strong moral support throughout the course of this study.

I would like to thank my examiners, Prof. Syed Mohammad Tauseef, Prof Bikarama Prasad Yadav, Dr. Suvendu Manna, and Dr. Amit Chawla for their useful suggestions and evaluation of the progress of my thesis work.

My special thanks to Mr. Rahul Silori, Mr. Durga Prasad Pandey and Mr Susanta Kumar Sethy for their courage and moral support.

I would like to thank Mr. Charu Pant, CIC lab, UPES for his help in XRD, FTIR and UV-Vis data acquisition, and Mr. Ram Sagar for helping sample preparation.

I wish to express my thanks to Dr.K Mohan Reddy, Prof. J. Deva Raju for being cordial and sharing all good and bad on many occasions.

Finally, and most importantly, I wish to express my deep gratitude to my mother, brother and sisters for their affection, encouragement, understanding and blessings which helped me to do my research work in an ideal environment. I would like to thank specially to my wife for her constant support and encouragement. I can not also forget to take names of my daughters who have been my strength.

Above all I bow my head before God Almighty to keep me in cheer and health during the course of this work.

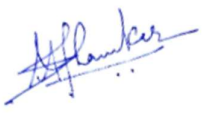

Date: _____ *(A. N. Shankar)*

List of Figures

Page No.

List of Tables

Page No.

CHAPTER-1

Introduction

In the construction industry Ordinary Portland Cement (OPC) has been used as base binding material of mortar and concrete. Constant efforts have been put by the researchers across the globe to improve its basic engineering properties including mechanical strength, hydration, setting time, filler properties, erosion of reinforced concrete etc. OPC based composites containing various nanomaterials of oxides and polymers are shown to be promising cementitious materials for construction industry with improved properties. However, it is quite challenging to achieve optimal content that may lead to modern economic and sustainable development for the construction industry. Furthermore, the physical and chemical mechanisms must also be understood in depth to achieve desired work functionality and future developments. Special emphasis is given to achieve smart properties, such as, photocatalytic dye degradation/pollutant removal, antimicrobial activity and corrosion resistance retaining its basic mechanical strength intact. To do so, attempts are being made to develop cementitious composites containing (a) oxides of Fe_2O_3, TiO_2, SiO_2, ZrO_2, (b) graphene and its derivatives such as graphene oxides (GO) and/or reduced graphene oxide (RGO), carbon nanotubes and nano-fibers, and (c) polymer-epoxy (PVA: polyvinyl alcohol, PMMA: polymethyl methacrylate). Studies show that addition of these functional nanomaterials accelerates cement hydration and formation of C-S-H gel, improving mechanical strength and exhibiting smart properties. A few representative recent developments are discussed below.

1.1. Cement composites containing functional nanoparticles

1.1.1. Cement composites containing oxides (Fe_2O_3, TiO_2, SiO_2)

Cement composites containing various oxide nanoparticles such as nano silica (SiO_2), nano titanium dioxide (TiO_2), iron oxide (Fe_2O_3) nanoparticles usually below 5 wt% show improvement in the mechanical strength in the range varying from 10-50%. Filling of pores by the oxide nanoparticles reduces pore volumes. The larger surface area available with the nanoparticles increase binding strength between nearing neighbours. Their presence in the OPC host also accelerates hydration producing faster C-S-H gel. Improvement in the compressive strength and flexural strength are mainly caused by the gel-phase. Nano silica

(SiO_2) can improve the compressive strength up to 25% due to the accelerated pozzolanic reactions and improvement in the microstructures [1]. With improved antimicrobial properties (self-cleaning or sterilizing the environment), nano TiO_2 is considered to be good candidate for smart cement composites. Nano TiO_2 shows better tensile and flexural strength, refinement of pores and prevention of shrinkage, better fatigue strength [2-5] and causes early strength due to the accelerated chemical process of C-S-H formation. Iron oxide (Fe_2O_3) nanoparticles are being considered to be highly effective too for improving mechanical strength. Optimum presence of Fe_2O_3 (~3wt%) improves microstructural properties, reduces micro-cracks and propagation (improved bonding strength) that resulted in improved binding [6]. Presence of oxygen groups in Fe_2O_3 improves water molecules accessibility accelerating cement hydration and C–S–H gel formation. It is reported recently that instead of one type of oxide nanoparticles a mixture of two or more different functional oxide nanoparticles (Fe_2O_3-SiO_2, TiO_2-SiO_2 etc) added together may result even better [7, 8, 9] flexural and compressive strength due to accelerated cement hydration and C-S-H gel formation, reduced pore volume (pore filling) forming more compact microstructures.

1.1.2. Cement composites containing GO/ RGO carbon nanostructures

Cement composites containing graphene and its derivatives (GO: graphene oxide, RGO: reduced graphene oxide), carbon nanotubes (CNTs) nanofibers (CNFs) are of current research interests for the sustainable developments. Graphene has excellent conductivity of heat & electricity, high Young's modulus (~ 1×10^{12} TPa (terapascals)) and intrinsic strength of ~ 130 GPa (gigapascals) [10]. It can increase compressive strength of about 40% at early stage of cement hydration when present at low wt% (< 1 wt%) [11]. Graphene oxide (GO) is found to be highly effective in enhancing tensile strength, reducing growth of crack and refining pore structure of concrete [12- 14]. Recently functionalized graphene oxide is considered to be influential in cement hydration that can highly increase flexural (49%) and compressive strength (35%) [15].

Carbon nanotubes and nanofibers are being incorporated into cementitious materials that may be considered as next generation promising high performance cementitious materials with high increase in compressive strength > 100% and >200% at as low as 0.1% carbon nanotubes and 0.2 wt% carbon fibers, respectively [16]. Improved flexural strength may be a result of better bridging action and acceleration in cement hydration process, while, inhibition of extension of cracks and pore refining or porosity reduction may cause improvement in the compressive strength [17, 18].

1.1.3. Cement composites containing polymers

Protecting infrastructures from chemical attack or environmental damage, cement composites containing polymer/epoxy may suitably be applied. However, it must be ensured that polymer containing composites maintain required level of mechanical strength at the same time when it is used for preventing corrosion or permeation chemicals. Eskander et al [19] has shown how cement-polymer composite prepared using recycled polystyrene foam waste in cement is effective for prevention of corrosion. Corrosion resistive polymer (fibre-reinforced polymer sheets) modified concrete is reported recently by Tu et al [20] showing significant improvement in the resistance to chloride ion attack. Rustum et al [21] have reported increase in bond strength due to incorporation of PMMA. It results in enhanced flexural and compressive strength. Chen et al [22] have shown better controlling of pores due to polymer loading. Polymer-cement nanocomposite may provide better strength and durability due to improved pore structure.

1.2. Challenges in the chosen topic (gap in the literature)

From the above background literature reports it is observed that PC based nanocomposites admixing with various nanoparticles/nanofibers may offer improved mechanical strength, filling properties, reduced cracks, corrosion & shrinkage, abrasion or erosion, microbial activity etc. Although a huge literature exists on the development of various cementitious materials showing appreciable improvement in the mechanical strength the real cause is still not clear. It is usually assigned to faster cement hydration and formation of C-S-H gel phase. However, understanding physical and chemical processes during cement hydration and curing through the study of structural and spectroscopic investigations is highly needed. At the same time, developing cementitious nanocomposites with smart properties, especially photocatalytic dye degradation and antimicrobial activity for cleaner production of environment maintaining mechanical strength at required level is highly desirable and challenging for future sustainable developments of civil infrastructures. Developing technologically viable smart cement nanocomposites would be first step in solving the above issues to large extent.

1.3. Objective of the proposed PhD works

Motivated by the above challenges existing in developing smart cement nanocomposites we propose the title of the work as '**Cement based smart nanocomposites containing metal oxides, graphene oxides and polymers for building applications.'** The objectives of the proposed thesis work are listed below:

1. To develop cement based smart nanocomposites containing oxides (Fe_2O_3, TiO_2, SiO_2) and metal (Cu) nanoparticles, and study of their structural and mechanical properties.
2. To develop cement based nanocomposites containing graphene oxides (GO) and reduced graphene oxides (RGO), and study of their structural and mechanical properties.
3. To develop cement based nanocomposites containing polymers (PVA: polyvinyl alcohol) to improve mechanical strength.
4. Study of photocatalytic dye degradation, antimicrobial properties and chemical stability on the developed cement based smart nanocomposites.

1.4. Working methodology/Flow Chart of the proposed work

1.4.1 Development of cement nanocomposites containing metal- oxide and metal nanoparticles, graphene oxide, reduced graphene oxide and polymers

We use Fe_2O_3, TiO_2, SiO_2, Cu nanoparticles, GO, RGO, and PVA in OPC at appropriate wt% to develop smart cementitious nanocomposites. Chemicals and other nanomaterials are purchased and used without further purification. Appropriate doses of additive nanomaterials are obtained by achieving optimized mechanical strength for each added nanomaterial. Compressive and flexural strengths are monitored at each stage of cement hydration (3 days, 7 days, 14 days and 28 days).

1.4.2 Mechanical strength measurements

Compressive strength and flexural strength are measured using compression testing machine (CTM) at each stage of cement hydration and curing (3 days, 7 days, 14 days and 28 days).

1.4.3 X-ray diffraction (XRD)

Microstructural properties of cement composites containing functional nanoparticles before and after the incorporation into OPC are investigated using X-ray diffraction.

1.4.4. Fourier transform infrared (FTIR)spectroscopy

Chemical changes at each state of cement hydration and formation of C-S-H gel phase are monitored using Fourier transform infrared spectroscopy.

1.4.5. UV-Vis spectroscopy

Visible light driven photocatalytic dye degradation (Rhodamine 6g) is studied on the smart cement composites using UV-Vis spectroscopy.

1.4.6. Antimicrobial studies

Antimicrobial activity was detected by using the disk diffusion method against *E. coli* (MTCC 2126). The plate was incubated at 37 ^{o}C inside a BOD incubator and observed for the zone of inhibition after 24 hours. The results are compared with that of OPC reference.

1.4.7. Chemical stability studies

Sample bricks are coated with optimized composite cement pastes and dipped in acid water solution for different time duration. Surface smoothness is monitored to compare with bricks surface coated with reference OPC paste.

1.5. Structure/chapter outline of the thesis

Chapter wise thesis content is organized as follows. In the chapter-1 we have presented introduction to the cement nanocomposites containing metal oxide and metal nanoparticles, graphene oxides and PVA. Research gap and subsequently thesis objectives are outlined. In the chapter-2 detailed literature survey relevant to the present thesis work is presented. In chapter-3, experimental techniques essential to prepare and characterize cement composites are outlined. Subsequently, in chapter-4 we have presented the details of the development of smart cement nanocomposites containing metal-oxide and metal nanoparticles and a systematic study of their mechanical and structural properties. In the chapter-5 development of the cement nanocomposites containing Fe_2O_3, graphene oxide and reduced graphene oxide is reported. Structural, mechanical and vibrational properties are discussed. Chapter-6 contains reports on the development of cement nanocomposite containing PVA, optimized Fe_2O_3, and GO. In the chapter-7, reports on the photocatalytic dye degradation, antimicrobial activity and effect of acid water treatment on the developed cement nanocomposites are presented. Conclusions and future scopes are outlined in the chapter-8. References are placed at the end.

CHAPTER-2

Literature Survey

Introduction: Interests in smart cement nanocomposites

Development of smart cement nanocomposites containing various functional nanomaterials such as oxides (TiO_2, Fe_2O_3, SiO_2, ZrO_2), graphene and its derivatives (GO/RGO), carbon nanomaterials (CNTs)/ nanofibers, and polymeric materials that are reported in last 10-15 years is discussed in this chapter.

Smart cement nanocomposites containing functional nanomaterials have been considered as potential candidates for long run sustainable developments in the construction industry. They have potential applications in cleaner production, especially, for photocatalytic dye degradation, air/water pollution control, hydrophobic surface and antimicrobial activities; in piezoelectric sensing, thermal and electrical conductivity, and in preventing chemical attack/ corrosion resistance [23-28]. These smart nanocomposites not only display smart properties but also retain their basic mechanical strength at desired level. Due to their modified and improvised mechanical properties and smart functionalities, they are of high demand worldwide. Portland cement (PC) being the basic ingredient of smart cement nanocomposites has been used widely in the construction industries. A variety of portland cements are existing depending upon their purpose of applications as shown in the Figure-2.1. Additive functional nanomaterials play crucial role in accelerating cement hydration and C-S-H (calcium-silicate-hydrate) gel formation that may result in faster development of mechanical strength. Usually, different metal oxides, metal nanoparticles, carbon nanomaterials and polymers are being added to ordinary portland cement (OPC) (at small weight percentage) to modify mechanical, physical & chemical properties of cement concretes. One of the key aspects of improving mechanical strength is to prevent cracks in the cement. Cracks may appear due to brittle nature of cement composites which may affect durability (Figure-2.2). Furthermore, porosity may also cause deterioration of concrete. Thus, maintenance is required to keep constructed building, walls, bridge etc at safe level but at the expense of extra cost. To mitigate microcracks and subsequent damage, and to increase compressive/tensile strength, various oxides, and functional nanomaterials such as carbon fibers,

Figure-2.1. Different types of portland cements that have different application purpose.

graphene and polymers are added to base cement. Metal and oxide nanoparticles have larger active surface compared to micro- and macro- particles; therefore, they may lead to stronger binding with surrounding cement components by filling of pores [29]. On the other hand, microfibers and macro fibers (large) play vital role in preventing microcracks and subsequent formation of macrocracks and their propagation through bridging action [30]. Hence, size of cement particles and various additive nanoparticles may play an effective role for achieving cement strength. Figure-2.2 shows a plot of surface area of various particles useful in construction Industry [31]. It shows high surface area associated with nanoparticles that may be useful for the preparation of high strength cement nanocomposites. As has been mentioned, one needs to incorporate various nanomaterials, such as, TiO_2 (titanium dioxide), Fe_2O_3 (iron oxide), SiO_2 (silicon dioxide), ZrO_2 (zirconium oxide)), GO (graphene oxide), RGO (reduced graphene oxide), carbon nanomaterials (CNTs (carbon nanotubes), CNFs (carbon nanofibers)), and polymers ((PMMA (polymethylmethacrylate)) to the base portland cement for achieving high cement strength [32, 33]. However, based on the fact that large volume of nanoparticle required in the construction may lead to multifold increase in the overall production cost. Furthermore, application specific choice of nanomaterials in cement nanocomposites needs optimization and deeper understanding through extensive research. In the past 10-15 years, researchers across the globe have put tremendous research efforts to fabricate novel cement nanocomposites containing various functional nanomaterials and

understand basic mechanical properties and smart properties. Year wise publications, as shown in Figure-2.3, reflect studies on a variety of cement nanocomposites containing various functional nanomaterials. For the plot google scholar search engine is used with appropriate 'string' of search as mentioned in the legend (with no further filtration). Figure shows strong research interests with increasing trend over the years. The chapter focuses on the recent developments of the cementitious materials that are reported in the last 10-15 years. Two aspects are considered for focused discussion: (a) basic mechanical properties (compressive and flexural strength) and (b) smart properties especially on the photocatalytic dye degradation, antimicrobial activity, hydrophobicity, piezoelectric property, corrosion resistance. After some basics we will discuss these aspects.

(a)

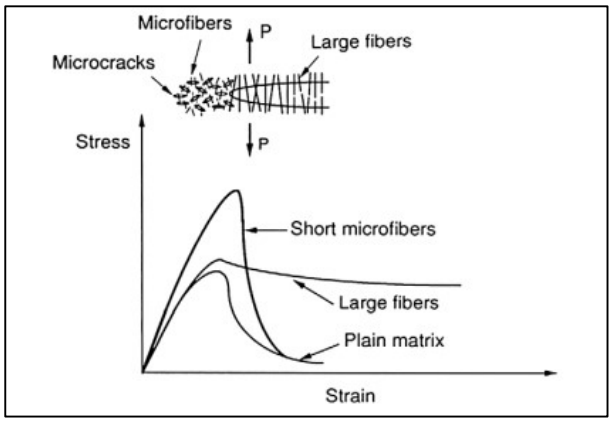

(b)

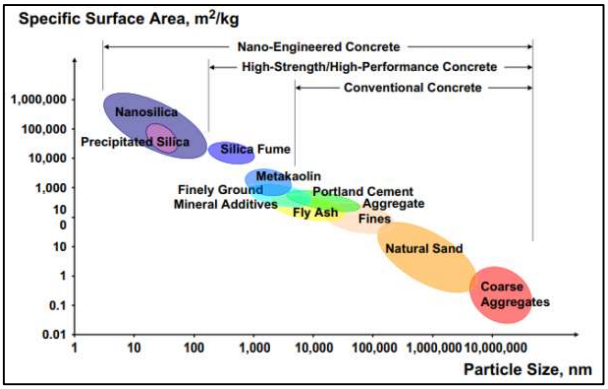

Figure-2.2. Relation between load & crack developed in the sample (a), and relative size of material used in construction industry (b). Figure source: (a) from Ref-7, and (b) from Ref-9.

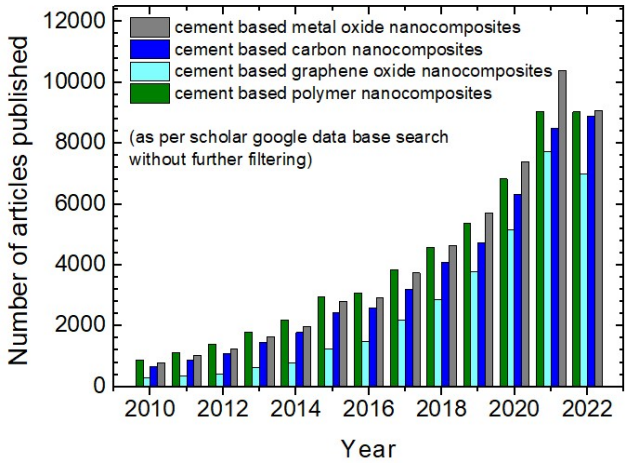

Figure-2.3. Year wise number of articles published on the topics as mentioned in the legend.

2.1 Cement basics

2.1.1 Cement compositions

The most common type of cement in the hydraulic cement category used for construction purpose is portland cement which is made of various silicates and oxides. When clinker minerals and water are mixed together the hydration process results in the hardening of the mixture.

Clinker phases are:

Alite (C_3S): $3CaO\ SiO_2$

Belite (C_2S): $2CaO\ SiO_2$

Tri-calcium Aluminate (Celite C_3A): $3CaO\ Al_2O_3$

Brownmillerite (Felite C_4AF): $4CaO\ Al_2O_3\ Fe_2O_3$

Limestone ($CaCO_3$) is burnt to produce CaO. This process release CO_2 (main source of carbon dioxide emission during calcination). CaO then reacts with SiO_2, Al_2O_3 to produce $2CaO\ SiO_2$/ $3CaO\ SiO_2$ and $3CaO\ Al_2O_3$, respectively and with Al_2O_3 and Fe_2O_3 to form $4CaO\ Al_2O_3\ Fe_2O_3$

$CaCO_3 \rightarrow CaO + CO_2$

$2CaO + SiO_2 \rightarrow 2CaO\ SiO_2$ (or Ca_2SiO_4)

$3CaO + SiO_2 \rightarrow 3CaO\ SiO_2$ (or Ca_3SiO_5)

$4CaO + Al_2O_3 + Fe_2O_3 \rightarrow 4CaO\ Al_2O_3\ Fe_2O_3$

The typical composition of portland cement [34] is

CaO: ~65%, SiO_2: ~20%, Al_2O_3: ~5%, Fe_2O_3: ~ 3%

Along with some other compound of minor quantity (such as MgO, SO_3, $CaSO_4$ etc)

2.1.2 Cement dispersion

Cement dispersion plays crucial role on initial cement hydration and microstructural properties. Water content to total available surface area of cement paste, mortar or concrete influences heat evolution and packing [35]. Well dispersion of additives is essential to achieve better workability of cement paste, mortar or concrete and reliable mechanical strength. Cement paste strength predominately varies depending upon w/c ratio of workable mix. It reduces as ratio increases as in the Figure-2.4, shown typically at 7 days of curing [36]. There are various models proposed in calculating strength of cement mix [37-40]. Elaborate discussion is beyond the scope of present review. However, it is noteworthy that simplistic models were given earlier by Feret [37] and Abrams [38], and subsequent improvements and/or discussions, and various other models are can be found in the references [39, 40]. Interested readers are referred to these references.

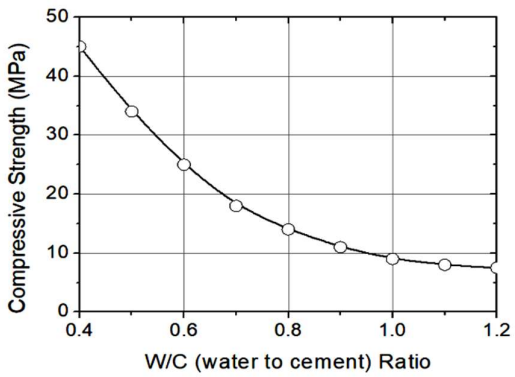

Figure-2.4. Influence of w/c ratio on the compressibility of cement mix typically at a curing of 7 days.

2.1.3 Cement hydration and setting time

Cement hydration is exothermic chemical reaction between cement & water when mixed together. Water to cement ratio (w/c), casting temperature, presence of C_3A and C_3S influence the overall hydration of cement. Furthermore, cement hydration also gets influenced by micro/nanostructures and fineness of mixed components. Reaction of C_3A, C_2S and C_3S with

water results in hydrated calcium aluminate, hydrated dicalcium silicate and hydrated tricalcium silicate along with CH (i.e. $Ca(OH)_2$), respectively. **A**ddition of water to cement results in initiation of cement hardening. This is an important process where optimum setting time is expected, as, too slow or quick may create problem of mixing, transportation and placing the cement mixture at the required places. Usually, half an hour to about 10 hours is considered to be ideal (according to IS 456-200 cement setting time can not be less than 30 minutes once water is mixed). Setting time gets influenced w/c ratio, admixtures and fineness of cement. A detailed discussion on the cement hydration using predictive models based on the dissolution and water diffusion theory can be found elsewhere [41]. These models can predict accurate cement hydration and concrete's performance evolution.

2.1.4 C-S-H gel formation in cement paste

Nanoscale building block of cement binder is calcium-silicate-hydrate (C-S-H) cohesive gel with no fixed composition and structure. Its formation starts when alite ((C_3S): 3CaO SiO_2) or belite ((C_2S): 2CaO SiO_2) reacts with water (chemical reactions are as follows: $2C_3S + 6\ H_2O \rightarrow 3\ CaO \bullet 2SiO_2 \bullet 3H_2O + 3\ CH$ + heat energy (high), and $2C_2S + 4\ H_2O \rightarrow 3\ CaO \bullet 2SiO_2 \bullet 3H_2O + CH$ + heat energy (low)) during the cement hydration process [41-45]. It is noteworthy that C_3S hydration is faster, and is responsible for early-stage cement strength (within first 7 days) while C_2S reacts with water slowly and results in latter stage (after 7-14 days) cement strength. Mechanism of C-S-H gel formation leading to cement setting is not straight forward which needs more study. Due to large surface area, cement hydration rate may be accelerated by the presence of C-S-H with increased precipitation in the capillary pores. The formation of gel phase/cement hydration process can be studied using X-ray diffraction (XRD) and Fourier transform infrared (FTIR) spectroscopies [46, 47] to understand chemical changes that occur during hydration process.

2.1.5 Consistency of cement paste

Cement consistency is useful to work with cement paste. It is the ability of cement paste to flow, and defined as the quantity of water required to make the cement paste of normal consistency. Vicat's apparatus is used to test cement paste consistency. Typically, 24% (wt%) water (or, if required, vary it from 26% to 33%) is added to 500g of cement and mixed, and plunger is gently released to obtain depth of penetration within 5-7 mm from the bottom.

2.1.6 Compressive strength

Compressive strength (CS) is the signature of cement strength defined by the ratio, $f_c = F/A$, where F = maximum force applied to the specimen before break, and A = area on which the force is applied. It is the capacity up to which the material withstands loads against compression or reducing size of the specimen. Compressive strength is measured upon standard sample size (for example: mold of dimension 70.6 × 70.6 × 70.6 mm, the sample cube size is in conformity with the Indian Standard, 516:1959). Test samples are cured at 3 to 28 days at an interval of 7 days. After normal drying (at ambient) the sample cubes are tested for compressive strength using compression testing machine (CTM).

2.1.7 Flexural strength

Ability of a material to withstand bending action due to applied load is termed as flexural strength (FS). It is also termed as modulus of rupture. Flexural strength is a measure of tensile strength indirectly. It can be measured from a three-point loading and centre-point loading test. Flexural strength is measured upon standard sample size (for example: mold of dimension 100 × 100 × 500 mm, IS 516:1959) cured for 3 days, 7 days, 14 days and 28 days.

2.2. Cement nanocomposites containing functional nanomaterials

We will now discuss detailed reports on the developments of cement nanocomposites containing various functional nanomaterials. It has already been mentioned in the previous section that cement nanocomposites containing various oxides, polymers and carbon materials are shown to accelerate cement hydration process with improved mechanical strength and other smart functionalities. A systematic discussion is presented below.

2.2.1. Cement nanocomposites containing TiO_2, SiO_2, Fe_2O_3 and ZrO_2

Incorporation of oxide nanoparticles, especially, TiO_2, SiO_2, Fe_2O_3 and ZrO_2 into cement host accelerates cement hydration improving compressive and flexural strength. It is usually safe to add non-toxic oxides to improve mechanical strength. For example, SiO_2 being one of the constituents of cement is added for further improvement of the mechanical strength of portland cement. Recently, flexural and compressive strength enhancement is reported by Ng et al [1]. They used nano-sized TiO_2, SiO_2, and Fe_2O_3 in cement mortar and showed improvement in the compressive strength in the range of 38-35%. Feng et al [2] showed how nano-TiO_2 in cement reduces microcracks and surface roughness using atomic force microscopy. Acceleration in pozzolanic reactions improves microstructures of concrete. In

this view, process of C-S-H gel formation plays major role in strengthening concrete (Singh et al [48]). Therefore, understanding pozzolanic reaction, cement hydration and subsequent acceleration in the formation of C-S-H gel have been considered as prime set points for developing futuristic smart cement composites. In the recent past, Han et al [3] has studied cement mortar and reported enhancement in tensile strength and flexural strength due to accelerated chemical process of C-S-H formation. Effect of nano-TiO_2 on hydration and shrinkage is studied by Zhang et al [4]. They showed enhanced compressive strength and pore refining and shrinkage. Phase of TiO_2 may play pivotal role in enhancing fatigue and FS of cement composites [5, 49].

Hematite (Fe_2O_3) nanoparticles may be considered as highly effective in improving mechanical strength due to their structural stability and possibility of physic-chemical binding and accelerating pozzolanic reaction at early stage [1, 6, 8]. On the surface of these nanoparticles C-S-H gel may grow which may further act as nucleation sites for the growth of C-S-H gel or β-phase, leading to the formation of more compact structure with reduced pores [1]. For example, Li et al [8] have shown experimentally that incorporating Fe_2O_3 and SiO_2 in to cement host increases compressive and FS of cement mortar which could be due to the reduction of pores or filling of pores by the added oxide nanoparticles. C-S-H growth is responsible for the enhancement in CS and FS, as reported by Kiamahalleh et al [6]. It is noted that optimum wt% of nanoparticles within the cement plays decisive role in enhancing mechanical strength and microstructural properties. This is also reported that reduction in micro-cracks results in improved bonding and hence mechanical strength. Optimum dose of Fe_2O_3 is found to be ~ 2.5 wt% in the cement mortar, showing influential effect of preventing the formation of microcracks and their propagation [6]. Furthermore, its presence is effective too in improving water molecules accessibility to the cement C–S–H and oxygen groups of Fe_2O_3 during cement hydration [6]. Among other oxides, effect of nano-sized ZrO_2 on PC is studied by Trejo-Arroyo et al [50]. They reported that mortar with ZrO_2 nanoparticles showed enhanced microstructural properties with high degree of compaction and increased compressive strength by ~ 9%. The presence of ZrO_2 nanoparticles inhibited growth of large $Ca(OH)_2$ crystals too.

2.2.2 Cement nanocomposites containing GO/ RGO and carbon nanomaterials

Cement nanocomposites containing graphene and graphene oxide have drawn significant research interests due to exotic properties of graphene. For example, it has excellent conductivity of heat & electricity, high Young's modulus (1 TPa) and intrinsic strength (130

GPa) (Alkhateb et al [10]). Only about 1wt% of graphene addition to cement may be sufficient to improve mechanical strength and other smart properties. Yang et al [11] have reported huge improvement in the compressive strength (~ 40%) when they added only 0.2 wt% of graphene to cement even within the aging of 3 days and 7 days. A considerable increase in the CS is observed too by Cao et al [12] when they added graphene nano-sheets. Babak et al [13] have reported increase in tensile strength by the use of 0.1 - 2 wt% GO (graphene oxide) along with 0.5 wt% super plasticizer. The presence of graphene oxide in composite reduces the growth of crack in cement mortar [14] and influences pore structures of concrete [51]. Recently functionalized graphene oxide and cement composite is studied by Wang et al [15]. Graphene oxide is functionalized with APTES (3-aminopropyl triethoxysilane) and amorphous SiO_2 to protect GO basal plane from alkaline environment and participate in to cement hydration process. With 0.15 wt% FGO (functionalized graphene oxide) in the cement composite a huge increase of about 49% and 35% in flexural and compressive strength was observed by the authors. This could be due to the improvement in the bonding between the nanoparticles and cement. Functionalized graphene oxide could be future potential candidate for cement industry. There are a few recent articles showing some studies on piezoelectric properties, thermal conductivity of concrete-GO/RGO, and multi-functionalities of cement-multilayered graphene. For example, Rehman et al [52] have prepared GNP cement composites and shown 30% increase in load carrying capacity. At maximum compressive load electrical resistivity drops by 42%. Recently Zhang et al [53] have developed a novel self-sensing cement composite using RGO in cement. They have seen improvement in the compressive strength (by ~ 29%), flexural strength (by ~ 49%) and electrical conductivity (by ~ 23%). A report by Sun et al [54] on cement composite containing multi-layer graphene shows 54% increase in compressive strength, 1.6 time higher shielding effectiveness, and ~ 7 times stronger absorption performance compared to composite without multi-layer graphene.

Other carbon nanomaterials, such as, SWCNTs (single walled carbon nanotubes) and MWCNTs (multiwalled carbon nanotubes) have strong influence too on mechanical, structural and optical properties. These are considered as next generation promising high performance materials for cement industry. Incorporation of short carbon fibers in to cement reduces porosity, increases stiffness of the materials and mechanical strength [55]. A very high increase in CS of cement mortar up to 154% & 217% is reported by Yazdani et al [16] when they just incorporated only 0.1% to 0.2% carbon nanotubes and fibers. In fact, carbon fibers help in arresting cracks and can show better load transfer mechanism [56].Carbon fibers with

strong interfacial formation can bridge cracks and improve surface quality by reducing pores, resulting in better bonding and C-S-H cement hydration. Addition of carbon nanotubes (0.5% CNT) along with SiO_2 (20%) increases compressive strength of cement mortar [57]. When CNT fibers and PVA (polyvinyl alcohol) are used in the composite an increase in the flexural strength is seen (Metaxa et al [58]). On the other hand, carbon nanotubes (SWCNTs and MWCNTs) in cement mortar also show considerable improvement in the compressive and flexural strength [17, 18, 59-61]. When MWCNTs and CNFs (carbon nanofibers) are added together to cement mortars, a significant enhancement in the flexural strength (~106%) is seen as reported by Gdoutos et al [59]. Uniform dispersion of carbon nanomaterials is necessary for improving mechanical strength. Effective dispersion can be made by functionalizing carbon nanomaterials with hydrophilic functional group such as COOH. Cement mortars containing COOH functionalized MWCNTs are studied by Sarvandani et al [60]. Various amounts of MWCNTs (0.05 % to 0.4% by weight) are added to cement mortars, and compressive and flexural strengths are studied at different environmental conditions. They have seen an increase in flexural strength which is a result of better bridging action. Furthermore, it may be noted that filler action may refines pores, improve mechanical and microstructure properties, inhibits cracks by better bridging actions with accelerated cement hydration process (C-S-H phase) [17, 18].

2.2.3. Cement nanocomposites containing polymers

Protecting infrastructures from chemical attack or environmental damage, cement composites containing polymer/epoxy may suitably be applied. However, it must be ensured that polymer containing composites maintain required level of mechanical strength. A study by Fan et al [62] has shown that cement composite containing 0.6 wt% PVA increases compressive strength of ~12%. They have also shown capillary water absorption decrease by ~60%. Another report by Eskander et al [19] has shown how cement-polymer composite (recycled polystyrene foam waste in cement) may be considered as effective for corrosion resistance. Corrosion resistive polymer (fibre-reinforced polymer sheets) modified concrete is reported recently by Tu et al [20] showing significant improvement in the resistance to chloride ion attack. Rustum et al [21] have reported increase in bond strength due to incorporation of PMMA. It results in enhanced flexural and compressive strength. Chen et al [22] have shown better controlling of pores due to polymer loading. Polymer-cement nanocomposite may provide better strength and durability due to improved pore structure.

2.3. Comparative study: Compressive strength, porosity, cracks, corrosion resistance

Admixing of various functional nanostructures of oxides, polymers and carbon materials shows improvement in the CS. This is caused by the accelerated hydration of cement and C-S-H gel formation which may lead to pores reduction and prevention of cracks formation and propagation. While addition of TiO_2, SiO_2 and Fe_2O_3 nanoparticles (at < 5 wt%) shows improvement in the compressive and flexural strength due to effective pore filling and cracks reduction [63-73], the addition of GO/RGO and CNTs results in even higher (beyond 100%) compressive and flexural strength due to accelerated cement hydration, bridging action, controlling of cracks and cracks propagation [13, 16, 74-77]. Furthermore, only < 1 wt% carbon nanomaterials are required to be added to the base cement. On the other hand, polymers are added to improve corrosion resistance and reduce permeation [27, 78, 79]. A comparative study is presented in a tabular form (Table-I) for easy guidance to these findings. Some selective representative reports on the developments are discussed.

Table-I: Various properties of cement nanocomposites

Portland cement (PC) based nanocomposites	Compressive strength	Filling of pores/microstructure improved?	Cracks/corrosion improved?	Ref
PC with 1 wt% Nano TiO_2	Increase by 12% with respect to control PC	up to 22%	30% reduction in cracks	[63]
PC with 10 wt% Nano TiO_2	Decreased by 10% with respect to control PC	-	Minor improvement in cracks reduction	[64]
PC with 1 to 5 wt% TiO_2	Increased abrasion resistance, good fatigue strength	Improved microstructure of concrete	-	[65]
PC with nano silica (~2.5 wt%)	~6% increase compared control sample	additional β-phase (C-S-H gel) formation	Increased impermeability by 23.9%, and increased resistance to chloride ions by 14.7%	[66]

Nano silica coated TiO_2 in reactive powder concrete (RPC)	~87% increase in FS and 12% increase in CS	Filler action and β-phase (C-S-H gel) formation caused by Pozzolanic action	Inhibition of cracks	[67]
Nano-SiO_2 up to 3 wt %	Increase in compressive strength by ~50% (60 MPa to 90 MPa at 28 days), increase in flexural strength by ~ 50% (10 MPa to 20 MPa at 28 days)	Porosity reduces, pore diameter also decreases	-	[68]
Nano-SiO_2 up to 4 wt%	Compressive strength increases by 106% (9 MPa to 17 MPa), flexural strength increases by ~ 67% (3 MPa to 5 MPa)	Reduces porosity and also refines pore structure (from 20-50 nm size to 20 nm size)	-	[69]
PC with 0.5 to 3 wt% Fe_2O_3& Fe_3O_4	Increase in compressive strength by up to 2-3%	2 to 3% can improve the hydration process	Improvements in micro-cracks	[70]
PC with 1, 3 and 5 wt% Fe_2O_3	Increase in compressive strength by up to 75% (from 25 MPa to 44 MPa), flexural strength increases by ~ 60% (from 4.2 MPa to 6.7 MPa)	Improvements of microstructure	-	[71]
PC with 1 to 5 wt% Fe_2O_3	Maximum compressive strength at 2.5% of Fe_2O_3 (from 26 MPa to 34MPa)	Porosity decreases	-	[72]
3 wt.% of nano-Fe_3O_4	Minor increase in compressive strength	Acted as a filler, improving microstructure of cementitious composite with reduction in porosity	-	[73]

PC with graphene oxide (0.1 to 2 wt% GO) and super-plasticizer (0.5 wt%)	Up to 48% increase in tensile strength	Good bonding between GO & Cement matrix found	Growth of cracks in controlled efficiently	[13]
0.05 wt% GO in cement	CS increased by 15-33% (31.3 MPa to 38.8 MPa) and FS by 41–59% (4.7 MPa to 7.0 MPa)	Addition of graphene oxide possibly promote the hydration process	Formation of barrier by GO sheet may prevent crack propagation	[74]
0.05 wt% GO in cement paste	The flexural strength increased by 90.5% after 28 days, and compressive strength increased by 40.4%	Addition of graphene oxide possibly promotes hydration, pore volume reduction, and accelerates crystallite formation	-	[75]
Multiwalled carbon nanotubes	Increase in both flexural & compressive strength	Decrease in porosity	-	[76]
0.1 to 0.2 wt% CNT & CNF to enhance CS & FS	Up to 150% increase in CS and 50% increase in FS	Reduction in porosity & more stiffness	Effective crack control	[16]
Multiwalled carbon nanotubes in cement mortar & paste	Increase in compressive strength by up to 40% is observed	Decrease in porosity	Can delay in micro cracks propagation	[77]
Polymer modified concrete (polymer modifiers: polyacrylic ester emulsion, organic silicon waterproof agent and styrene-butadiene rubber latex)	Generally, compressive strength gets reduced. Addition of fly ash may improve compressive strength	Pore structure and compactness of concrete may be improved through polymer modification	Polymer modified concrete shows improvement in the resistance to chloride ion penetration	[78]

2.4. Smart properties of cement nanocomposites

Cement nanocomposites with smart properties are of recent research interests due to potential applications in self-cleaning and photocatalytic activities [80-90], antimicrobial activities [91-97], piezoelectric (PZT) smart properties [98-100], corrosion and shrinkage [101-104], mechanical, thermal and electrical properties [105-109] and hydrophobic coatings [110-116]. This smart sensing has now been possible due to technological developments and discovery of novel functional nanomaterials. Smart materials show unique signature property in response to the external excitations. Primarily, the addition of nano-sized materials to OPC would not only improve the basic mechanical strength of the cementitious materials but also exhibit certain smart properties. In the present review, photocatalytic activity, dye degradation, self-cleaning and antimicrobial properties are specifically discussed for composites containing oxide materials such as TiO_2, Fe_2O_3, SiO_2, CuO, ZnO, Al_2O_3 and CdS as main additives (they are potential photocatalysts and antimicrobial agents). Graphene and its derivatives, carbon nanomaterials are discussed for shrinkage and bridging effect. Tyre-rubber, crumb-rubber materials are important to generate hydrophobicity within cement composites. Piezoelectricity, corrosion and thermal stability are also discussed to show potentials applications and sustainable developments. It is noted that for enhancing various properties, nanomaterials need to be added at an optimum level. Higher dosage may lose effectiveness. Furthermore, sometimes, co-addition of two different nanomaterials may also result in better performance than that with one type of nanomaterial. In the Table-II, we have outlined some important smart properties that are achieved with the addition of different nanomaterials. From the large available literature reports we have picked up only some representative references for the discussion.

Table-II: Smart functionalities of cement nanocomposites

Cementitious composites	Specific purpose addressed	Level of improved	Ref
Graphene/TiO_2 nanocomposites coating on cement mortar	Under visible light discoloration of RhB (self-cleaning) and removal of NO (air purification)	The performance is compared among (a) no coating on cement mortar, (b) TiO_2coating on cement mortar, (c) TiO_2/graphene coating on cement mortar. Graphene (2D planar conjugated π-structure)	[80]

		favours adsorption of target pollutants due to higher specific surface area. This results in more effectiveness of TiO_2/graphene in the composite	
Nano-TiO_2 cement concrete, Nano-TiO_2 is used by IDM (internal doping method) and SPM (spraying method)	Photocatalytic dye (methyl orange (MO)) degradation	Nano-TiO_2 may be used by both the methods (for better photocatalytic performance) that may depend on the type of application: IDM for pavement materials, and SPM for wall building materials	[81]
Cement Composites containing Fe_2O_3, TiO_2 and Cu (copper) nanoparticles	Photocatalytic dye degradation (of Rhodamine-6G)	Enhanced dye-degradation is observed. Highest degradation rate of about 2.5 times faster (OPC containing Fe_2O_3) compared to control sample is observed	[82]
Photocatalytic additive (TiO_2) in mortars	To study degradation rate of common urban pollutant, NO_x	1% of TiO_2 addition results in reasonable degradation rate of NO_x without losing mechanical strength	[83]
Anatase-type TiO_2/cement mortar system for dye degradation	Photocatalytic dye (Methylene Blue (MB)) degradation under UV light	TiO_2-mortar cementitious materials show photocatalytic activities without damaging of mechanical properties. Highest MB degradation of ~76.6% happens in 4.5 hours with 1% TiO_2. Other concentration is less effective.	[84]

TiO_2-cement mortar cementitious materials	Photocatalytic activity: NO_X removal	Addition of TiO_2 shows photocatalytic activity without significant change in FS and the CS of the modified cements	[85]
Cement mortar containing Ag-TiO_2 photocatalysts	Photocatalytic dye (methyl orange (MO) and methylene blue (MB)) degradation under ultra violet (UV) and visible light	Dye degradation rate: (a) For MO, it is 95.5% at 30 minutes under UV light (b) For MB, it is 69.8% at 40 minutes under visible light	[86]
Cu-TiO_2/SiO_2 photocatalyst coating on concrete	Self-cleaning and air-pollution reduction	Addition of Cu in to TiO_2 photocatalyst (up to ~5% wt) promotes photocatalytic activity. 95% MB (methylene blue) degradation occurs within 60 min. Photocatalytic activity decreases for Cu doping beyond 5wt% may be due to defect states (trap states)	[87]
CdS/TiO_2-cement-nanocomposite catalyst	Photocatalytic dye degradation	Under UV light, TiO_2-cement composites result better dye degradation, whereas, CdS-TiO_2-cement composite is more efficient under visible light	[88]
Nitrogen and carbon co-modified TiO_2 photocatalyst in cement pastes for photocatalytic activity	Self-cleaning/dye degradation upon UV-Vis light exposure	Modified TiO_2 shows better photocatalytic efficiency than unmodified TiO_2	[89]
Cement samples containing BiOBr precursor for RhB degradation and NOx removal under visible light	RhB dye degradation and NOx removal	BiOBr precursor in cement matrix shows better photocatalytic activity compared to control sample	[90]
ZnO or ZnO–SiO_2 and lignin-	Prevention or slower	ZnO-enriched systems showed	[91]

cement composites	bacterial growth (antimicrobial study)	high antimicrobial resistance, $ZnO–SiO_2$ showed deterioration of the antimicrobial effect, with lignin showed lower growth than other systems	
Silica-titania (SiO_2/TiO_2) core-shell nanostructures-cement mortar	Self-cleaning, bactericidal, and photocatalytic properties	It acts as filler, self-cleaning and bactericidal properties under UV exposure are also observed	[92]
Antimicrobial Activity of Al_2O_3 (aluminum oxide), CuO (copper oxide), Fe_3O_4 (ferrosoferric oxide) and ZnO (zinc oxide) nanoparticles in cement-based building materials	Antimicrobial properties	Proper mixing of metal oxide nanoparticles in cement nanocomposite is important in observing antimicrobial response. Unproper dispersion may not be effective. Furthermore, even antimicrobial response of different strains from same species may be different.	[93]
PMMA based cement composites: Addition of silver nanowires for antibacterial activity	To enhance antibacterial activity	Silver nanowires (1 wt%) will enhance antibacterial activity against aureus	[94]
Inhibition ability of growth of bacteria and fungi due to the presence of copper(II) oxide, zinc oxide and titanium(IV) oxides in the cementitious material (cement mortars)	Inhibition ability of growth of E. coli or P. aeruginosa (bacteria) and C. albicans (fungi)	0.1% ZnO, 0.5% CuO, and 1% TiO_2 can be used separately for inhibition of growth of bacteria and fungi with highest inhibition with CuO. The dispersion is an important factor that may affect the workability and strength. This may even affect antimicrobial activity.	[96]
ZnO nano-needles in white	Enhanced	ZnO nano-needles in white	[97]

cement for photocatalytic, hydrophobic and antimicrobial property	photocatalytic, hydrophobic and antimicrobial property	cement showed significant improvement in the photocatalytic, antimicrobial activity	
Piezoelectric cement (30–70% PZT (lead zirconate titanate) with w/c of 0-20%)	Piezoelectric properties	Improvement in piezoelectric properties	[98]
Piezoelectric cement composites	Dielectric and piezoelectric properties	Properties depend on the interfacial microstructure between the matrix and the piezoelectric insertion	[99]
Piezoresistive properties of cement mortar doped with graphene nanoplatelets (GNPs)	Piezoresistive properties	For optimal piezo-resistivity GNP may be used in the range of 0.05% to 0.1%	[100]
Nanoclay and graphite in cement (0 to 1 wt% of cement) composite for the reduction of shrinkage	Reduction of shrinkage	Plastic shrinkage reduction by ~ 70% is achieved (independent of nanomaterial type)	[101]
Carbon nanotubes-cement mortars incorporation of	Shrinkage and bridging effects	About 0.05–0.1% of CNTs mixing reduces early-stage shrinkage by ~ 62%. Reduction of capillary stresses by filler and nucleation effect of smaller diameter CNTs decreasing fine pores between the hydration products may be responsible	[102]
Cement mortar and concrete prepared with distilled and electrolyzed water (30 min)	Corrosion resistance study (sodium sulphate: Na_2SO_4, sodium chloride: NaCl, and a combined mixture of Na_2SO_4 &	The cement mortars and concretes prepared with electrolyzed water show less attack	[103]

	NaCl solution)		
Cementitious composites: addition of nano-TiO_2 and effect on microstructural and corrosion resistance properties	Corrosion resistance to acidic solution, tap and saline water	Corrosion inhibition efficiency is good up to 5% of nano-TiO_2 for all the environments	[104]
Nano titanium dioxide ($nTiO_2$) in EGA (expanded glass aggregates)-mortar	Improvement in the mechanical properties and resistance to water	Nano TiO_2 improves mechanical properties and water resistance ability	[105]
Reduced graphene oxide (RGO) in cement mortar	Enhancing thermal properties of cement mortar by incorporating RGO	1.2 wt. % RGO doping enhances thermal conductivity and thermal diffusivity coefficient by 7.8 % and 29 %, respectively	[106]
Graphene oxide (GO) in cement mortar	Improving thermal conductivity	Thermal conductivity increases by 8.6% when 0.02 wt% GO is added to cement mortar	[107]
GO in cement (paste/mortar)	Electrical conductivity	Electrical conductivity is 50% higher than control sample when 0.03 wt% GO is added to cement	[108]
Addition of nanosilica into cementitious material	Thermal stability	Considerable enhancement of thermal stability due to addition of nanosilica (5wt%). Sample that does not contain nanosilica shows more damage at elevated temperature. Pozzolanic activity and reduction in CH seem to be the primary reason for minimum damage and higher stability.	[109]
Ionic paraffin emulsions (IPEs) in cement nanocomposite	To improve hydrophobicity	Addition of 4.0% NPE (non-ionic paraffin emulsion) in cement mortar exhibits outstanding hydrophobicity compared to anionic and cationic	[110]

		paraffin emulsions	
Different hydrophobic agents (stearic acid, DryCit, rapeseed oil) in cement composites (1-2 wt%)	To improve internal hydrophobicity	Water resistance in the pore protection factor test increases between 21% to 33%	[111]
Waste tire rubber in mortar	Hydrophobicity	Decrease in water absorption and increase in corrosion resistance due to better hydrophobicity	[112]
Amorphous carbon powder (ACP) in cement paste	Hydrophobicity and electrical properties	Addition of 15% ACP by weight reduces water absorption by 23% and electrical conductivity of cement paste by 65%	[113]
Tyre rubber (TR) addition to cementitious material (cement paste)	Improving hydrophobicity	Smaller grain size results in better hydrophobic characteristics	[114]
Addition of crumb rubber cement paste	Improving hydrophobicity to reduce water penetration	Rubberized cement paste shows reduced water penetration due to improved hydrophobicity of paste treated with crumb-rubber	[115]
Multifunctional cementitious composites containing graphene nanoplate (GNP) and silicone hydrophobic powder (SHP)	Piezo-resistivity, and hydrophobic behaviour	Addition of SHP (2%) shows better reduction (~15 times) of water absorption. Along with isolation effect of GNP, the SHP powder helps in improving hydrophobicity in the specimen surface and other places such as pores and cracks. This effect reduces water absorption and help in achieving stable piezo-resistivity.	[116]

CHAPTER-3

Experimental Techniques

Introduction

This chapter deals with the discussion the experimental techniques involved in preparing and characterizing the smart cementitious materials containing TiO_2, Fe_2O_3, SiO_2, Cu nanoparticle, graphene and its derivatives (GO/RGO), and PVA materials usually at low wt% (1-5 wt% or less). After the preparation, mechanical strength is measured for initial testing of compatibility. Compressive and flexural strength are monitored at different days of curing and cement hydration. Thermal stability is measured when and where necessary. Once the mechanical strength is achieved with optimum dosage of nanomaterials, the samples are then tested further for achieving smart properties, such as photocatalytic dye degradation and antimicrobial activity.

3.1 Sample preparation and mechanical strength measurements

OPC (ordinary portland cement) of grade 43 is taken as the basic binding material. Various additives, such as, TiO_2, Fe_2O_3, SiO_2 and Cu (copper) nanoparticles are used as received (Sisco Research laboratories, India & Otto Chemie Pvt Ltd, Maharashtra, India) without further purification or chemical modification. To make smart OPC nanocomposites, oxide nanoparticles and metal nanoparticles are being mixed with OPC at various weight%. A total of 12 cubes of cement paste are made with each cube volume of 351.89 cm^3 (70.6 mm × 70.6 mm × 70.6 mm). Consistency test is carried out for OPC grade 43 which is found to be 32%. After casting, 24 hours are allowed for natural setting before putting them in to water for curing. Mechanical properties (compressive strength (CS) and flexural strength (FS)) are studied after standard curing time of 3 to 28 days at a step of 7 days. Capacity of Compression Testing Machine (CTM) is 2000kN and rate of loading for compression is 0.6kN/sec. The CS (f_c) is determined using the relation, $f_c = P/A$, where P = maximum or ultimate load, and A = cross-sectional area of sample cube (= 49.84 cm^2 in this case). Flexural strength (f_s) is measured on the sample beam (100 mm × 100 mm × 500 mm). FS (flexural strength) measurement is carried out by placing the specimen beam in middle of the supports (2-point loading) (Figure-3.1). Modulus of rupture or flexural strength is given by, f_s (MPa) = $(P \times L)/(B \times D^2)$, where, P = load when specimen fails (kN≡ kilo Newton), D = depth of beam

specimen (mm), L = minimum distance between the edge and breaking point, B = width of specimen beam.

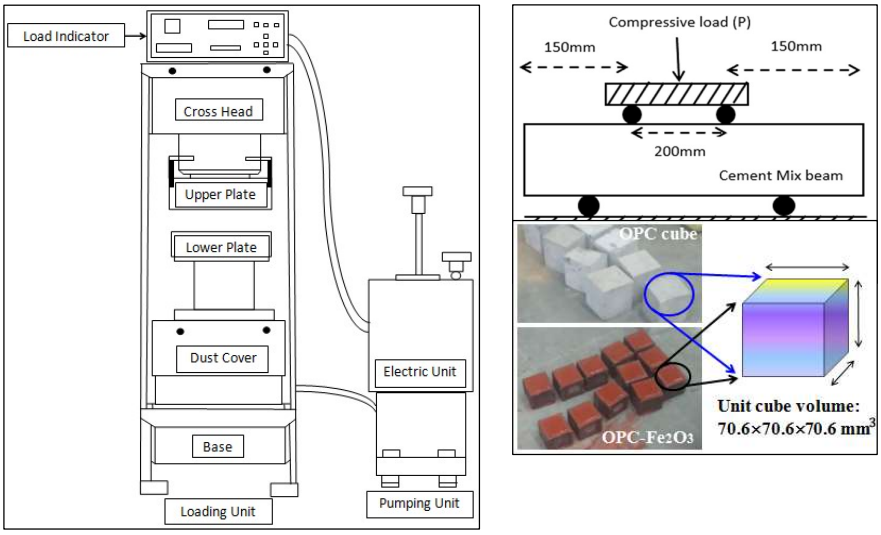

Figure-3.1 Compressive strength measurements using typical system (layout: left panel), flexural strength measurements (layout: right panel-top). Typical samples prepared with OPC (as reference) and OPC-Fe_2O_3 (as test sample) are shown in the right panel (bottom). Unit cube dimensions are as mentioned in the figure (right panel: bottom).

3.2 Structural characterization

Microstructural characterization is carried out using x-ray diffractometer (BRUKER:D8 advanced diffractometer, Germany with Cu $K\alpha_\alpha$ radiation, λ (wavelength) = 1.5406 Å) in the 2θ range of 20 degrees to 80 degrees. Crystallite sizes of oxide and metal nanoparticles are calculated from the peak diffraction of respective nanoparticle using Scherrer's formula [117]. The X-ray diffraction facility at CIC of UPES is utilized.

3.3 Scanning electron microscopy study

Scanning electron microscopy (SEM) was carried out to analyze surface morphology using ZEISS SEM. EDAX (Energy dispersive X-ray) was carried out to analyze elemental presence in the cement nanocomposites.

3.4 Fourier transform infrared (FTIR) spectroscopy study

FTIR spectroscopy studies of GO/RGO admixed OPC-Fe_2O_3 cementitious materials are carried out using Perkin Elmer Spectrum One instrument from 450 to 4400 cm^{-1} at 4 cm^{-1} resolution. Spectra are recorded in the transmission mode. Usually, >10 scans are employed for the better signal to noise ratio. KBr (potassium bromide) is added with the sample powder (small part of cube of each sample specimen is finely ground) for enhancing transparency, and sample palette (10 mm diameter) of each sample is made. Thickness of palette is made very thin to retain transparency.

3.5 UV-Vis photocatalytic/dye degradation studies

Photocatalytic study is carried out on OPC, and other cementitious materials containing oxide (Fe_2O_3, TiO_2, SiO_2) nanomaterials, GO/RGO, polymer (PVA) and other OPC-Fe_2O_3, OPC-TiO_2, OPC-Cu cement composites using UV-Vis spectroscopy (Lambda 35 from Perkin Elmer). Small part of sample cube cured at 28 days is finely ground using mortar and pastel. In 80 ml deionised water (DI water) 25 mg of finely ground powder of each composite sample is dispersed and ultrasonicated for 1 minute. Rhodamine-6G of 25 mg of is added in 100 ml DI water. Next, 20 ml of Rhodamine solution is added separately to the 80 ml sample solution. Thus, a total of four separate solution mixtures (100 ml each) are being prepared. All the solution mixtures are exposed to 100 watts visible light (bulb is kept 10 cm away from the solution surface) with frequent stirring using glass rod. UV-Vis absorption spectra are recorded for each solution to record spectral response. Before visible light exposure the recorded spectra are treated as references. Subsequently, after every 1 hour exposure spectra are recorded to monitor exposure dependent dye degradation.

3.6 Antimicrobial studies

Antimicrobial activity was detected by using the disk diffusion method against *E. coli* (MTCC 2126). 100 µl of 24-hour-old *E. Coli* broth culture was spread over a sterile nutrient agar plate. The sample disc (pellet size of 1 cm diameter and 1mm thick made of OPC (reference) and other cementitious materials was sterilized using UV irradiation for 15 minutes and placed over the agar in sterile environment inside a biosafety cabinet. The plate was incubated at 37 ºC inside a BOD incubator and observed for the zone of inhibition after 24 hours.

CHAPTER-4

Development of cement composites containing metal and oxide nanoparticles and study of their mechanical and structural properties

Introduction

Preparation and characterization of cement nanocomposites containing metal and oxide nanoparticles are reported in this chapter. These nanoparticles are added in minor weight percentage (wt%) to ordinary portland cement (OPC). It has been found that minor quantity of various metal oxides such as Fe_2O_3, TiO_2, SiO_2, metal nanoparticles such as Cu added to OPC changes its mechanical strength, more specifically, improves by ~10-30%. Minor addition of these oxide nanoparticles also improves various smart properties including dye degradation, antimicrobial affect etc retaining their basic mechanical strength intact. In the present studies we have prepared OPC based smart cement composite paste containing Fe_2O_3, TiO_2, SiO_2 and Cu nanoparticles in the range of 0.5-5 wt%. Prepared samples are cured at standard curing time and at each stage mechanical, microstructural properties are investigated systematically. Highest compressive strength (CS) improvement is seen for OPC-Fe_2O_3 nanocomposite paste that shows ~33% improvement in the CS and ~20% in FS. This improvement is caused by the faster cement hydration and β phase (C-S-H gel phase) formation whose presence is confirmed by X-ray diffraction measurements. Thermal stability measurements show micro cracks formation when annealed temperature goes beyond 100 ^oC.

4.1 Sample preparation and experimental measurements

Nanomaterials of Fe_2O_3, TiO_2, SiO_2, and Cu nanoparticles are added to OPC at different wt% as in the Table-4.1. Water consistency test for OPC results in 32%. A total of 12 cubes of each cement composite (OPC, OPC-Fe_2O_3 composite, OPC-TiO_2 composite, OPC-SiO_2 composite, OPC-Cu composite) are made. After casting, 24 hours are allowed for natural setting before putting them in to water for curing. Mechanical properties (compressive and flexural) are studied after standard curing time of 3 to 28 days at a step of 7 days. Microstructures are investigated using x-ray diffractometer in the 2θ range of 20 degrees to 80 degrees. In order to understand thermal effect on mechanical properties of cement composite we have exposed the

optimized cement composite cubes cured at 28 days to thermal annealing. The reference OPC cube and OPC-Fe_2O_3, OPC-TiO_2, OPC-Cu cube samples (3 cubes of each type) exposed to oven at 100 ^oC, 200 ^oC, 300 ^oC, 400 ^oC at one go (no cumulative exposure). Time of thermal annealing is of 30 minutes.

Table-4.1: Oxide and metal nanoparticles based OPC cement nanocomposites at different wt% of oxides or metal nanoparticles.

OPC-Composite Type	OPC: Fe_2O_3 (g: g)	OPC: TiO_2 (g: g)	OPC: SiO_2 (g: g)	OPC: Cu (g: g)
0.5 wt%	-	-	600: 03	600: 03
1wt%	600: 06	600: 06	600: 06	600: 06
2wt%	600: 12	600: 12	600: 12	600: 12
3wt%	600: 18	600: 18	600: 18	600: 18
4wt%	600: 24	600: 24	600: 24	-
5wt%	600: 30	600: 3	600: 30	-

4.2 Results and discussions

Microstructures and mechanical properties of cement composites may get affected by the doses of added nanoparticles. This addition may also have influential effect on cement hydration and C-S-H gel phase formation, binding and bridging with active nanoparticles, pre-filling and reduction of pores. Details of systematic studies are presented below.

4.2.1 Compressive strength of OPC paste containing Fe_2O_3, TiO_3, SiO_2 and Cu nanoparticles

The compressive strength of the OPC composites containing Fe_2O_3, TiO_3, and SiO_2 and Cu nanoparticles with different weight percentage (wt%) are shown in the Figure-4.1 (a-d). Cement composite containing Fe_2O_3 nanoparticles shows increase in compressive strength with curing time (Figure-4.1 (a)). This trend is observed for all the samples with different concentration (1% to 5%) of Fe_2O_3 (wt%) with respect to that of the reference OPC [1]. Maximum compressive strength of ~ 33% is measured for the OPC- Fe_2O_3 composite with 3wt% cured at 28 days. The observed considerable improvement in the CS is expected to be caused by the reduction of porosity and strong bonding by the β-phase (C-S-H gel phase) formation. Similarly; we have studied OPC-TiO_2, OPC-SiO_2 and OPC-Cu cement composites. The OPC-TiO_2 composites (1% to 5% wt% TiO_2) show enhanced CS compared to pure OPC

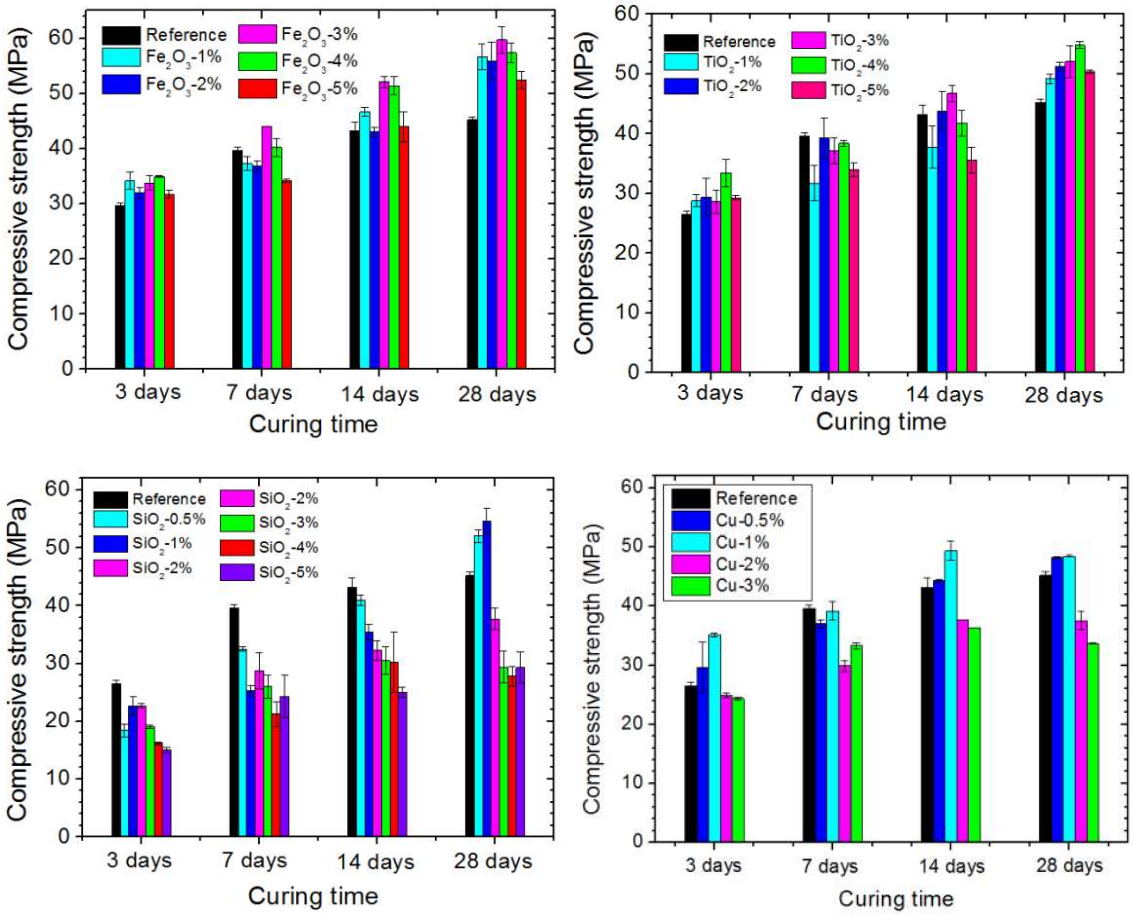

Figure-4.1. CS of composites containing Fe_2O_3 (top-row left), TiO_2 (top-row right), SiO_2 (bottom-row left) and Cu nanoparticles (bottom-row right). Standard curing time is considered to be of 3 to 28 days at a step of 7 days. Different added wt% is as indicated in the respective legend.

reference (Figure-4.1 (b)), especially after 28 days of curing. However, OPC-TiO_2 cement composites show lesser enhancement compared to that with OPC-Fe_2O_3 composites. OPC-SiO_2 composites show different trend. Enhanced CS is observed for the samples with 0.5 wt% and 1 wt% and only at 28 days of curing. For all the other wt% and curing compressive strength is less than that of OPC reference (Figure-4.1(c)). The CS of the OPC-Cu composites is shown in the Figure-4.1(d). It shows increase in compressive strength with curing time for 0.5 wt% and 1 wt% OPC-Cu composites only. For all the other concentrations it is lesser than that of OPC reference (for all curing time). Up to 1wt% Cu can be considered as effective in

enhancing compressive strength for all curing ages. From the study it is evident that 3wt% Fe_2O_3 in OPC-Fe_2O_3, 4 wt% TiO_2 in OPC-TiO_2, 1wt% SiO_2 in OPC-SiO_2 and 1 wt% Cu in OPC-Cu may be considered as optimum dose to achieve highest strength at 28 days. It is also seen that as compared to OPC reference, no composites containing oxides with optimum dose of nanoparticle show saturation trend except OPC-Cu.

4.2.2 Flexural strength of OPC cement paste containing Fe_2O_3, TiO_3 nanoparticles

Based on the compressive strength data we have prepared samples typically with 3wt% Fe_2O_3 and 4wt% TiO_2 in OPC separately to study flexural strengths at curing time of 3 to 28 days at a step of 7days, as presented in Figure4.2. Both, OPC-Fe_2O_3 and OPC-TiO_2 composites show increase in FS with the aging. It is also seen that the enhancement with aging is better in

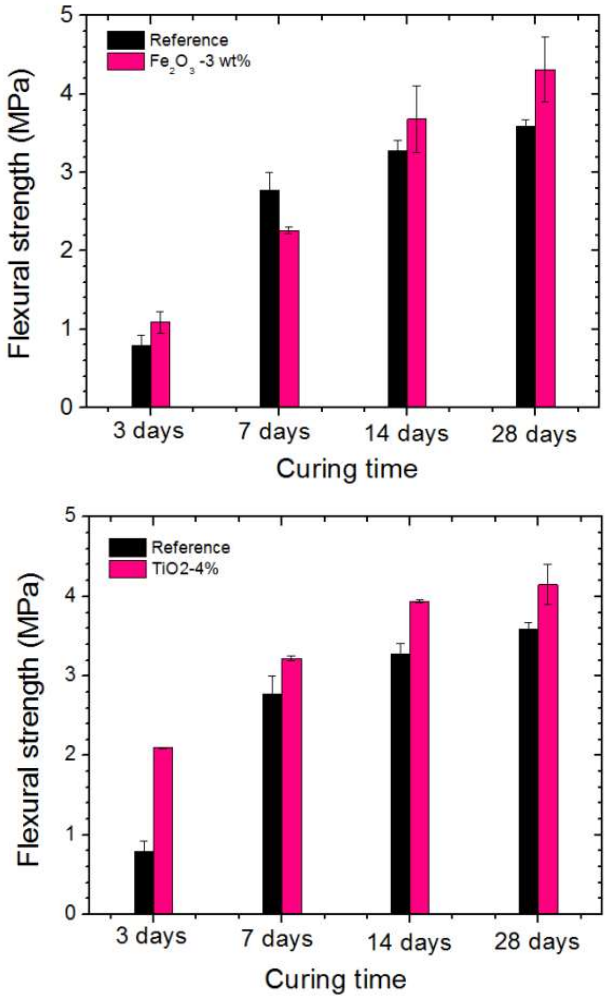

Figure-4.2. Flexural strength of cement composite containing Fe_2O_3 (top), TiO_2 (bottom) nanoparticles at the curing ages of 3 to 28 days at a step of 7 days. The strength of Fe_2O_3 in OPC-Fe_2O_3 is 3wt% and that of TiO_2 in OPC-TiO_2 is 4wt%.

OPC-TiO_2 composite than OPC-Fe_2O_3 composite in most of the aging time. Flexural strength is increased by about 10 to 15% with respect to the OPC in both the cases. It is further noted that OPC-TiO_2 composite shows a saturation trend, although no such trend is observed for OPC-Fe_2O_3 composite. Non saturation of flexural strength in the OPC-Fe_2O_3 composite suggests possibility of further enhancement at longer aging. Faster increase and subsequent saturation observed in OPC-TiO_2 can be attributed to faster cement hydration and better bonding with TiO_2, and the enhanced strength may be caused by the reduction of pores or filling of pores by nanoparticles and better bridging the gaps by C-S-H hydration.

4.2.3 Microstructural properties of OPC-Fe_2O_3, OPC-TiO_2 and OPC-Cu nanocomposites

In order to understand the role of microstructures of added nanoparticles to enhance mechanical and other smart properties we have studied X-ray diffraction (XRD) of cement composite samples containing nanoparticles before and after the mixing with OPC. X-ray diffraction spectra of OPC-Fe_2O_3, OPC-TiO_2 and OPC-Cu composites after 28 days of aging at various concentrations (0.5wt% to 5wt%) are shown in the figure below. XRD spectrum of OPC cube after 28 days of aging is also shown for comparison. For reference, XRD spectra of pure OPC (powder), Fe_2O_3, TiO_2 and Cu nanoparticles have also been incorporated and studied. Typical measurement range is considered to be from 20 degrees to 65 degrees (2θ values). X-ray diffraction spectra of OPC-Fe_2O_3 samples are shown in the Figure 4.3. Various peaks related to crystal planes are observed at 2θ values of 24.15, 33.15, 35.65, 40.85, 49.45, 54.02, 62.42, and 64.02 degrees which correspond to the hexagonal α-Fe_2O_3 (hematite) with planes (012), (104), (110), (113), (024) (116), (214) and (300), respectively [117, 118]. In the same figure we have plotted XRD of pure OPC (cube) after 28 days of aging shows several distinct peaks denoted by α, β, γ that correspond to CaO-H_2O, C-S-H (i.e. CaO-SiO_2-H_2O) and C_3S (i.e. 3CaO-SiO_2), respectively of OPC constituents [46, 119]. From the figure, it is also evident that the addition of Fe_2O_3 in to OPC does not change crystalline properties of OPC constituents appreciably. However, β-phase (C-S-H gel) is relatively more prominent in samples with 2wt% and 3wt% Fe_2O_3. Addition of Fe_2O_3 in to OPC beyond 3wt% makes β-phase less prominent. This study reveals that up to 3wt% addition of Fe_2O_3, C-S-H gel formation gets accelerated as shown in the figure (bottom row: right). Pure OPC powder XRD spectrum is shown here to differentiate gel formation (β phase) as occurred in the OPC cube sample aged at 28 days. This observation is consistent with the observation of enhanced mechanical strength in OPC-Fe_2O_3 composites as discussed in the previous section.

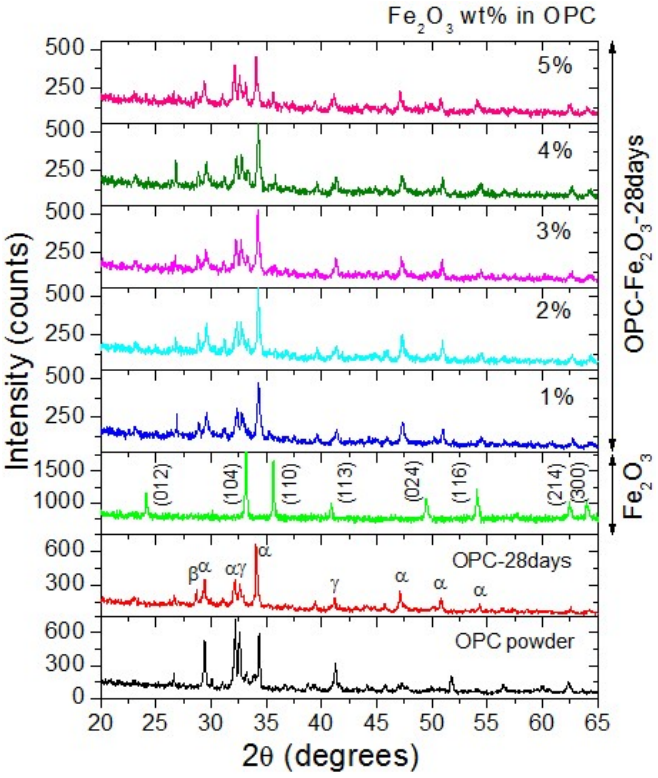

Figure-4.3. X-ray diffraction spectra of cement composites containing Fe_2O_3 nanoparticles in OPC at different doses (added wt% of nanoparticles in OPC). Samples cured at 28 days.

Similar x-ray diffraction study on OPC-TiO_2 samples with various wt% of TiO_2 in OPC is carried out. The spectra are shown in the top right panel of the Figure 4.4. Spectrum of pure TiO_2 powder shows mixed phases of TiO_2. Peaks corresponding to various lattice planes of co-existed anatase and rutile phases are indexed, as shown in the figure. Addition of TiO_2 at various wt% in OPC shows the appearance of β-phase (at 28.97 degrees and 27.85 degrees). It is noted here that the TiO_2 associated (110)r phase is close to the β-phase, hence, cement hydration in the presence of TiO_2 may get affected. With increasing wt% of TiO_2, the β phase strength or cement hydration rate is seen to increase resulting in the enhancement of compressive strength. With highest TiO_2 wt%, however, the overall gel phase strength is seen to be less that may reduce compressive strength as shown in the figure. This is indeed observed as in Figure 1 (top right) indicating the consistency of the results. Relative strength

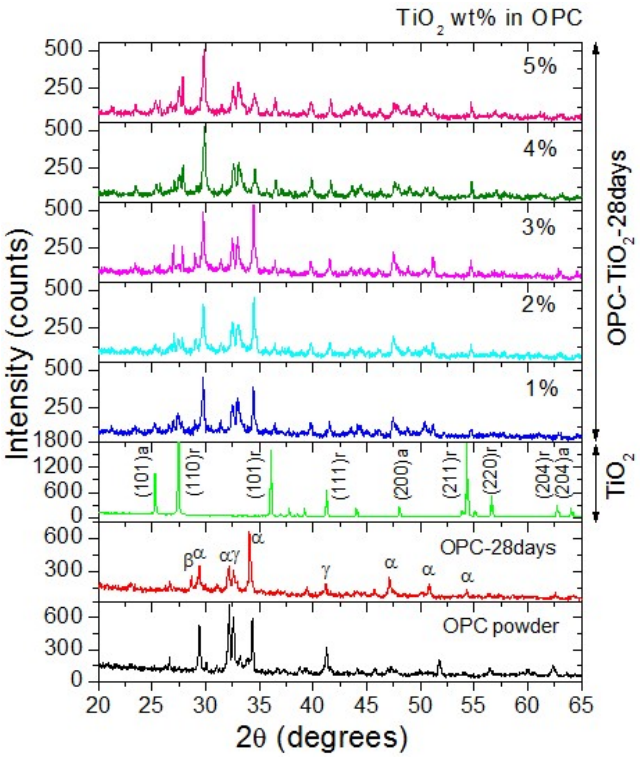

Figure-4.4. X-ray diffraction spectra of cement composites containing TiO_2 nanoparticles in OPC at different doses (added wt% of nanoparticles in OPC). Samples cured at 28 days.

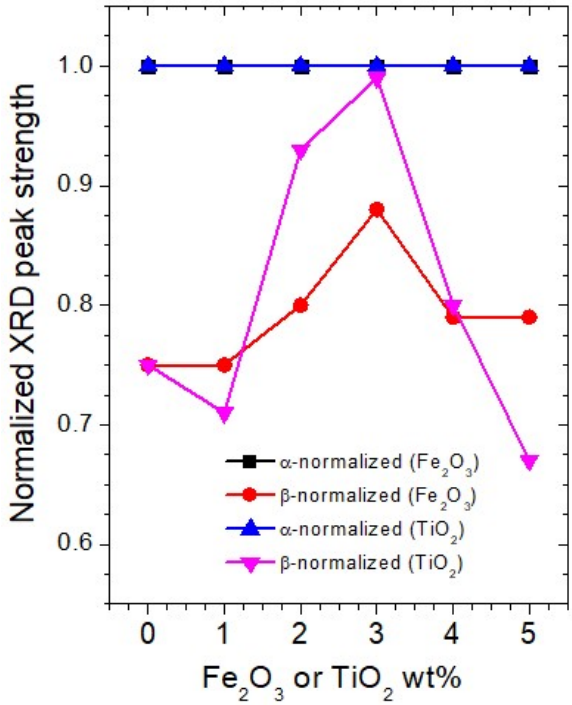

Figure-4.5. A plot of normalized XRD peak strength of α-phase (typically at 29.45 degrees) and β-phase (with respect to α-phase).

of α-phase at 29.45 degrees and β-phase at 28.67, typically considered for Fe_2O_3 and TiO_2 at various wt% in OPC. The α-phase strength is normalized for both Fe_2O_3 and TiO_2. However, β-phase (at 28.67) is normalized with respect to α-phase. It is seen that while strength of β-phase reaches a maximum at certain concentration of additive oxide nanoparticles as shown in the Figure 4.5. This increase can be considered as the indication of cement hydration and gel phase formation. This clearly indicates the favourable mechanism of cement hydration where β-phase plays crucial role. Furthermore, optimum strength of β-phase is indicative of optimum concentration of additives for achieving highest compressive strength as seen previously (Figure 4.1). Hence, increase in compressive strength, β phase strength and Fe_2O_3 wt% are in well correlation.

XRD spectra of OPC-Cu nanocomposites with varying Cu concentration (0.5 to 3 wt%) are shown in the bottom panel of Figure 4.6. Pure Cu metal nanoparticles show crystalline properties with two strong peaks corresponding to (111) and (200) planes of cubic phase of Cu. Addition of Cu metal nanoparticles helps a little to the C-S-H gel formation, confirming β phase weakly observed at higher wt% of Cu, as evident in the 0.5wt% OPC-Cu composite. However, addition of Cu beyond 1wt% shows Cu cubic phase separately, which is

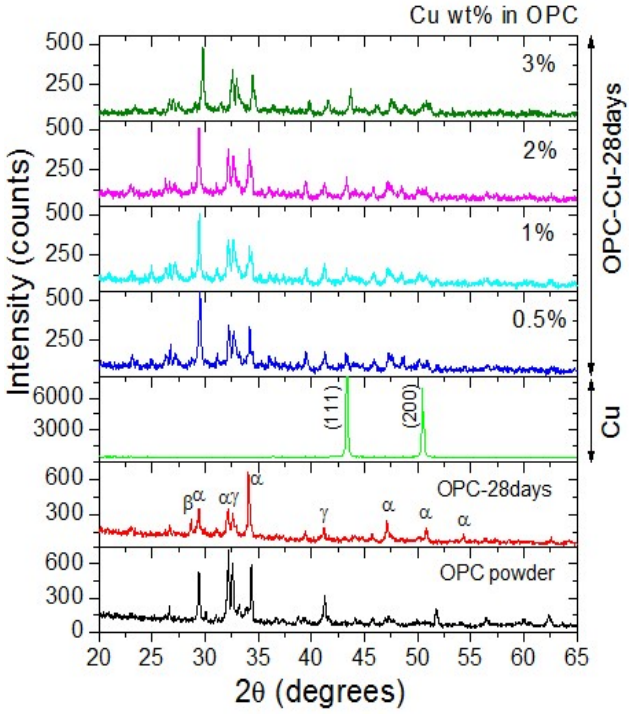

Figure-4.6. X-ray diffraction spectra of cement composites containing Cu nanoparticles in OPC at different doses (added wt% of nanoparticles in OPC). Samples cured at 28 days.

probably the indication of existence of separate Cu nanoparticles domain within the composite. This is not favourable for forming C-S-H cement hydration and may not help in enhancing compressive strength. Thus, x-ray diffraction studies corroborate well with the compressive strength data.

4.2.4 Effect of thermal annealing on mechanical and microstructural properties

4.2.4.1 Mechanical properties

In order to understand thermal effect on CS of cement composite we have exposed the optimized cement composite cubes cured at 28 days to thermal annealing. The reference OPC cube and OPC-Fe_2O_3, OPC-TiO_2, OPC-Cu cube samples (3 cubes of each type) exposed to oven at 100 ºC, 200 ºC, 300 ºC, 400 ºC at one go (no cumulative exposure). Time of thermal annealing is of 30 minutes. Figure-4.7 (top panel) shows the compressive strength of all the samples at different stages of thermal annealing. Figure shows decrease in the CS for all the

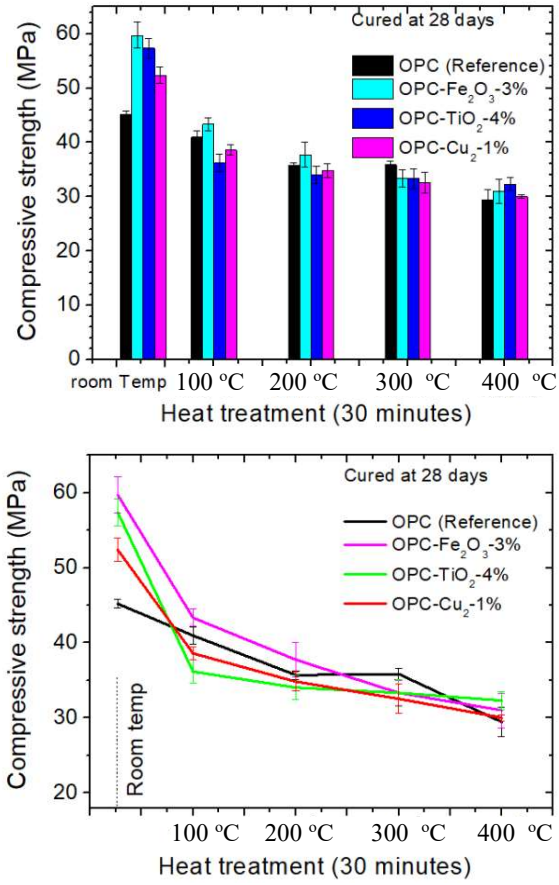

Figure-4.7. Compressive strength of OPC, OPC-Fe_2O_3, OPC-TiO_2 and OPC-Cu cement composites annealed at the temperature range from 100 ºC to 400 ºC at a step of 100 ºC. All the samples cured at 28 days before annealing.

temperatures. However, rate of fall is different for different composites. For the case of OPC-Fe_2O_3 compressibility fall is rapid than pure OPC. This trend similar for OPC-TiO_2 and OPC-Cu composites too. Although fall is rapid but it slows down at higher temperature. Bottom panel figure shows this trend explicitly. It is noteworthy that at 300 ºC and 400 ºC some cracks develop and the cracks are zigzag which are not necessarily through the voids as shown in the Figure 4.8. The images are captured using a digital camera. Similar surface cracks are observed at higher temperatures (300 ºC and 400 ºC) for all other composites (not shown here). Hair-line cracks at 300 ºC become very prominent at 400 ºC. Reduction of mechanical strength is attributed to the formation of cracks.

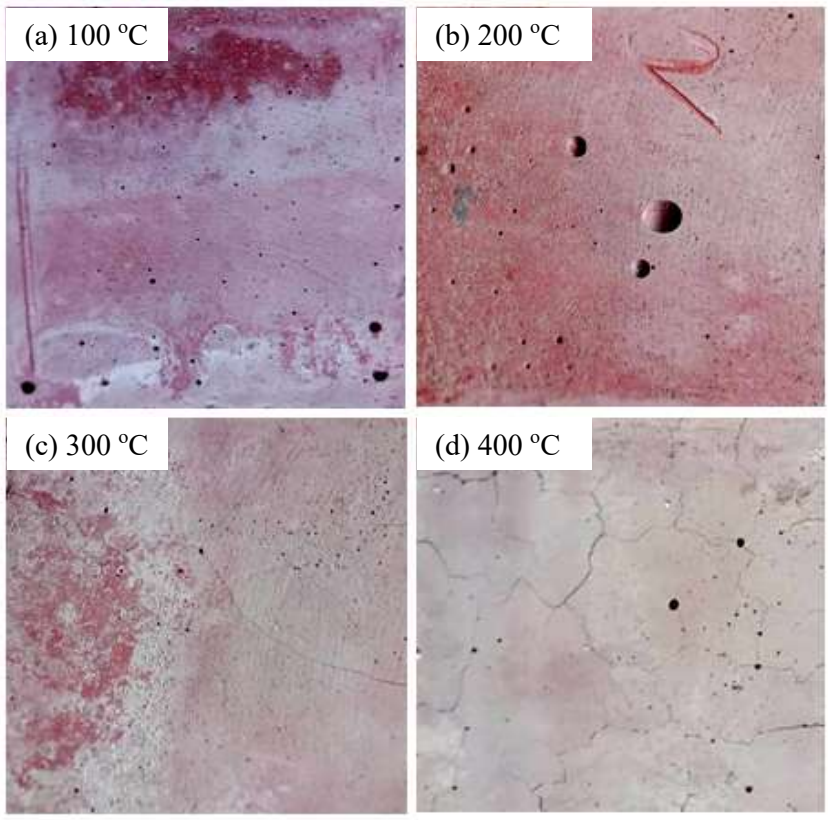

Figure-4.8. Digital photographs (not in scale, area ~ 7×7 cm^2) of OPC-Fe_2O_3 cement composite samples (typical) cured at 28 days and annealed at different temperatures, as mentioned above. Cracks form at 300 ºC (c) and 400 ºC (d) as observed clearly.

4.2.4.2 Microstructural properties: X-ray diffraction

Microstructural properties of annealed cement composites are studied using X-ray diffraction. All the cement composites, OPC-Fe_2O_3, OPC-TiO_2, OPC-Cu, and OPC cured at 28 days are

considered for the study. At each stage of thermal annealing X-ray spectrum on each sample is recorded and plotted as in the Figure-4.9 and Figure-4.10. For OPC-Fe_2O_3 composite sample, spectra show no significant changes for all the annealing temperatures, although; at elevated temperature such as 300 ºC and 400 ºC samples show some improvement in the diffracted peaks (peaks are indicted by symbols, '*' (gypsum) and '#' (Belite (C_2S): 2CaO SiO_2)). Peak at lower 2θ (as marked with #) peak becomes more prominent, especially for OPC-Fe_2O_3 and OPC-TiO_2. Improvement in the other characteristic peaks is also visible for the other composites and OPC. From the study it is clear that thermal annealing even at reasonably higher temperature does not change structural properties significantly. Crystalline quality may have improved with temperature due to reorganization of the crystallites within the composite and OPC samples. It is noteworthy that C-S-H peak that appeared due to cement hydration still exists at high temperature, which is suggestive of slower rate of reduction of compressibility at higher temperature, and is consistent with the observations as in the Figure-4.7.

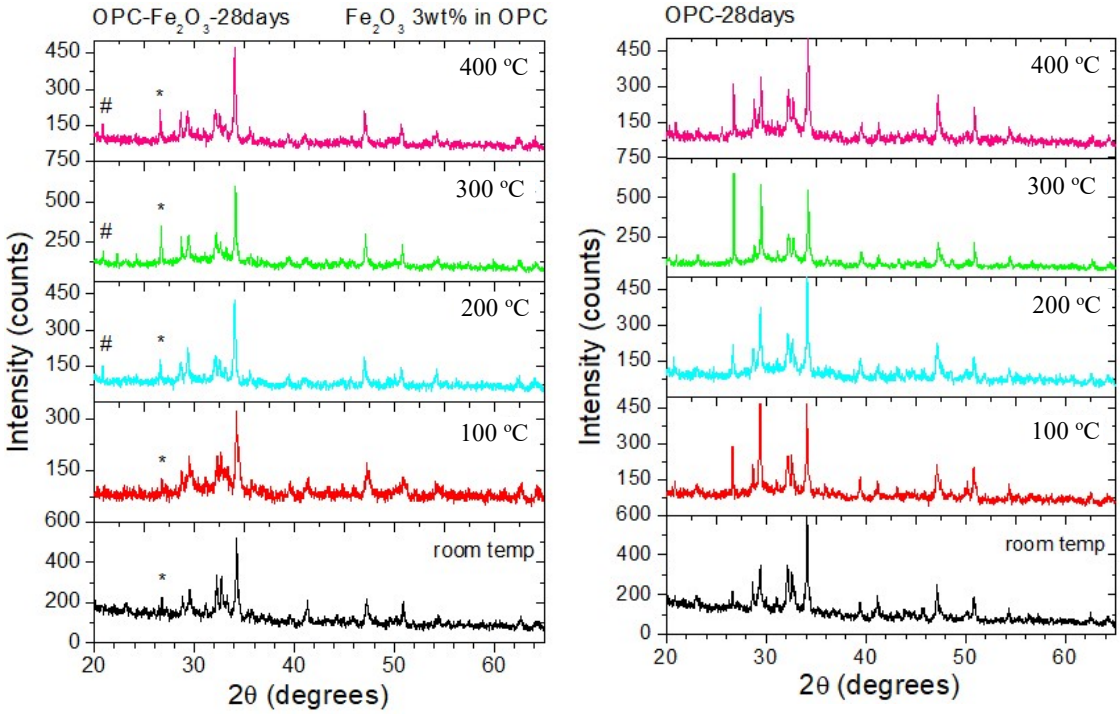

Figure-4.9. X-ray diffraction spectra of heat treated OPC-Fe_2O_3 composite and pure OPC. Anneal temperatures are as indicated in the figure.

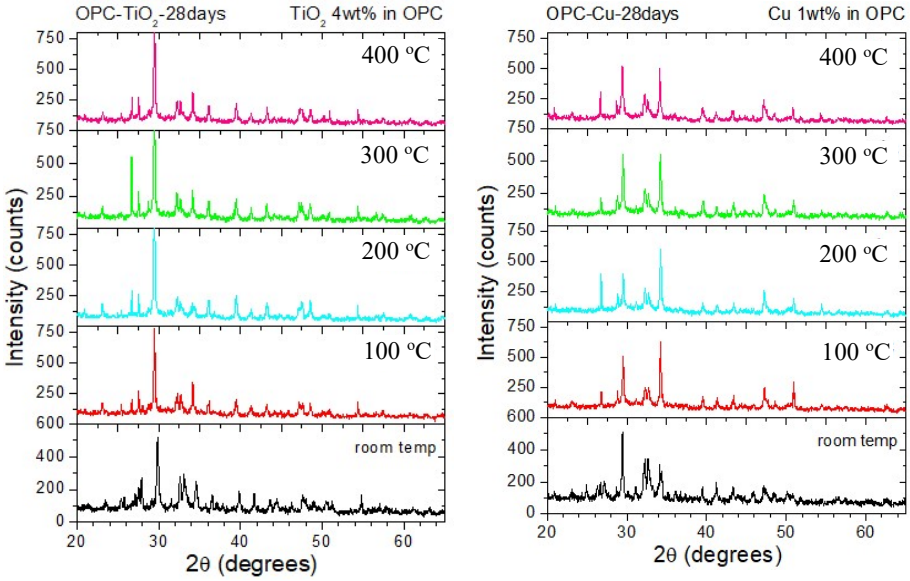

Figure-4.10. X-ray diffraction spectra of heat treated OPC-TiO_2 (left panel) and OPC-Cu (right panel) composite (1wt% Cu in OPC, cured at 28 days). Anneal temperatures are as indicated in the figure.

CHAPTER-5

Effect of GO/RGO additives on the cement hydration, mechanical, microstructural properties of OPC-Fe_2O_3 cement paste

Introduction

This chapter deals with the preparation of cement composites by adding GO (graphene oxide), RGO (reduced graphene oxide) and Fe_2O_3 (iron oxide) showing improved mechanical, and microstructural properties compared to that of OPC paste. Suitable amount of (wt%) GO and RGO are added to OPC-Fe_2O_3 (optimized Fe_2O_3 in OPC). Improved compressive strength (CS) is caused by the faster cement hydration and β-phase (C-S-H gel-phase) formation which is confirmed by detailed studies using XRD and FTIR spectroscopies at each stage of curing. These spectroscopic investigations also confirm the superior characteristics from GO admixed OPC-Fe_2O_3 compared to that from RGO admixed OPC-Fe_2O_3.This could be due to the presence of higher amount of OH, COOH in GO than in RGO.

5.1. Sample preparation and experimental measurements

Graphene oxide and reduced graphene oxides are mixed with OPC-Fe_2O_3 to prepare OPC-Fe_2O_3-GO and OPC-Fe_2O_3-RGO cement composites. OPC-Fe_2O_3 composite is prepared by mixing 3wt% Fe_2O_3 with OPC [82]. GO or RGO is added to OPC-Fe_2O_3 by 0.1wt% separately to make OPC-Fe_2O_3-GO and OPC-Fe_2O_3-RGO final composites. In this preparation, OPC (grade 43), GO and RGO are used as received with no further purification or chemical modification. Each sample cube has volume of 352 cm^3 (70.6 × 70.6 × 70.6 mm^3). Appropriate amount of water (32%, as revealed from water consistency test) is added to make final composite cement pastes. Cubes are allowed overnight (24 hours) for natural setting before placing them in water for curing at different days (3 to 28 days at a step of 7 days).

Compression Testing Machine (CTM) is used for compressive strength measurement with limiting capacity of 2000kN. The compression loading rate is set to 0.6kN/sec. CS is defined as the maximum bearable load divided by A (cross-sectional area) of sample cube. X-ray diffraction is carried out with Cu Ka_α radiation (wavelength, λ = 1.5406 Å) in the 2θrange

of 20-80^{o} for all the samples. FTIR spectroscopy studies of OPC-Fe_2O_3-GO and OPC-Fe_2O_3-RGO. FTIR spectroscopy has been used to obtain qualitative and quantitative information about the chemical bonding of molecules. In the present study, Perkin Elmer Spectrum One instrument is used from 450 to 4400 cm^{-1} at 4 cm^{-1} resolution. FTIR spectra are recorded in the transmission mode. Usually, >10 scans are employed for the better signal to noise ratio. KBr (potassium bromide) is added with the sample powder (small part of cube of each sample specimen is finely ground) for enhancing transparency, and sample palette (10 mm diameter) of each sample is made. Thickness of palette is made very thin to retain transparency.

5.2. Results & Discussions

As mentioned OPC based cement nanocomposites containing graphene or its derivatives (GO/RGO) exhibit attractive mechanical, thermal/electrical/piezoelectric, photocatalytic and antimicrobial activities. Effective dispersion plays key role in enhancing these characteristics. Effective dispersion can be increased by incorporating nanosized metal oxide nanoparticles or nanomaterials containing COOH, OH, C-O-C oxygen groups. Graphene oxide and reduced graphene oxide seem to be effective in this regard. GO/RGO content in cement composites is expected to show higher mechanical strength with improved microstructural properties due to the formation of β-phase (C-S-H gel phase) playing vital role in filling the pores and bridging the gaps existing among larger cement particles. To understand underlying mechanical, structural and chemical changes leading to improved properties we have investigated in details compressive strength, X-ray diffraction and FTIR spectroscopy of OPC-Fe_2O_3-GO and OPC-Fe_2O_3-RGO nanocomposite cement pastes. The detailed results are presented systematically below.

5.2.1 Compressive strength of cement composites: OPC-Fe_2O_3-GO and OPC-Fe_2O_3-RGO

Compressive strength of the OPC-Fe_2O_3 paste containing 0.1wt% GO and RGO at different aging time is shown in the Figure-5.1 and Figure-5.2. In the Figure-5.1, compressive strength of reference OPC, OPC-Fe_2O_3 (3wt%) and OPC-GO (0.1wt%) are also plotted for explicit understanding of the changes in the compressive strength. With curing time (days) increase in compressive strength is seen for pure OPC paste. A saturation trend attaining highest CS of ~ 45 MPa at 28 days is seen. When Fe_2O_3 nanoparticles (3wt%) is added to OPC, the compressibility of OPC-Fe_2O_3 sample increases with curing time with no trend of saturation. For all the curing time, compressive strength of OPC-Fe_2O_3 is seen to be higher than that of pure OPC. Compressive strength of OPC-Fe_2O_3 attains its highest value to ~ 60 MPa at 28

days of curing. This is about 35% more than the OPC reference value [82]. Similarly, we have studied OPC-GO cement composite which shows reduction in CS at all the curing time as compared to the OPC reference, except at 28 days, when CS is seen to be a little higher (~48 MPa). It is noteworthy here that optimum content of GO is obtained separately (different wt% of GO is added to OPC and compressive strength is measured to achieve highest strength at 28 days) before adding it to OPC-Fe_2O_3 composite (data not shown here). With the optimum content of Fe_2O_3 (3wt%) and GO (0.1wt%) we have prepared OPC-Fe_2O_3-GO cement composite and its compressibility is shown in the Figure-5.1. Interestingly, compressive strength shows higher strength for all the curing time. Unlike OPC-Fe_2O_3 and OPC-GO, this composite, however, shows slight saturation trend. Saturation and non-saturation trend is

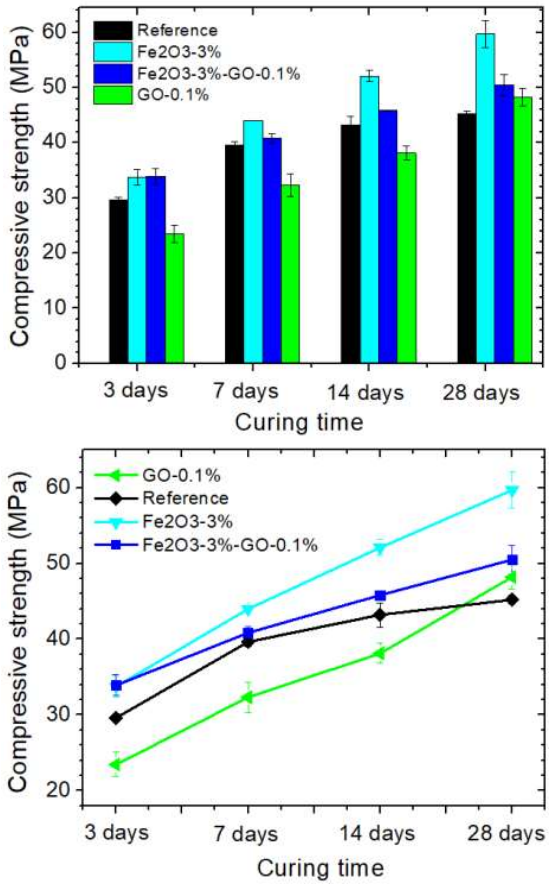

Figure-5.1. Compressive strength of OPC-Fe_2O_3-GO cement nanocomposite paste at standard curing time of 3 to 28 days at a step of 7 days. Top panel: bar graph and lower panel: scattered point plot. Colours identification is as in legend.

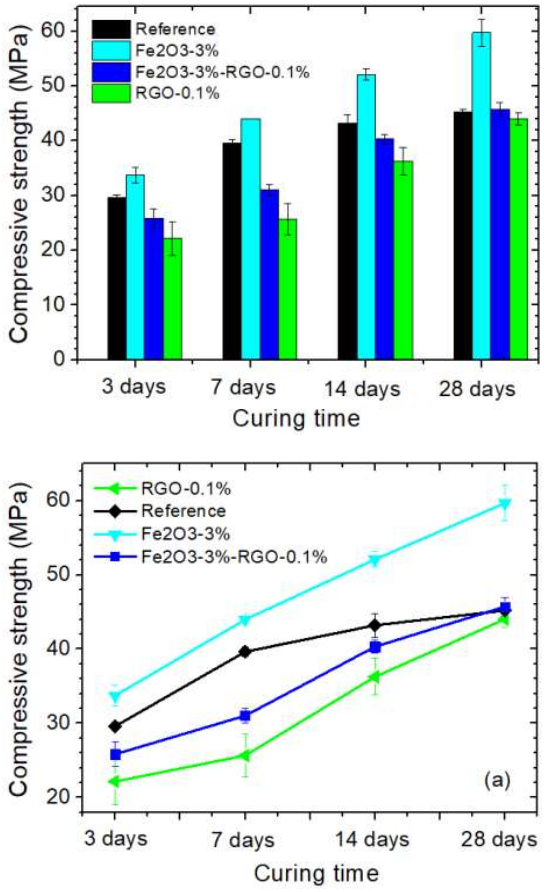

Figure-5.2. Compressive strength of OPC-Fe_2O_3-RGO cement nanocomposite paste at standard curing time of 3 to 28 days at a step of 7 days. Left panel: bar graph and right panel: scattered point plot. Colours identification is as in legend. Bar graph: top panel and scattered plot (lower panel).

explicitly seen from the right panel of the figure. The presence of functional GO and Fe_2O_3 accelerates β-phase (C-S-H gel phase) formation that makes stronger bonding between the neighbouring particles. Formation of β-phase (C-S-H gel phase) and effective filling of pores lead to the considerable improvement in the compressive strength [15, 120-122]. Higher compressive strength in the OPC-Fe_2O_3-GO is considered to be effective for smart application due to existence of functional components, GO and Fe_2O_3. Similar compressive strength measurements are carried out on the OPC-Fe_2O_3-RGO cement composite paste as shown in the Figure-5.2. It shows reduced CS for all the curation time except at 28 days where it is comparable to that of OPC reference. It is noteworthy that compressive strength of OPC-Fe_2O_3-GO is always higher than that of OPC-Fe_2O_3-RGO.

5.2.2 X-ray diffraction of OPC-Fe_2O_3-GO and OPC-Fe_2O_3-RGO cement composites

Microstructures of OPC constituents, Fe_2O_3, GO, RGO nanoparticles, OPC cube, OPC-Fe_2O_3-GO and OPC-Fe_2O_3-RGO cement composites are studied using XRD. Figure-5.3 (top panel) shows XRD spectra of all the samples (as purchased as well as 28 days cured samples). XRD spectra of OPC (as purchased) and OPC cube (28 days cured) show multiple peaks denoted by α (at 29.46°, 32.1°, 34.07°, 47.13°, 50.82°, 54.38°), β (at 28.67°), γ (at 32.62°). These peaks correspond to CaO-H_2O (α-phase), C-S-H (CaO-SiO_2-H_2O, β-phase) and C_3S (3CaO-SiO_2, γ-phase) of constituents of OPC cube cured at 28 days [82, 117, 118]. XRD spectrum of as purchased OPC powder shows similar peaks except β-phase. XRD spectrum of Fe_2O_3 show peaks at 2θ of 24.15, 33.15, 35.65, 40.85, 49.45, 54.02, 62.42, and 64.02 degrees. These correspond to hexagonal α-Fe_2O_3 (hematite) with planes indexed as (012), (104), (110), (113), (024) (116), (214) and (300), respectively [82, 117, 118]. It is interesting to note that when 3wt% Fe_2O_3 is added to OPC, no peaks corresponding to pure Fe_2O_3 are observed. This observation indicates that Fe_2O_3 does not change international microstructure of OPC constituents. Furthermore, no separate peaks corresponding to pure Fe_2O_3 are observed which indicates no separate phase existing within the OPC paste or minor quantity of Fe_2O_3 is mixed homogeneously without affecting microstructures of OPC. XRD spectrum of GO shows (001) phase at 2θ value of 42.3°, although OPC-GO composite (0.1wt% GO in OPC) does not show this signature. XRD spectrum of OPC-Fe_2O_3-GO composite shows the presence of peaks as observed from hydrated OPC cube. It is also observed that peaks at 26.68° and 29.29° related to CaO-H_2O (α-phase) become more prominent. Phase at 23.15° (δ) is attributed to $CaCO_3$ of OPC constituent. C-S-H gel phase (β phase) still present but with reduced strength relative to that observed in OPC-Fe_2O_3 composite, signifying that binding would be less effective in OPC-Fe_2O_3-GO composite than OPC-Fe_2O_3 composite. This is, in fact, observed that the CS of OPC-Fe_2O_3-GO is less than CS for OPC-Fe_2O_3 composite attributed to the effect of GO within the OPC-Fe_2O_3. In order to understand microstructural change at each stage (3, 7, 14, and 28 days of curing) of cement hydration, we have captured XRD spectrum at each stage and plotted in the bottom panel of the figure. The spectra show improvement in the β phase (intensity) with curing. Thus, XRD results are in well corroboration with the compressive strength data.

In similar manner we have systematically studied OPC-Fe_2O_3-RGO cement composite at various curing time, and corresponding XRD spectra are shown in the Figure-5.4 (top and bottom panels). The study reveals that the results (top panel XRD spectra) are not different

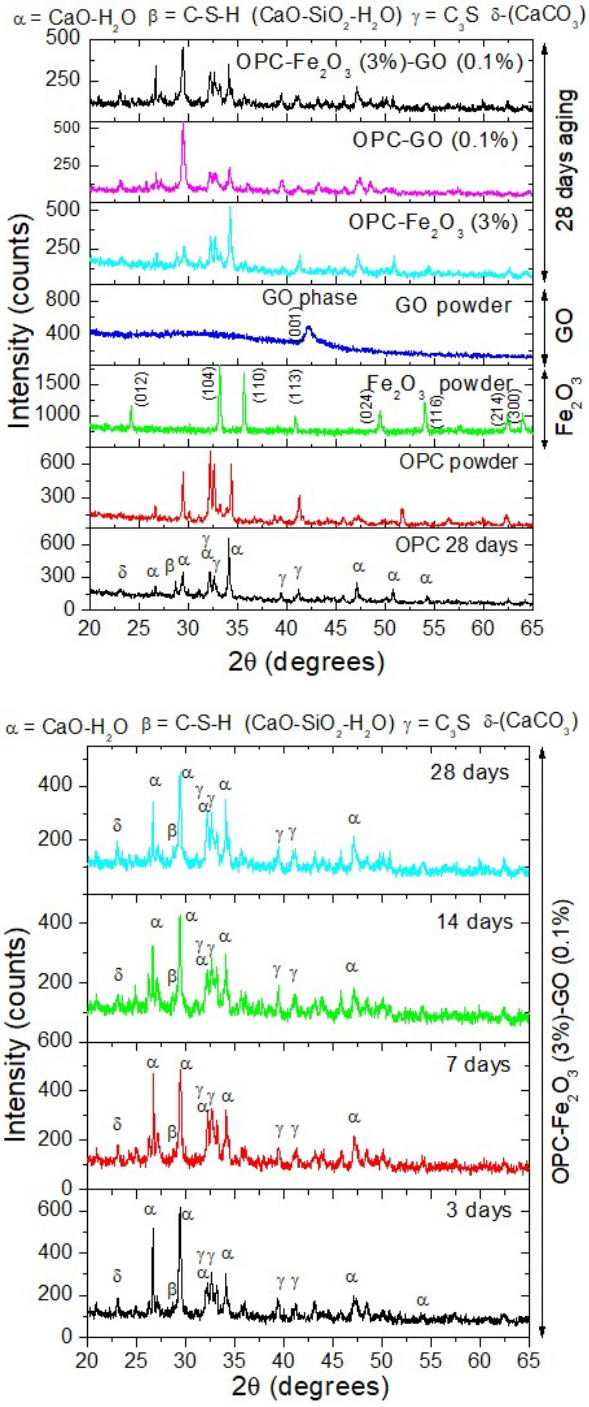

Figure-5.3. XRD spectra of cement composites containing Fe_2O_3 (3wt%) and GO (0.1wt%) at different stages of cement hydration. Top panel: for comparison, XRD spectrum of OPC (OPC cube cured at 28 days), OPC powder (as purchased), GO powder (as purchased), Fe_2O_3 powder (as purchased), OPC-Fe_2O_3cube cured at 28days and OPC-GO (0.1wt%) cured at 28 days. Bottom panel: OPC-Fe_2O_3-GO composite after curing at different days, as above.

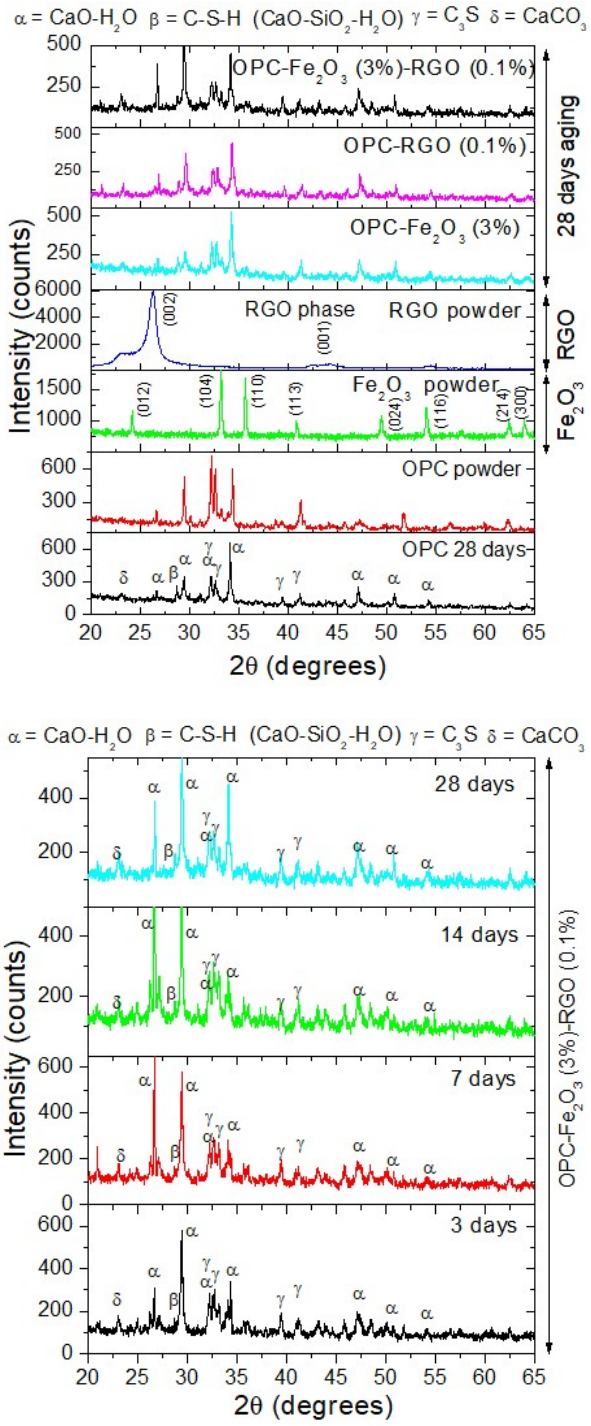

Figure-5.4. XRD spectra of cement composites containing Fe_2O_3 (3wt%) and RGO (0.1wt%) at different stages of cement hydration. Top panel: for comparison, XRD spectrum of OPC (28 days cured OPC), OPC powder (as purchased), RGO powder (as purchased), Fe_2O_3 powder (as purchased), OPC-Fe_2O_3 cube cured at 28days and OPC-RGO (0.1wt%) cured at 28 days. Bottom panel: OPC-Fe_2O_3-RGO cement composite after curing at 3, 7, 14, and 28 days.

significantly from that of OPC-Fe_2O_3-RGO cement composite. However, due to the existence of (002) plane of RGO at 26.24^o the hydrated OPC cement phase (α-phase) at 26.68^o and 29.29^o gets enhanced. This enhancement is stronger than that appeared in the case of OPC-Fe_2O_3-GO cement composite. In all these cases (OPC-Fe_2O_3-GO and OPC-Fe_2O_3-RGO cement composites) β phase is weakly seen. Curing time dependent studies (bottom panel) also show weak improvement in the β phase.

5.2.3 FTIR studies of OPC-Fe_2O_3-GO and OPC-Fe_2O_3-RGO cement composites

Vibrational bonding information of OPC-Fe_2O_3-GO and OPC-Fe_2O_3-RGO cement composites is obtained by studying FTIR. In order to observe detailed changes during cement hydration of composite we have investigated systematically step by step. All the spectra are compared with OPC (28 days cured) reference spectrum. Furthermore, FTIR spectrum of individual added component (Fe_2O_3, GO, RGO) is also recorded and compared. FTIR spectra of the cement composite (OPC-Fe_2O_3-GO) and reference OPC are shown in the Figure-5.5 (top and bottom panel). In top panel, FTIR spectrum of OPC cube cured at 28 days (reference spectrum) shows vibrational modes, M0 (3641 cm^{-1}), M1 (3433 cm^{-1}), M2 (2923 cm^{-1}), M3 (2850 cm^{-1}), M4 (1633 cm^{-1}), M5 (1477 cm^{-1}), M6 (1414 cm^{-1}), M7 (1092 cm^{-1}), M8 (998 cm^{-1}), M9 (863 cm^{-1}), M10 (718 cm^{-1}) and M11 (522 cm^{-1}) corresponding to cement constituents as assigned in Table-5.1 [11, 123-127]. When we compared these modes with that of as procured OPC we observe that all these modes are present in the OPC. This signifies that the modes are due to the constituents of OPC. However, it is noticed that strong M11 mode is reduced to the insignificant level when OPC is hydrated (i.e. OPC cube cured at 28 days). Furthermore, the insignificant and submerge M9 mode (as in OPC procured) is now very prominent and distinct. The appearance of M9 mode is attributed to β-phase (C-S-H gel phase) formation. The 28 days cured OPC-Fe_2O_3 composite also shows strong M9 mode along with all the other characteristic modes. A systematic monitoring is carried out on the OPC-Fe_2O_3-GO composite at different curing time. All the spectra are shown in the bottom panel of the figure. At early curing of 3 days, M9 mode is very prominent, and remains intact significantly till 28 days of curing. The addition of GO during the composite preparation has influential effect on the vibrational signature of OPC-Fe_2O_3-GO composite. As procured GO shows no vibrational signature related to M8, M9, M10, and M11. Addition of GO reduces the strength of M8, and is only weakly observed as a hump. However, presence of GO is seen to increase M9 strength even more in the OPC-Fe_2O_3-GO than OPC cube and OPC-Fe_2O_3 cube

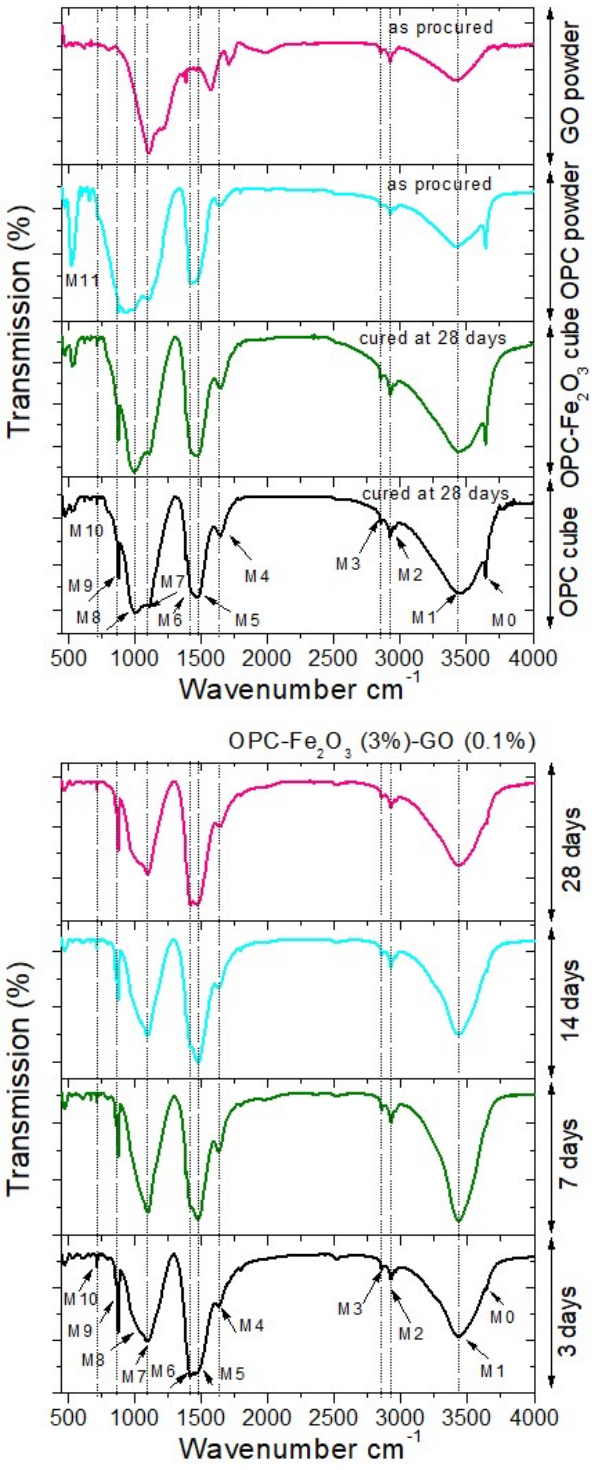

Figure-5.5. FTIR spectra of cement composites containing Fe_2O_3 (3wt%) and GO (0.1wt%) at different stages of cement hydration. Top panel: for comparison, FTIR spectra of pure OPC (28 days cured OPC cube), OPC-Fe_2O_3 cube (28days cured), OPC powder (as purchased), GO powder (as purchased) are plotted. Bottom panel: OPC-Fe_2O_3-GO cement composite after curing at 3, 7, 14, and 28 days.

(hydrated at 28 days). This is expected because the oxygen containing groups that are present may help in achieving better cement hydration. The acceleration in early cement hydration and C-S-H gel formation help in achieving better strength of OPC-Fe_2O_3-GO paste. This is, in fact, observed as in Figure-5.1 earlier, where increase in compressive strength is seen to be faster and higher at early curing time.

To understand the effect of less available oxygen containing functional groups, we have prepared OPC-Fe_2O_3-RGO composite paste where RGO expectedly contains less oxygen containing groups. FTIR spectra of OPC cube (cured at 28 days), OPC powder (as procured), OPC-Fe_2O_3 cube (cured at 28 days) are already discussed and re-plotted here for comparison purpose only (top panel of Figure-5.6). The spectrum of RGO as procured is also shown for explicit understanding of change in chemical bonding. It is noteworthy that, in RGO, C=O absorption band at 1228 cm^{-1} (C–O–C vibrations), and at 1098 cm^{-1} (C–O vibrations (alkoxy group)) are less prominent than that observed in GO. Furthermore, in RGO, the COOH vibrational band at ~ 1704 cm^{-1} is absent too. Effect of this has direct influence on the cement hydration of OPC-Fe_2O_3-RGO cement paste. The β-phase (C-S-H gel phase) is poorly seen at early curing time (3 and 7 days) (bottom panel of Figure-5.5). For longer duration, C-S-H gel phase strength becomes stronger. These observations are consistent with the earlier observations on the compressive strength measurements which are seen to be stronger only at longer hydration time.

Table-5.1: Various vibrational modes of cement constituents in OPC-Fe_2O_3-GO and OPC-Fe_2O_3-RGO cement composites

Modes	Transmission dip position (cm^{-1})	Band assignment	Source of vibration
M0	3641	O-H stretching	Portlandite ($Ca(OH)_2$)
M1	~ 3433 (broad band)	O-H stretching (symmetric & antisymmetric)	Water molecule
M2	2923	C-H	Not identified
M3	2850	C-H	Not identified
M4	1633	O-H vibration (deformation)	Water molecule
M5	1477	C-O vibration	$CaCO_3$
M6	1414	C-O vibration	$CaCO_3$
M7	1092	SO_4^{2-} ion	Calcium sulphate (OPC constituent)
M8	998	C-O vibration	$CaCO_3$
M9	863	C-S-H gel	$CaO.SiO_2.H_2O$
M10	718	C-O vibration	$CaCO_3$
M11	522	Si-O out of plane vibration	C_3S

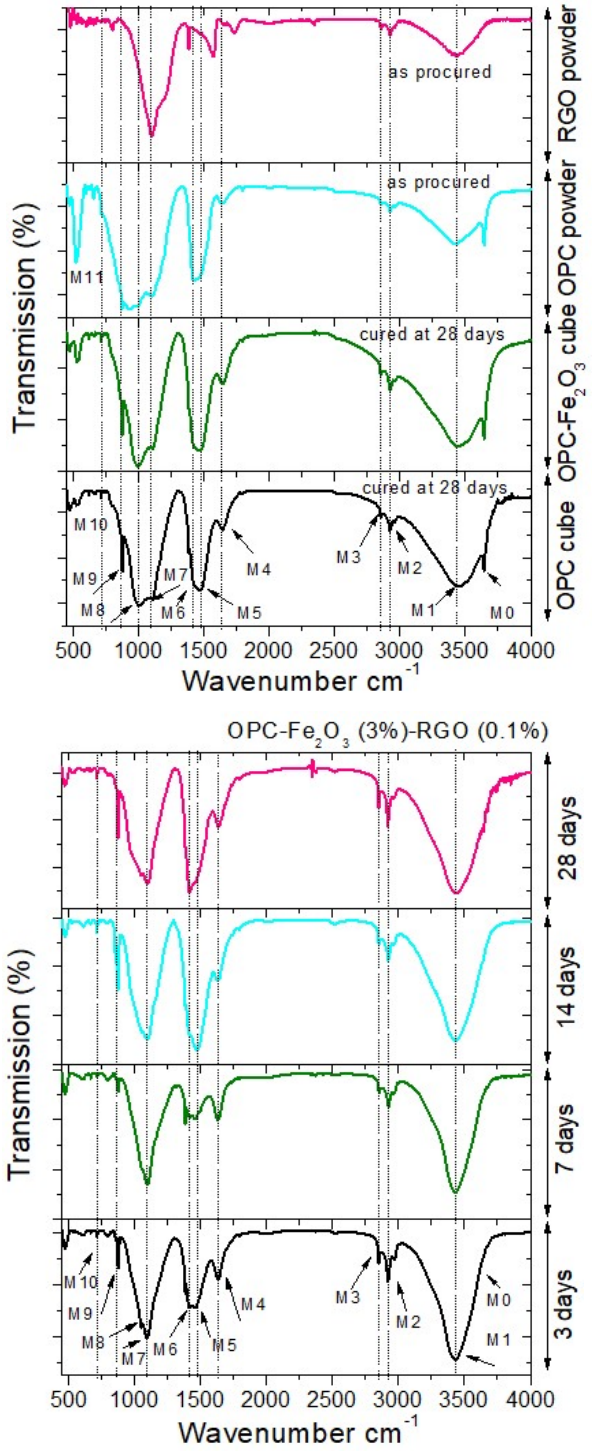

Figure-5.6. FTIR spectra of cement composites containing Fe_2O_3 (3wt%) and RGO (0.1wt%) at different stages of cement hydration. Top panel: for comparison, FTIR spectrum of pure OPC (28 days cured OPC cube), OPC-Fe_2O_3 cube cured at 28days, OPC powder (as purchased), RGO powder (as purchased). Bottom panel: OPC-Fe_2O_3-RGO cement composite after curing at 3, 7, 14 and 28 days.

5.2.4 Scanning electron microscopic (SEM) study and elemental analysis using EDAX

Presence of oxygen containing group is studied using scanning electron microscope (SEM) and energy dispersive X-ray analysis (EDAX). SEM micrographs are useful in surface, interface, microstructural imperfection studies, whereas, EDAX shows possible distribution of additives and their strength. In fact, uniform dispersion plays crucial role in improving mechanical strength. Due to the superior characteristics of OPC-Fe_2O_3-GO samples we have

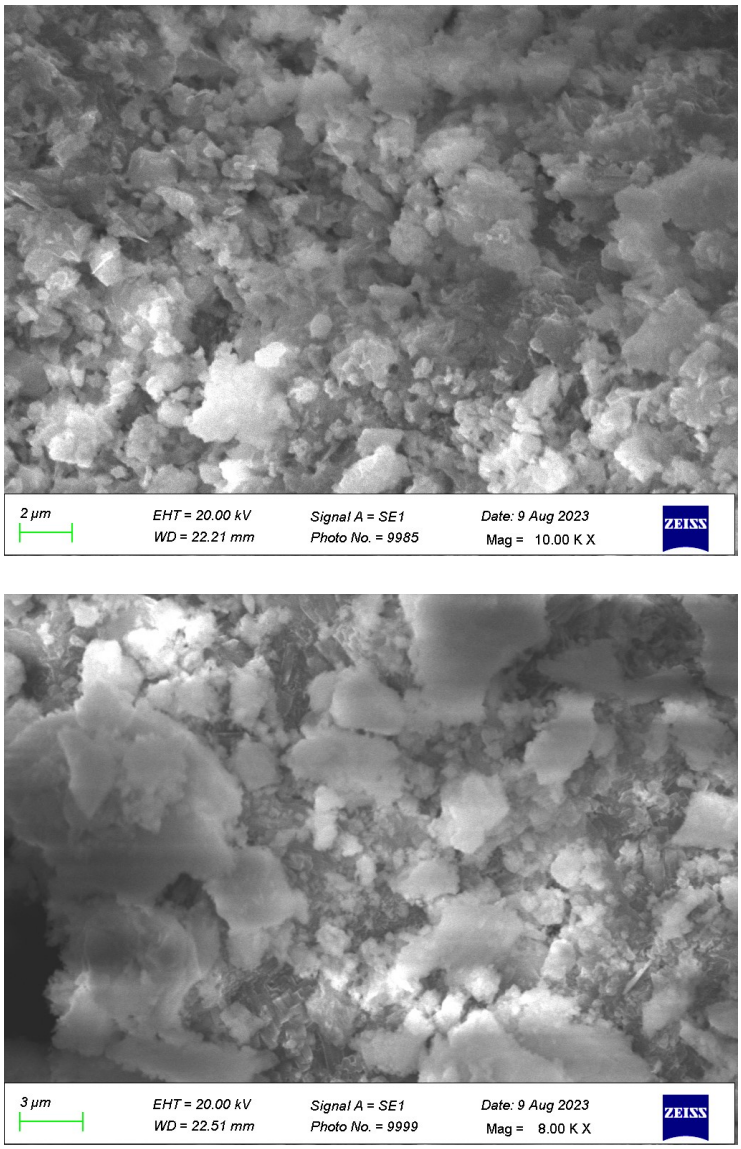

Figure-5.7. SEM micrographs for OPC-Fe_2O_3-GO cement nanocomposite (top panel) and OPC reference (lower panel) samples.

conducted SEM and EDAX studies on this sample and the results are compared with that of pure OPC reference sample. Scanning electron micrographs are shown below in the Figure-5.7. SEM micrograph of OPC-Fe_2O_3-GO shows better distribution (less voids or pores) compared to pure OPC. EDAX elemental scans, especially for iron (Fe) and oxygen (O) and carbon (C) are shown in the Figure-5.8. Estimated concentration (at wt%) is summarized in Table-5.2. The elemental analysis shows carbon content is higher in OPC-Fe_2O_3-GO compared to OPC which is expected. Similarly, Fe content is higher than that observed in OPC. Thus, SEM and EDAX analysis are corroborated well with the observations from XRD and FTIR studies confirming uniform dispersion and higher C-S-H gel in OPC-Fe_2O_3-GO that result in improved compressive strength.

Table-5.2: Elemental analysis (EDAX) of cement constituents in OPC-Fe_2O_3-GO cement nanocomposite (left) and OPC reference sample (right)

Element	Weight %	Atomic %
C K	1.9	3.6
O K	45.1	64.9
Ca K	37.8	21.7
Fe K	3.7	1.5

Element	Weight %	Atomic %
C K	0.6	1.2
O K	44.5	65.1
Ca K	38.7	22.6
Fe K	1.8	0.7

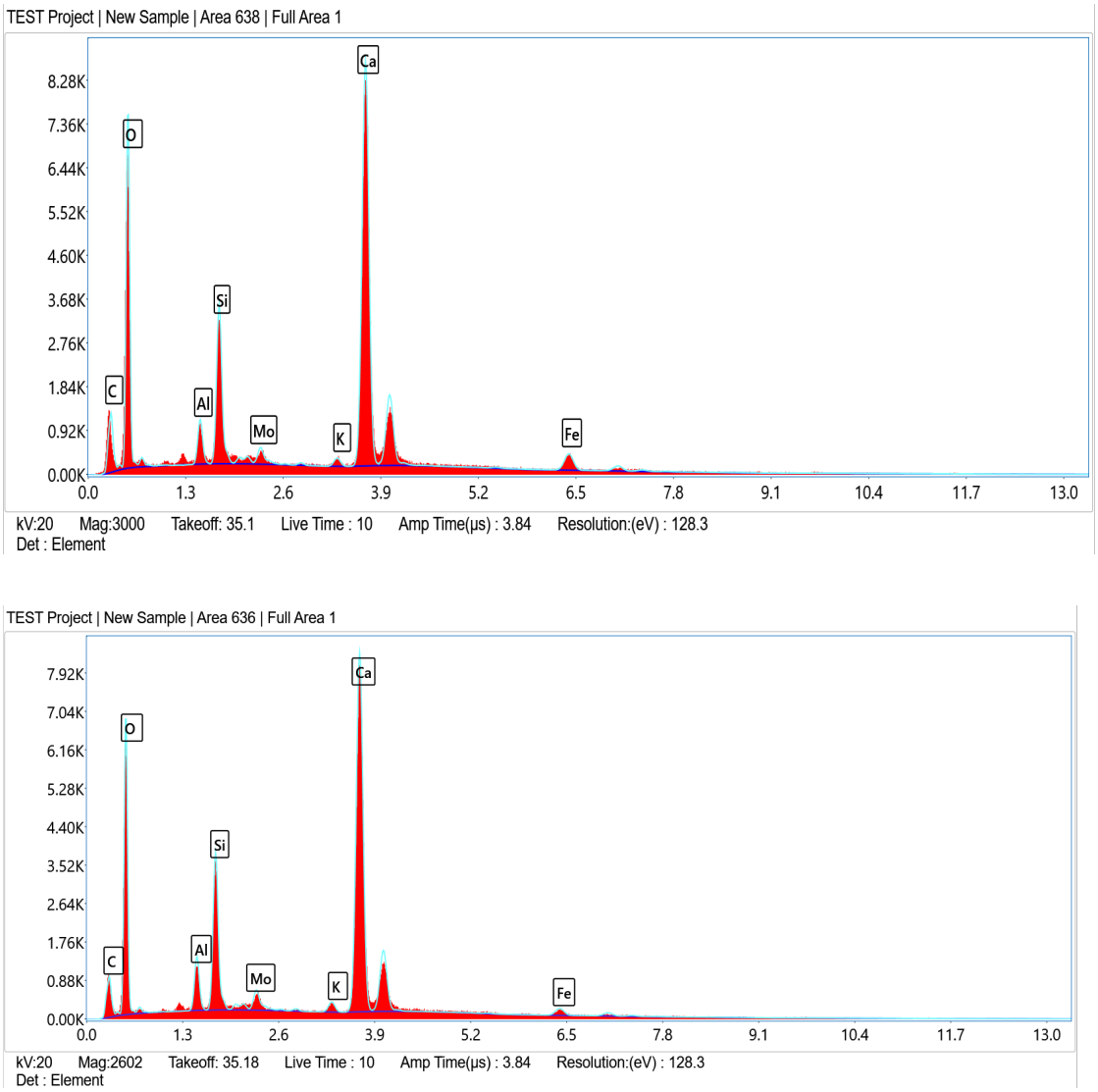

Figure-5.8. EDAX elemental analysis with energy dispersive spectra for OPC-Fe_2O_3-GO (top row) and OPC (lower row).

CHAPTER-6

Development of total composite cement pastes containing Fe_2O_3, GO and PVA, and study of their mechanical, microstructural properties

Introduction

Cement composites containing polyvinyl alcohol (PVA), polymer (PMMA) are attractive as they show improved mechanical strength, and simultaneously capable of preventing from chemical attack, decrease in capillary water absorption [21, 62]. In the previous chapters we have seen the effect of GO and RGO on the mechanical, structural and antimicrobial properties of Fe_2O_3 admixed OPC cement. Further addition of polymer/epoxy may result in additional benefit of environmental stability such as chemical attack. In the present chapter work total composite cement paste containing Fe_2O_3, GO and PVA is prepared, and mechanical and structural properties are investigated. The content of Fe_2O_3, GO in OPC is optimized individually in the previous chapters. At first optimization of PVA content in OPC is carried out. Subsequently total composite with optimized content of Fe_2O_3, GO and PVA is prepared by studying compressive strength measurements. Microstructural changes are studied using XRD spectroscopy.

6.1 Preparation of OPC-PVA composite paste and experimental measurements

OPC-PVA composites are prepared by adding PVA with different wt% (0.05wt% to 1wt%) to OPC. In the Table-6.1 samples compositions are shown. Standard curing procedure is followed for aging as mentioned in the previous chapters (after casting, 24 hours are allowed for natural setting before putting them in to water for curing). Compressive strength measurements and XRD studies are carried out at each stage of curation.

Table-6.1: Compositions of OPC-PVA cement composites.

OPC-Composite Type	OPC: PVA(g:g)
0.05 wt%	600: 0.3
0.1wt%	600: 0.6
0.5wt%	600: 03
1wt%	600: 06

6.2 Results and discussions

6.2.1 Compressive strength of OPC paste containing PVA

The compressive strength (along with error bar) of the OPC composites containing PVA with different weight percentage (wt%) are shown in the Figure-6.1. Cement composite containing 1wt% and 0.5wt% PVA shows decrease in compressive strength with respect to the compressive strength of OPC reference (bar graph (a)). This trend is observed for all the

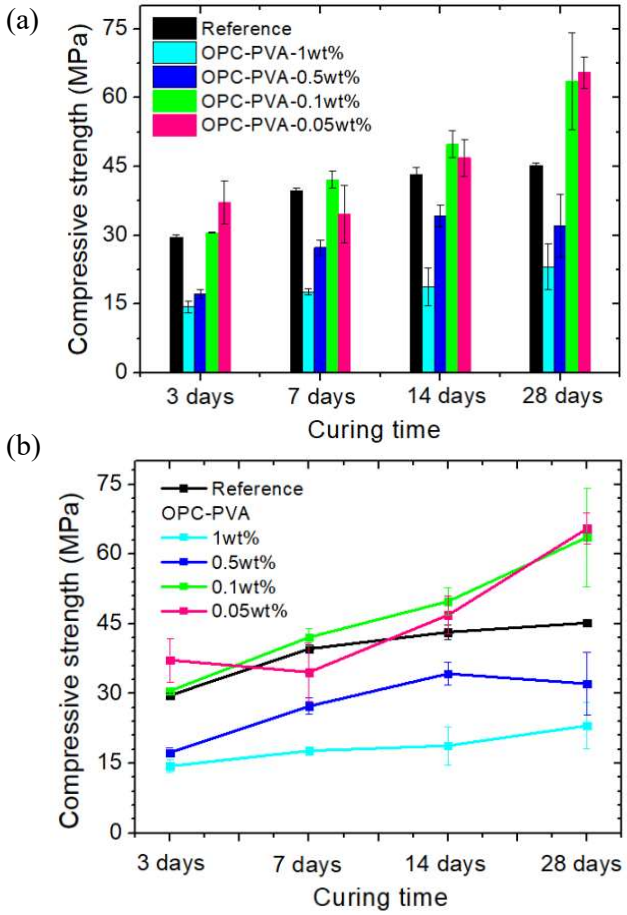

Figure-6.1. Bar graph of CS (compressive strength) (along with error bar) of cement composites containing PVA at different wt% and curing time (a). Standard curing time of 3 to 28 days at a step of 7 days, as mentioned above. The line plot (b) is presented explicitly just to show any saturation trend is present or not.

curation time. The compressive strength, however, remains at higher side for 0.5wt% OPC-PVA composite than 1wt% composite. Furthermore, when PVA wt% is decreased to 0.1wt%, the compressive strength is significant increased for all the curation time [21, 62]. This is true

for 0.05wt% PVA containing OPC too. At highest curing time, the compressive strength is considerably large compared to that of OPC reference. This could be due to the improved pore structure or pore refinement within OPC. No saturation trend is seen in the compressive strength (as seen from the Figure-b). For higher compressive strength, 0.1wt% or less PVA can be added to OPC.

6.2.2 Microstructural study of OPC paste containing PVA

Microstructural properties of OPC-PVA composite have been studied using XRD. From the compressibility study, as we have seen the highest compressive strength occurs for the cement composite with 0.1wt% PVA, we have chosen only this wt% in the composite for all the remaining studies (XRD, antimicrobial, chemical treatment). X-ray diffraction spectrum at each curing stage (3 to 28 days at a step of 7 days) is shown in the Figure-6.2. Typical measurement range is considered to be from 20 degrees to 65 degrees (2θ values). At all the

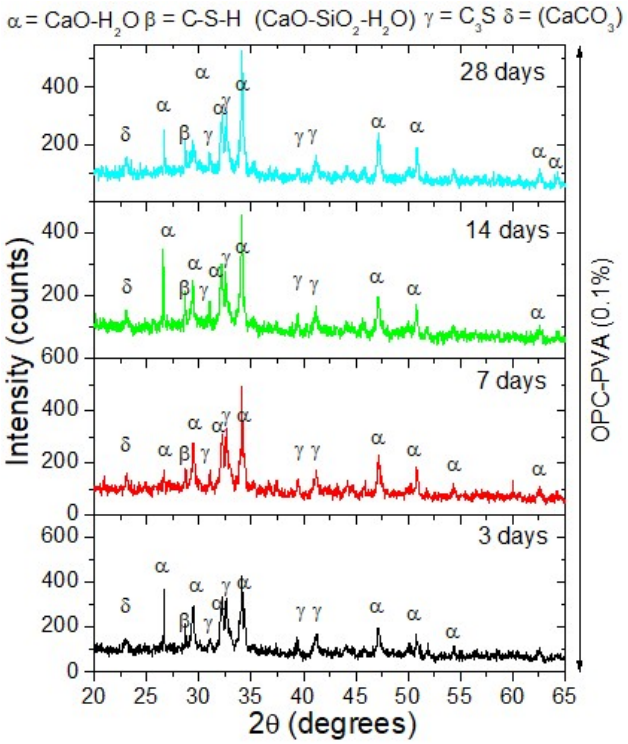

Figure-6.2. XRD spectra of OPC-PVA at different curing time as mentioned. Standard curing time is as mentioned above (3 to 28 days at a step of 7 days).

stages of curing various peaks related to crystal planes are observed at 2θ values of 23.04, 26.60, 28.65, 29.48, 32.10, 32.64, 34.15, 39.40, 41.15, 47.18, 50.75, 54.31, 62.55, and 64.32

degrees corresponding to various phases of hydrated OPC (28 days) as discussed in the previous chapter. The phases (α, β, γ, δ) are identified and attributed to the presence of CaO-H_2O (α), C-S-H (β), C_3S (γ) and $CaCO_3$ (δ) phases. Minor presence of PVA does not affect the microstructural properties.

6.2.3 Compressive strength of total composite cement paste

We are now in a position to prepare total cement composite that contains optimum contents of Fe_2O_3, GO and PVA which are 3wt%, 0.1wt% and 0.1wt%, respectively. The compressive strengths (CS) (with respective error bars) of the total cement composite at various curing stages (days) are shown in the Figure-6.3. CSof OPC-Fe_2O_3-GO-PVA is systematically

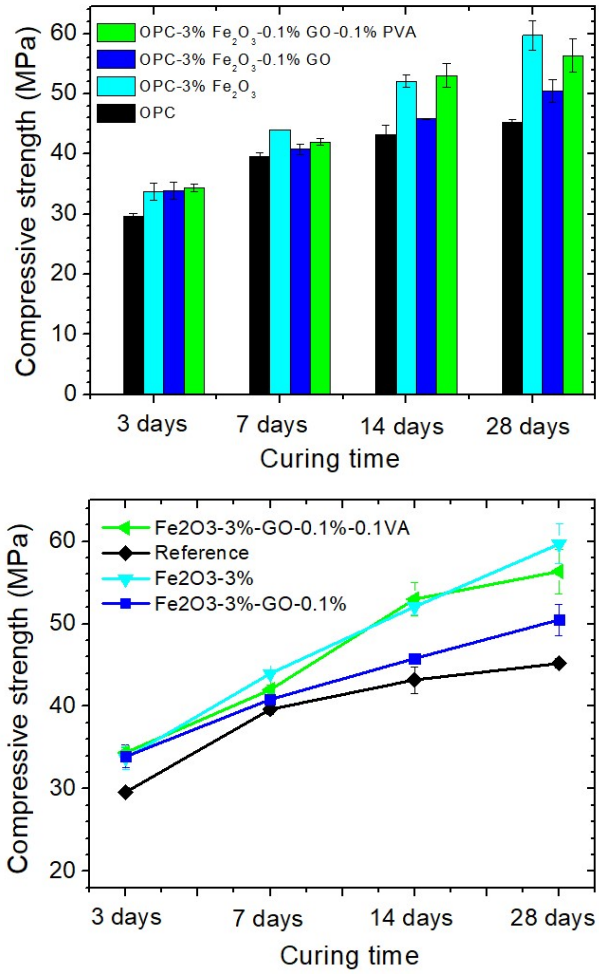

Figure-6.3. Left panel: bar graph of compressive strength (along with error bar) of total composite cement paste containing 3wt% Fe_2O_3, 0.1wt% GO and 0.1wt% PVA at standard curing time of 3 to 28 days, as above. Right panel: the line plot just to show explicitly any existence of saturation trend.

compared with the compressive strength of OPC (reference), OPC-Fe_2O_3, OPC-Fe_2O_3-GO cement composites at each stage of curing. Total composite shows increase in compressive strength with curing time. A saturation trend is seen for this composite. Figure in right panel is presented explicitly to show this trend. This is consistent with the compressive strength of OPC (reference), OPC-Fe_2O_3, OPC-Fe_2O_3-GO cement composites. At highest curing time, the compressive strength of total composite remains considerably high compared to that of OPC (reference) and OPC-Fe_2O_3-GO. It is slightly less than that of OPC-Fe_2O_3 at higher curing time (28 days). This study thus clearly indicates the suitability of total composite in civil infrastructural developments and smart applications.

6.2.4 Microstructural study of total composite cement paste

X-ray diffraction study on the total composite is carried out at each stage of curing to understand the structural change during cement hydration. X-ray diffraction spectra at each curing stage are shown in the Figure-6.4. Typical measurement range is considered to be from 20 degrees to 65 degrees (2θ values). At all the stages of curing various peaks related to crystal

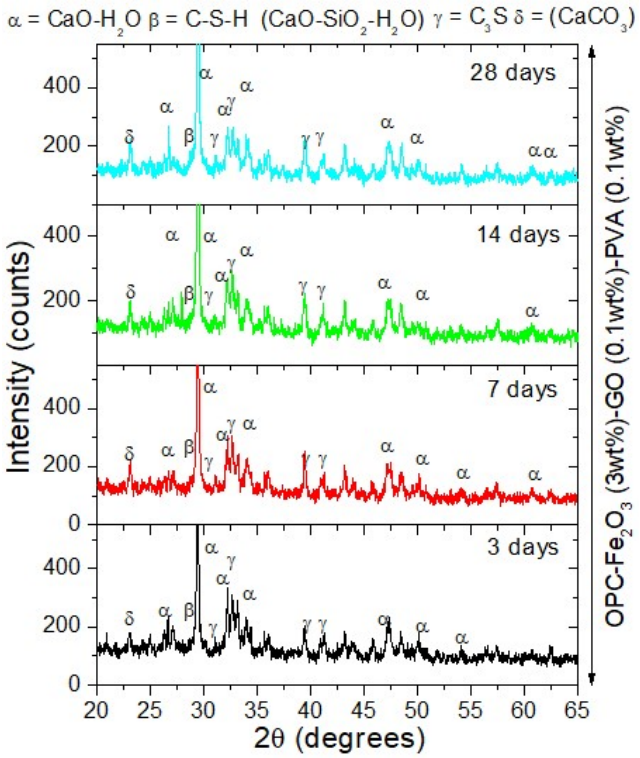

Figure-6.4. XRD spectra of total cement composite OPC-Fe_2O_3-GO-PVA (3wt% Fe_2O_3, 0.1wt% GO and 0.1wt% PVA) at different curing time of cement hydration. Standard curing time is as indicated above.

crystal planes are observed at 2θ values of 23.04, 26.60, 28.65, 29.48, 32.10, 32.64, 34.15, 39.40, 41.15, 47.18, 50.75, 54.31, 62.55, and 64.32 degrees. These peaks correspond to the various phases of hydrated OPC (28 days) as discussed in the previous chapter. The phases (α, β, γ, δ) appear due to the presence of CaO-H_2O (α), C-S-H (β), C_3S (γ) and $CaCO_3$ (δ). Minor presence of PVA does not affect the microstructural properties.

CHAPTER-7

Photocatalytic dye degradation, antimicrobial and chemical stability of cement based smart nanocomposites containing oxides, GO/RGO and PVA

Introduction

Photocatalytic and antimicrobial activities are important areas of research for producing cleaner environment and sustainable developments as mentioned previously. We have developed smart cement nanocomposites that are expected to be highly effective for modern civil infrastructural applications that are capable of showing smart activities simultaneously. In the present chapter smart photocatalytic dye degradation, antimicrobial properties and chemical stability are studied on the developed cement nanocomposites. The types of cement nanocomposite pastes on which the smart properties are investigated are: OPC containing (a) Fe_2O_3, TiO_2 and Cu nanoparticles, (b) Fe_2O_3 and GO, and (c) Fe_2O_3, GO and PVA. In all these cases typical concentrations of additives are considered due to the fact that the optimized concentration offered improved mechanical strength. Furthermore, our aim is to get effective smart properties keeping mechanical strength intact. Rhodamine 6G is used for photocatalytic dye degradation while for antimicrobial activity is detected by using the disk diffusion method against *E. coli* (MTCC 2126). To test chemical stability sample bricks are coated with pure OPC paste and OPC-Fe_2O_3-GO-PVA nanocomposite paste into water solution of diluted H_2SO_3 for different time. Change in surface smoothness is observed after different dipping time.

7.1 Photocatalytic dye degradation

Photocatalytic study is carried out on OPC, and cement nanocomposites containing Fe_2O_3, TiO_2, SiO_2 and Cu nanoparticles using UV-Vis absorption spectroscopy. A part of sample cube of OPC, OPC-Fe_2O_3, OPC-TiO_2 and OPC-Cu cured at 28 is finely ground. A water solution of 25 mg finely ground powder in 80 ml is dispersed with 1 minute ultrasonication. A water solution of 25 mg Rhodamine-6G in 100 ml DI water is prepared. Subsequently, 20 ml Rhodamine solution from total 100 ml solution is added to the 80 ml sample solution (containing cement nanocomposite powder). This way, a total of four separate solution

mixtures (100 ml each) are being prepared. All the solution mixtures are exposed to 100 watt visible light with stirring using glass rod and UV-Vis absorption spectra are monitored after every 1 hour.

UV-Vis spectra of Rhodamine 6G dye degradation are shown in the Figure-7.1 for OPC and OPC-Fe_2O_3. Figure (top panel) shows characteristic absorption of R6G between from 400 nm to 600 nm peaking between 475 nm to 550 nm. Before exposure very high absorption within the entire stated wavelength range is seen. After first 1 hour of exposure absorption spectra show drastic reduction in absorption. Full width at half maxima is reduced drastically too. After 2 hours the reduction trend continues, although after two hours the rate

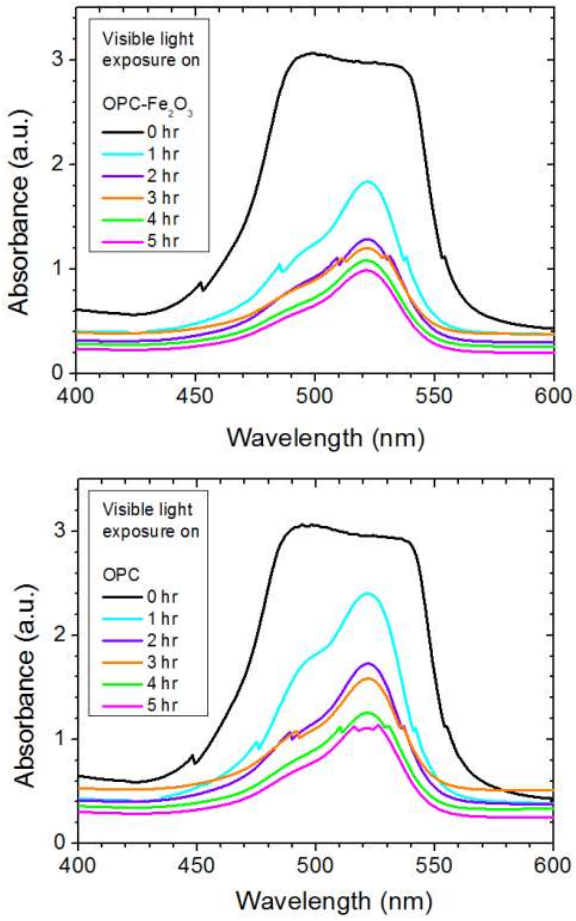

Figure-7.1. UV-Vis absorbance spectra of Rhodamine dye (R6G) degradation as a function of visible light exposure duration (hours) for OPC-Fe_2O_3 (top panel) and pure OPC (lower panel). , and decay of peak absorbance and its best exponential decay fit (bottom-row). The exponential fit is carried out on OPC and OPC-Fe_2O_3 samples typically to show rate of decay.

of reduction slows down. The absorption characteristics of pure OPC also show similar behaviour (lower panel). However, apparently it is seen that reduction rate is higher in the OPC-Fe_2O_3 nanocomposite solution compared to that of pure OPC. After 4 hours of exposure the reduction becomes almost flat.

Similar dye degradation is observed for OPC-TiO_2 and OPC-Cu samples as shown in the Figure-7.2. For explicit understanding we have plotted peak absorbance (at 521.6 nm) with exposure duration for all the samples as is shown in the Figure-7. The corresponding decay fits with exponential decay function, $y = y_0 + a_0 e^{-t/\tau}$ (y as absorbance, t as exposure duration in minutes, y_0 as starting absorbance value, and a_0 as weight factor) for OPC and OPC-Fe_2O_3 are shown in the right panel of bottom row figure. Compared to OPC reference all the samples show faster decay, especially for OPC-Fe_2O_3. The best fits show decay rates (τ) for OPC and OPC-Fe_2O_3 are 2.87 hr (standard deviation: 0.78 hr) and 1.14 hr (standard deviation: 0.09 hr), respectively. This observation suggests about 2.5 times faster decay in the

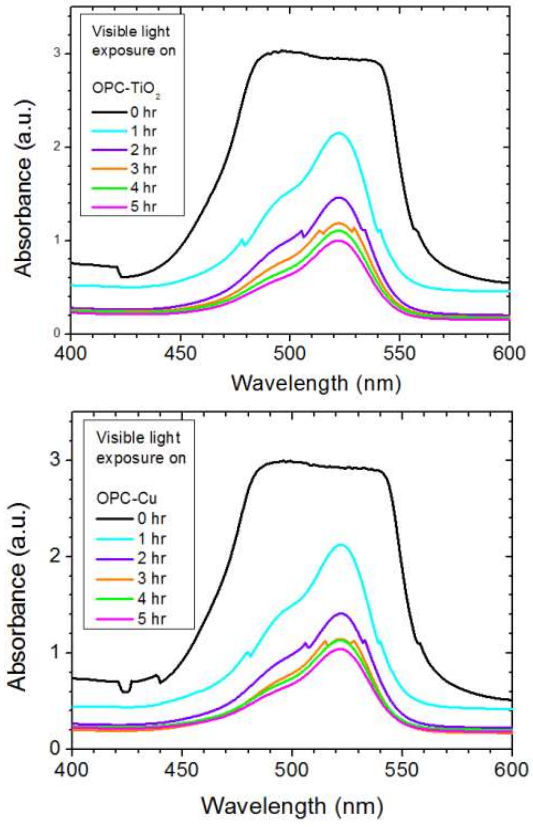

Figure-7.2. UV-Vis absorbance spectra of Rhodamine dye (R6G) degradation as a function of visible light exposure duration (hours) for OPC-TiO_2 (top panel) and OPC-Cu (lower panel).

oxide nanoparticles containing composites. Increase dye degradation is previously observed with various oxide nanoparticles in cement by other researchers [84-88]. Added metal oxide and metal nanoparticles with large surface to volume ratio play additional decay channels for Rhodamine dye molecules to decay. The enhanced photo-degradation in the presence of oxide and metal nanoparticles can be considered for effective removal path of organic dye pollutants. The results signify the potential of developed nanocomposites for civil infrastructure applications and modern sustainable development of cleaner environment.

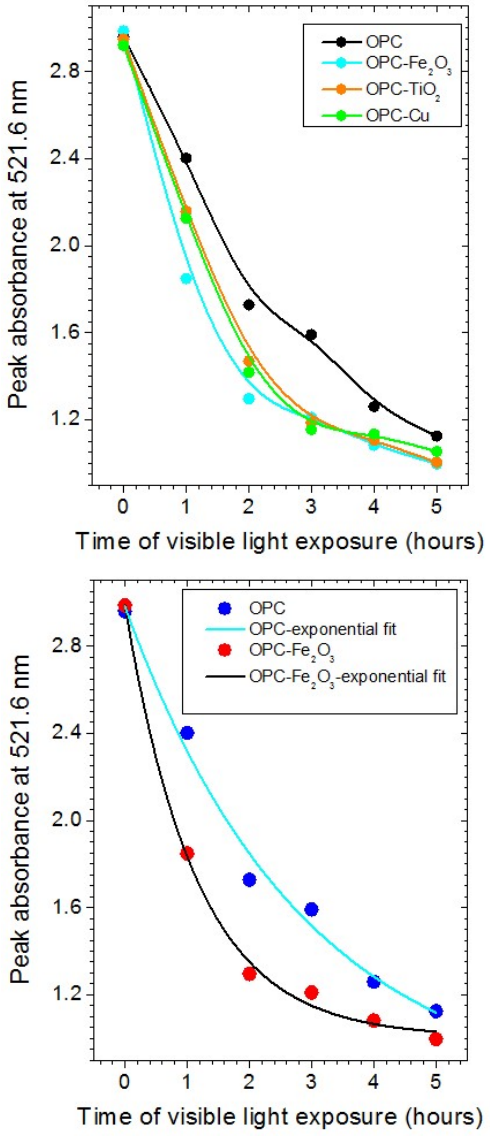

Figure-7.3. Plot of peak of absorption decay with exposure duration (top panel). Highest decay for OPC-Fe_2O_3 is separately plotted in the lower panel along with the best fitting. To extract rate of decay and compare the decay rate of OPC is also plotted and fitted with best fitting. Colour and symbols are as mentioned in the legends.

7.2. Antimicrobial test

7.2.1 Antimicrobial test on OPC-Fe_2O_3-GO nanocomposite

Antimicrobial activity is carried out against *E. coli* (MTCC 2126) by the disk diffusion method as mentioned earlier. Two sample pellets of both the samples (OPC reference and OPC-Fe_2O_3-GO cement composites) are kept inside the sterile nutrient agar plate containing *E. Coli* (spread over) as shown in the Figure-7.4 (a-b). After incubation period gets over, the inhibition zone area is calculated in terms of diameter of the reference samples as well as composite ones. The average inhibition length (diameter) of composite sample is found to be 1.8 cm and that for reference (control) sample is 1.5 cm. The composite sample shows ~20% higher inhibition strength than OPC indicating cement composite (OPC-Fe_2O_3-GO) to be more antimicrobial than reference OPC.

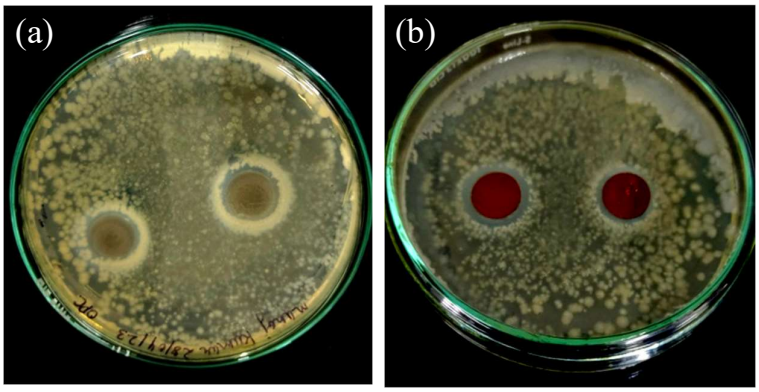

Figure-7.4. Antimicrobial activity of OPC (a) and OPC-Fe_2O_3-GO (b) against *E. coli* (MTCC 2126). Incubation period: 24 hours at 37 ^oC.

7.2.2 Antimicrobial test on OPC-Fe_2O_3-GO-PVA nanocomposite

Antimicrobial activity is carried out against *E. coli* (MTCC 2126) by the disk diffusion method as mentioned earlier. Two sample pellets of both the samples (OPC reference and OPC-Fe_2O_3-GO-PVA cement composites) are kept inside the sterile nutrient agar plate containing *E. Coli* (spread over) as shown in the Figure-7.5 (a-b). The average inhibition length (diameter) of composite sample is found to be 1.69 cm and that for reference (control) sample is 1.45 cm. The composite sample shows ~16% higher inhibition strength than OPC indicating cement composite (OPC-Fe_2O_3-GO) to be more antimicrobial than reference OPC.

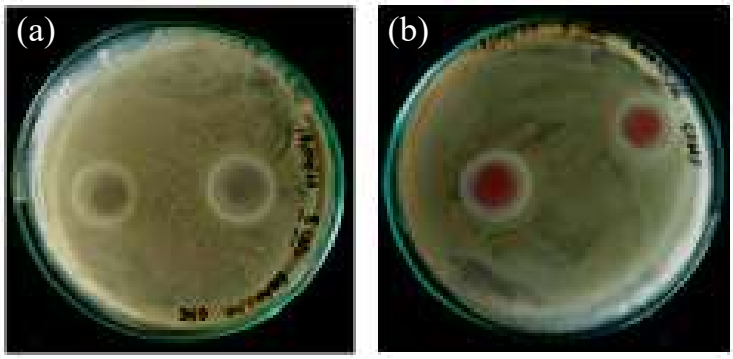

Figure-7.5. Antimicrobial activity of (a) OPC and (b) OPC-Fe_2O_3-GO-PVA against *E. coli* (MTCC 2126). Incubation period: 24 hours at 37 ºC.

7.3. Chemical stability test on OPC-Fe_2O_3-GO-PVA nanocomposite

Chemical attack and subsequent change in the bricks' surface coated with OPC-Fe_2O_3-GO-PVA are studied. The Change in the surface roughness (corrosion or voids/pores formation) is compared with the bricks' surface coated with OPC paste. For the purpose we have considered weak H_2SO_3 acid (0.1M). Firstly OPC-Fe_2O_3-GO-PVA cement nanocomposite paste is coated on to bricks' (2 sample bricks) surface before and allowed for 24 hours setting. Subsequently they are put in to water for curing for 28 days. Similarly, OPC paste is also coated on to the surface of bricks (2 sample bricks) and allowed for setting for 24 hours before putting in to water for curing for 28 days. Finally sample bricks are dipped in to water solution of H_2SO_3 (water : acid = 10 liters : 20 ml) for 3 days and 7 days. Changes in the surface roughness (macro)are photographed with a digital camera. Before dipping the surface photographs are also taken for better comparison. Photographs are shown in the Figure-7.6. The as prepared (without chemical treatment) bricks' surfaces coated with OPC and OPC-Fe_2O_3-GO-PVA show smooth surface feature (top row). After dipping in to the chemical solution for reasonable time (3 days and 7 days), the surfaces do not show much difference (middle row and bottom row). These observations signify the effectiveness of the total composite samples for various smart activities including chemical stability. Moreover, the prepared nanocomposite cement paste has superior compressive strength than OPC paste.

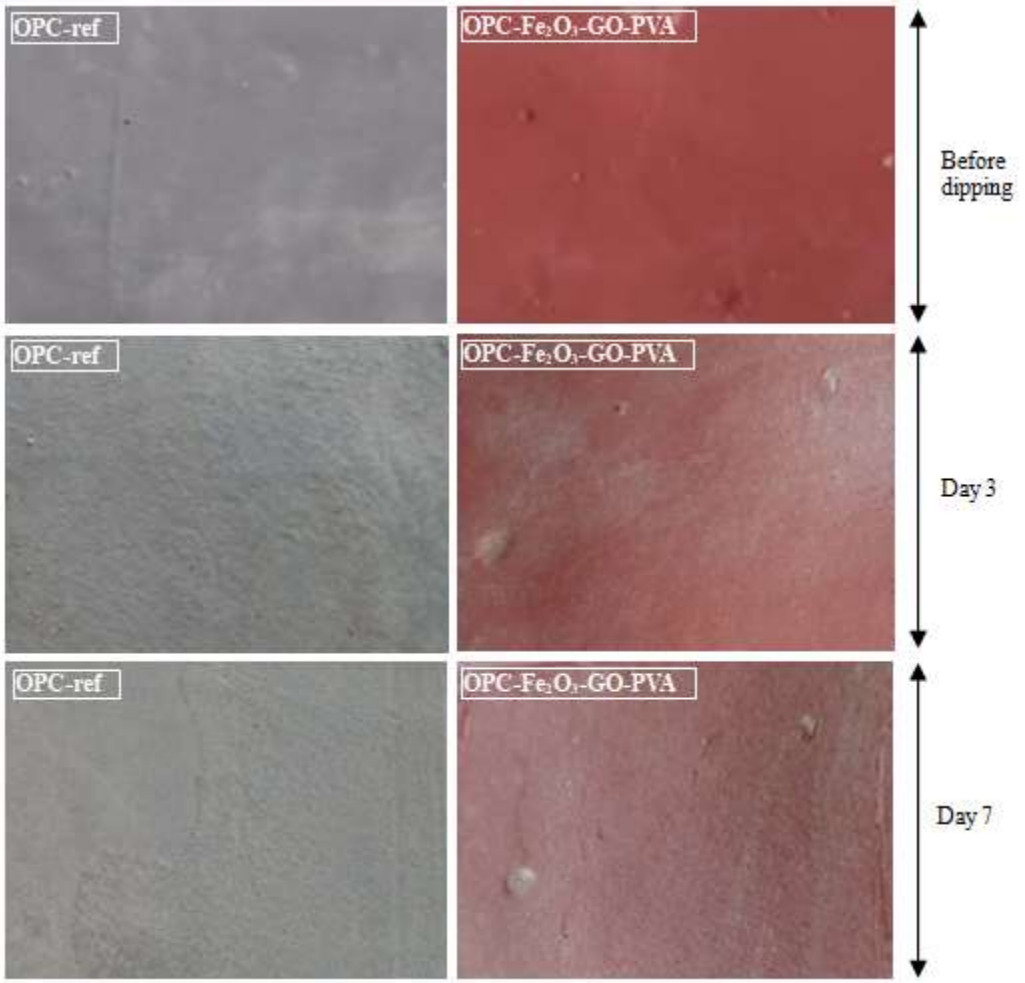

Figure-7.6. OPC and OPC-Fe2O3-GO-PVA coated bricks surface before and after dipping in water solution of H_2SO_3 (water : acid = 20 liters : 100 ml). Before dipping (top row), after dipping for 3 days (middle row) and after dipping for 7 days (bottom row).

CHAPTER-8

Conclusions and future scopes

This chapter summarizes the PhD thesis work carried out. Conclusions drawn on each chapter work is presented separately. At the end future scopes are presented.

8.1 Conclusions

8.1.1 Cement composites containing metal and oxide nanoparticles

OPC nanocomposite pastes containing oxide nanoparticles such as Fe_2O_3, TiO_2, SiO_2, and metal (Cu) nanoparticles at different wt% (usually in the range ≤5wt%) are prepared. A total of 12 cubes of each cement nanocomposite are considered for the study. The prepared cubes of OPC-Fe_2O_3, OPC-TiO_2, OPC-SiO_2, OPC-Cu and pure OPC are dipped into water for different curing time. Before dipping, the cubes are allowed for natural setting of 24 hours. Standard curing procedures are followed. Mechanical strengths (compressive and flexural) are measured after standard curing time (3 to 28 days at an interval of 7 days). Sample cubes are sun dried (1-2 hours) before testing. After mechanical strength measurements, a small piece of broken cube is finely ground for microstructural study using X-ray diffractometer in the 2θ range of 20 degrees to 80 degrees. Optimized cement paste is studied further for stability under thermal agitation. Compressive and flexural strength measurements show increase in strength with increasing days of curing for all the composite cement pastes. It is also observed that with increasing dosage of nanoparticles compressive strength increases first and decreases afterwards. Addition beyond this wt% leads to the reduction of mechanical strength which may be due to the formation of nanoparticle agglomeration and form separate nanoparticle phase. Compressive strength reaches to its maximum that depends on the additive types. For different types of oxide nanoparticles and metal (Cu) nanoparticles optimum dosage is different. For cement paste containing Fe_2O_3shows about 3wt% is optimum showing ~30% higher compressive strength compared to OPC reference. For OPC-TiO_2 cement nanocomposite paste optimum concentration lies nearly in the range of 2-4 wt%. OPC-SiO_2 cement nanocomposite even at lower concentration of SiO_2 (≤ 1wt%) shows higher compressive strength. OPC-Cu cement nanocomposite also shows maximum compressive strength for ≤ 1wt% Cu. Although, OPC-Fe_2O_3, OPC-TiO_2 and OPC-SiO_2 nanocomposites show reasonable improvement in the compressive strength at optimized composition, OPC-Cu hardly shows any improvement. Improved compressive strength is due to the faster

cement hydration and C-S-H gel-phase (β-phase) formation. Microstructural studies show the presence of β-phase whose strength is maximum at the optimum additive concentration for each composite. These observations clearly indicate the role of β-phase in the cement hydration and improvement mechanical strength. The thermal stability is tested on the typical Fe_2O_3 admixed OPC paste that showed highest improvement in compressive and flexural strength. At different temperature when cubes are treated the compressive strength continues to fall. Beyond 100 ^oC the compressive strength falls slowly and shows saturation trend. At 300 ^oC cubes show fine cracks that become prominent at 400 ^oC. At high temperature, beyond 200 ^oC, the fall in compressive strength may be caused by the developments of cracks. Microstructural studies on the thermally annealed samples show no appreciable change in the structural properties. Furthermore, crystalline quality is seen to be improved due to reorganization of the crystallites within the composite and OPC samples. The β-phaseexistence is less significant at elevated temperature which is consistent with the observations that the slow reduction of compressibility at higher temperatures are due to the cracks and voids, not due to the reduction in gel phase strength.

8.1.2 Cement composites containing Fe_2O_3, GO and RGO

OPC-Fe_2O_3-GO and OPC-Fe_2O_3-RGO cement nanocomposite pastes are prepared by mixing GO and RGO at low wt% (0.05 to 1 wt%) with OPC-Fe_2O_3. We have considered OPC-Fe_2O_3 (3wt% Fe_2O_3) as base material as this composite shows highest compressive strength among other composites containing TiO_2, SiO_2 or Cu nanoparticles. InOPC-Fe_2O_3-GO sample GO content is varied from 1 to 0.05 wt% and compressibility test is carried out for different curing time (3 to 28 days). Increase in compressive strength with curing time is seen for additive concentration of up to 0.1wt%. Beyond this concentration compressive strength falls once again. Optimized concentration of GO is found to be ~ 0.1wt%. Similar compressive strength measurement is carried out on OPC-Fe_2O_3-RGO sample with varying additive concentration. At each curing stage mechanical (compressive strength) and structural (XRD) studies are carried out to correlate improvement and the role of β-phase (C-S-H phase). Oxygen containing groups are monitored by FTIR spectroscopy to know the details of chemical changes that occur during cement hydration and formation of β-phase (C-S-H gel phase).

The improvement is attributed to faster cement hydration and formation of β-phase (C-S-H gel phase). XRD and FTIR studies corroborate well with this observation. Both the spectroscopic studies confirm the presence of β-phase. Interestingly, GO admixed OPC-Fe_2O_3 composite shows superior characteristics than that of RGO admixed OPC-Fe_2O_3. This is

because the presence of more oxygen containing groups such as OH, COOH in GO rather than RGO playing important role in accelerating cement hydration process. Due to improved mechanical and microstructural properties, GO admixed OPC-Fe_2O_3 is considered further for antimicrobial studies to exhibit effective smartness of the composite. Antimicrobial test results show the colonial growth of *E*-coli is restricted by ~ 20% more than that of OPC. Present studies show the significance of GO admixed OPC-Fe_2O_3 for civil construction and smart infrastructural applications producing cleaner environment.

8.1.3 Cement composites containing Fe_2O_3, GO and PVA

OPC-PVA nanocomposites are prepared by adding PVA with different wt% (0.05wt% to 1wt%) to OPC. Samples are cured at standard curing time (3 to 28 days at a step of 7 days). Compressive strength measurements on these nanocomposites shows optimized concentration is about 0.1 wt% at which compressive strength is maximum. Structural measurements also show the presence of β-phase with highest strength for 0.1 wt% PVA when samples are cured at 28 days. With this optimization, total nanocomposites (OPC-Fe_2O_3-GO-PVA) are prepared with optimized concentration of 3wt% Fe_2O_3, 0.1wt% GO and 0.1wt% PVA. Compressive strength is measured and compared with that of OPC-Fe_2O_3, OPC-Fe_2O_3-GO and pure OPC. Measurements show the mechanical (compressive) strength of total composite is slightly less than that of OPC-Fe_2O_3 but remains at higher side compared to that of OPC-Fe_2O_3-GO and pure OPC. The superior characteristic is further supported by the microstructural study which confirmed the stronger strength of β phase (C-S-H gel phase). It clearly indicates the suitability of total composite in civil infrastructural developments.

8.1.4 Smart properties of cement nanocomposites containing Fe_2O_3, GO and PVA

Photocatalytic and antimicrobial activities are important areas of research for producing cleaner environment and sustainable developments as mentioned previously. We have developed smart cement nanocomposites that are expected to be highly effective for modern civil infrastructural applications that are capable of showing smart activities simultaneously. In the present chapter smart photocatalytic dye degradation, antimicrobial properties and chemical stability are studied on the developed cement nanocomposites. The types of cement nanocomposite pastes on which the smart properties are investigated are: OPC containing (a) Fe_2O_3, TiO_2 and Cu nanoparticles, (b) Fe_2O_3 and GO, and (c) Fe_2O_3, GO and PVA. In all these cases typical concentrations of additives are considered due to the fact that the optimized concentration offered highest compressive strength. Furthermore, our aim is to get effective

smart properties keeping mechanical strength at its best level. Rhodamine 6G is used for photocatalytic dye degradation while for antimicrobial activity was detected by using the disk diffusion method against *E. coli* (MTCC 2126). To test chemical stability sample bricks are coated with pure OPC paste and OPC-Fe_2O_3-GO-PVA nanocomposite paste into water solution of diluted H_2SO_3 for different time. Change in surface smoothness is observed after different dipping time. For photocatalytic dye degradation Rhodamine 6G is used. All the cement nanocomposites show faster dye degradation compared to that observed with OPC. OPC-Fe_2O_3 composite shows highest dye degradation rate which ~ 2.5 times higher than that observed with OPC. Antimicrobial test with *E. coli* (MTCC 2126) shows about 18-20% better restricted colonial growth of E-coli compared to plain OPC. Furthermore, chemical stability check shows bricks that are coated with OPC-Fe_2O_3-GO-PVA nanocomposite paste are comparably stable when treated with acid-water solution.

8.2 Future scopes

Smart cement nanocomposites are important cementitious materials for the developing modern sustainable developments. Various smart cement nanocomposites can be realized by adding various functional oxide nanomaterials, nano carbon materials and polymers. These functional additive nanomaterials play important role in filling pores and binding properties, bridging gaps between nearing neighbours, and preventing crack developments. As a result, they show superior mechanical properties as well as smart properties. However, underlying physical and chemical mechanisms of such improvement and exotic smart properties are poorly understood. Even the basic understanding of formation of β-phase (C-S-H gel phase), chemical changes and structural phases are not very clear till date. Therefore, focused research is necessary to understand these mechanism and further developments. Challenges lie in developing cementitious materials with smart functionalities and optimized parameters retaining basic mechanical strength intact. In depth research is necessary on the toxicity of various nanomaterials and safe level of exposure. Finally, various ways of producing functionalized nanomaterials and their cost-effectiveness must be looked at seriously.

REFERENCES

[1] Ng, D.S., Paul, S.C., Anggraini, V., Kong, S. Y., Qureshi, T., Rodriguez, C.R., Liu, Q.F., Savija, B. (2020). Influence of SiO_2, TiO_2 and Fe_2O_3 nanoparticles on the properties of fly ash blended cement mortars. *Construction and Building Materials*, 258, 119627 https://doi.org/10.1016/j.conbuildmat.2020.119627

[2] Feng, D., Xie, N., Gong, C., Leng, Z., Xiao, H., Li, H., Shi, X. (2013). Portland cement paste modified by TiO_2 nanoparticles: a microstructure perspective. *Industrial & Engineering Chemistry Research*, 52, 11575-11582. https://doi.org/10.1021/ie4011595

[3] Han, B., Li, Z., Zhang, L., Zeng, S., Yu, X., Han, B., Ou, J. (2017). Reactive powder concrete reinforced with nano SiO_2-coated TiO_2. *Comp. part A, Appl. Sci. & Manufacturing*, 101, 143-150. https://doi.org/10.1016/j.conbuildmat.2017.05.065

[4] Zhang, R., Cheng, X., Hou, P., Ye, Z. (2015). Influences of nano-TiO2 on the properties of cement-based materials: Hydration and drying shrinkage. *Const. & Build. Mater.*, 81, 35-41. https://doi.org/10.1016/j.conbuildmat.2015.02.003

[5] Jalal, M., Tahmasebi, M. (2015). Assessment of nano-TiO_2 and class F fly ash effects on flexural fracture and microstructure of binary blended concrete. *Sci. Eng. Compos. Mater.*, 22, 263–270. https://doi.org/10.1515/secm-2013-0211

[6] Kiamahalleh, M.V., Alishah, A., Yousefi, F., Astani, S.H., Gholampour, A. (2020). Iron oxide nanoparticle incorporated cement mortar composite: Correlation between physico-chemical & physico-mechanical properties. *Materials Advances*, 1, 1835-1840. DOI: 10.1039/D0MA00295J

[7] Slosarczyk, A., Klapiszewska, I., Klapiszewski, L. (2022). Influence of nanosilica and binary oxide systems on the selected physical and mechanical properties of cement composites. *Physicochem. Probl. Miner. Process*, 58, 144184

[8] Li, H., Xiao, H.G., Yuan, J., Ou, J. (2004). Microstructure of cement mortar with Nano particles. *Composites Engineering Part B*, 35, 185-189 https://doi.org/10.1016/S1359-8368(03)00052-0

[9] Shchelokova, E.A., Tyukavkina, V.V., Tsyryatyeva, A.V., Kasikov, A.G. (2021). Synthesis and characterization of SiO_2-TiO_2 nanoparticles and their effect on the strength of self-cleaning cement composites. *Construction and Building Materials*, 283, 122769 https://doi.org/10.1016/j.conbuildmat.2021.122769

[10] Alkhatab, H., Al-Ostaz, A., Alexander, H., Cheng, D., Li, X. (2013). Material Genome for Graphene-Cement Nanocomposites. *J. Nanomech. Micromech.*, 3, 67-77. https://doi.org/10.1061/(ASCE)NM.2153-5477.0000055

[11] Yang, H., Monasterio, M., Cui, H., Han, N. (2017). Experimental study of the effects of graphene oxide on microstructure & properties of cement paste composites. *Composites: Part A*, 102, 263-272. https://doi.org/10.1016/j.compositesa.2017.07.022

[12] Cao, M.L., Zhang, H.X., Zhang, C. (2016). Effect of Graphene on mechanical properties of cement mortars. *J. Cent. South Uni.*, 28, 19. https://doi.org/10.1007/s11771-016-3139-4

[13] Babak, F., Abolfazl, H., Alimorad, R., Parviz, G. (2014). Preparation & Mechanical properties of Graphene Oxide: Cement Nanocomposites. *The Scientific World Journal*, 2014, 276323. https://doi.org/10.1155/2014/276323

[14] Lv, S., Ma, Y., Qiu, C., Sun, T., Liu, J., Zhou, Q. (2013). Effect of graphene oxide Nano-sheets of microstructure & mechanical properties of cement composites. *Const. & Build. Mater.*, 49, 121-127. https://doi.org/10.1016/j.conbuildmat.2013.08.022

[15] Wang, N., Wang, S., Tang, L., Ye, L., Cullbrand, B., Zehri, A., Tebikachew, B.E., Liu, J. (2020). Improved Interfacial Bonding Strength and Reliability of Functionalized Graphene Oxide for Cement Reinforcement Application. *Chemistry - A European Journal*, 26, 6561-6568. https://doi.org/10.1002/chem.201904625

[16] Yazdani, N., Mohanam, V. (2014). Carbon Nano-Tube & Nano-fiber in Cement Mortar: Effect of Dosage rate & water-cement ratio. *Int. J. Mater. Sci.*, 4, 45-52. Doi: 10.14355/ijmsci.2014.0402.01

[17] Wang, B., Pang, B. (2020). Properties improvement of multiwall carbon nanotubes-reinforced cement-based composites. *J. Composite mater.*, 54, 2379-2387. https://doi.org/10.1177/0021998319896835

[18] Lu, S., Wang, X., Meng, Z., Deng, Q., Peng, F., Yu, C., Hu, X., Zhao, Y., Ke, Y., Qi, F. (2019). The mechanical properties, microstructures and mechanism of carbon nanotube-reinforced oil well cement-based nanocomposites. *RSC Adv.*, 9, 26691-26702. DOI: 10.1039/C9RA04723A

[19] Eskander, S. B., Saleh, H. M., Tawfik, M. E., Bayoumi, T. A. (2021). Towards potential applications of cement-polymer composites based on recycled polystyrene foam wastes on construction fields: Impact of exposure to water ecologies. *Case Studies in Construction Materials*, 15, e00664. https://doi.org/10.1016/j.cscm.2021.e00664

[20] Tu, Y., Liu, D., Yuan, L., Zhang, Y. (2020). Corrosion resistance of concrete strengthened with fibre-reinforced polymer sheets. *Magazine of Concrete Research*, 72, 2000042

http://doi.org/10.1680/jmacr.20.00042

[21] Rustum, M.K., Eweed, K.M. (2020). The effect of partial replacement of PMMA on the compressive and Flexural strength of cement Mortar. *European Journal of Engineering Research and Science*, 5, 443-447. http://dx.doi.org/10.24018/ejers.2020.5.4.1833

[22] Chen, C.H., Huang, R., Wu, J.K. (2077). Preparation and properties of polymer impregnated concrete. *J. Chinese Inst. Engineers.*, 30, 163-168.
https://doi.org/10.1080/02533839.2007.9671240

[23] Du, M., Jing, H., Gao, Y., Su, H., Fang, H. (2020). Carbon nanomaterials enhanced cement-based composites: advances and challenges. *Nanotechnol. Rev.*, 9, 115–135.
https://doi.org/10.1515/ntrev-2020-0011

[24] Sharma, N., Sharma, P. (2021). Effect of hydrophobic agent in cement and concrete : A Review. *IOP Conf. Series: Mater Sci & Engg.*, 1116, 012175.
DOI: 10.1088/1757-899X/1116/1/012175

[25] Hamidi, F., Aslani, F. (2019). TiO_2-based Photocatalytic Cementitious Composites: Materials, Properties, Influential Parameters, and Assessment Techniques. *Nanomaterials*, 9, 1444. https://doi.org/10.3390/nano9101444

[26] Zhen, L., Ding, S., Yu, X., Han, B., Ou, J. (2018). Multifunctional cementitious composites modified with nano- titanium dioxide: A review. *Comp. Part A: Appl. Sci. Manuf.*, 11, 11-137. https://doi.org/10.1016/j.compositesa.2018.05.019

[27] Qiu, L., Dong, S., Ashour, A., Han, B. (2020). Antimicrobial concrete for smart and durable infrastructures: A review. *Const. Build. Mater.*, 260, 120456.
https://doi.org/10.1016/j.conbuildmat.2020.120456

[28] Suo, Y., Guo, R., Xia, H., Yang, Y., Zhou, B., Zhao, Z. (2022). A review of graphene oxide/cement composites: Performance, functionality, mechanisms, and prospects. *J. Build. Engg.*, 53, 104502. https://doi.org/10.1016/j.jobe.2022.104502

[29] Brandt, A. M. (2008). Fibre reinforced cement-based (FRC) composites after over 40 years of development in building and civil engineering. *Composite Structures*, 86, 3-9
https://doi.org/10.1016/j.compstruct.2008.03.006

[30] Zainal, S. M. I. S., Hejazi, A. F. N. A. A., Jaafar, M. S. (2020). Effects of Hybridized Synthetic Fibers on the Shear Properties of Cement Composites. *Materials*, 13, 5055
https://doi.org/10.3390/ma13225055

[31] Sanchez, F., Sobolev, K. (2010). Nanotechnology in concrete-A review. *Construction and Building Materials*, 24, 2060-2071 https://doi.org/10.1016/j.conbuildmat.2010.03.014

[32] Li, W., Qu, F., Dong, W., Mishra, G., Shah, S.P. (2022). A comprehensive review on self-sensing graphene/cementitious composites: A pathway toward next-generation smart concrete. *Construction and Building Materials*, 9, 127284 https://doi.org/10.1016/j.conbuildmat.2022.127284

[33] Li, Z., Ding, S., Yu, X., Han, B., Ou, J. (2018). Multifunctional cementitious composites modified with nano titanium dioxide: a review. *Composites part a: applied science and manufacturing*, 111, 115. https://doi.org/10.1016/j.compositesa.2018.05.019

[34] https://www.civilengineeringrealities.com/2020/08/cement-its-ingredients-and-their-functions.html

[35] Zhu, W., Feng, Q., Luo, Q., Bai, X., Lin, X., Zhang, Z. (2021). Effects of pce on the dispersion of cement particles and initial hydration. *Materials*, 14, 3195. https://doi.org/10.3390/ma14123195

[36] Shankar, A.N. (2020). Structural Concrete. 1st Edition, *24by7Publishing*, India

[37] Feret, R. (1892). On the compactness of hydraulic mortars. *Annales des Ponts et Chaussees*, 7, 5–164.

[38] Abrams, L.D. (2019). Properties of Concrete. 3rd edn. *Pitman Publishing*, London, UK.

[39] Chidiac, S.E., Mahmoodzadeh, F., Moutasem, F. (2013). Compressive strength model for concrete. *Mag. Concrete Res.*, 65, 557–572.

[40] Biswas, R., Rai, B. (2019). Efficiency Concepts and Models that Evaluates the Strength of Concretes Containing Different Supplementary Cementitious Materials. *Civil Eng. Journal*, 5, 18-32. http://dx.doi.org/10.28991/cej-2019-03091222

[41] Qi, T., Zhou, W., Liu, X., Wang, Q., Zhang, S. (2021). Predictive Hydration Model of Portland Cement and Its Main Minerals Based on Dissolution Theory and Water Diffusion Theory. *Materials*, 14, 595. https://doi.org/10.3390/ma14030595

[42]https://www.engr.psu.edu/ce/courses/ce584/concrete/library/construction/curing/Hydration.htm as on 21-6-2023

[43] https://en.wikipedia.org/wiki/Alite as on 21-6-2023

[44] https://en.wikipedia.org/wiki/Belite as on 21-6-2023

[45] Hakamy, A. (2021). Influence of SiO2 nanoparticles on the microstructure, mechanical properties, and thermal stability of Portland cement nanocomposites. *J. Taibah Uni. Sci.*, 15, 909. https://doi.org/10.1080/16583655.2021.2011594

[46] Kourti, I., Deegan, D., Boccaccini, A.R., Cheeseman, C.R. (2013). Use of DC Plasma Treated Air Pollution Control (APC) Residue Glass as Pozzolanic Additive in Portland Cement. *Waste Biomass Valorization*, 4, 719-728.

https://doi.org/10.1007/s12649-013-9210-6

[47] Horgnies, M., Chen, J.J., Bouillon, C. (2013). Overview About The Use Of Fourier Transform Infrared Spectroscopy To Study Cementitious Materials. *WIT Transac. Eng. Sci.*, 77, 251-262. doi:10.2495/MC130221

[48] Singh, L.P., Goel, A., Bhattachharyya, S.K., Ahalawat, S., Sharma, U., Mishra, G. (2015). *Int. J. Concrete Struc. & Mater.,* 9, 207-217.

[49] Li, H., Zhang, M.H., Ou, J.P. (2007). Flexural fatigue performance of concrete containing nano-particles for pavement. *Int. J. Fatigue*, 29, 1292-1301. https://doi.org/10.1016/j.ijfatigue.2006.10.004

[50] Trejo-Arroyo, D.L., Acosta, K.E., Cruz, J.C., Valenzuela-Muñiz, A.M., Vega-Azamar, R.E., Jiménez, L. F. (2019). Influence of ZrO_2 Nanoparticles on the Microstructural Development of Cement Mortars with Limestone Aggregates. *Appl. Sci.*, 9, 598. https://doi.org/10.3390/app9030598

[51] Liu, C., Huang, X., Wu, Y.Y., Deng, X., Liu, J., Zheng, Z., Hui, D. (2020). Review on the research progress of cement-based & geo-polymer materials modified by graphene & graphene oxide. *Nanotechnol. Rev.*, 9, 155-169. https://doi.org/10.1515/ntrev-2020-0014

[52] Rehman, S.K., Ibrahim, Z., Memon, S.A., Jayed, M.F., Khushnood, R.A. (2017). A sustainable graphene based cement composite. *Sustainability*, 9, 1229. https://doi.org/10.3390/su9071229

[53] Zhang, N., She, W., Du, F., Xu, K. (2020). Experimental Study of Mechanical & functional properties of reduced Graphene Oxide/ Cement Composites. *Materials*, 13, 3015. https://doi.org/10.3390/ma13133015

[54] Sun, S., Ding, S., Han, B., Dong, S., Yu, X., Zhou, D., Ou, J. (2017). Multi-layer graphene-engineered cementitious composites with multifunctionality/intelligence. *Comp. part B Engineering*. 129, 221-232. https://doi.org/10.1016/j.compositesb.2017.07.063

[55] Konsta-Gdoutos, M.S, Metaxa, Z.S., Shah, S.P. (2010). Highly dispersed carbon nanotube reinforced cement based materials. *Cement & Concrete Res.*, 40, 1052–1059. https://doi.org/10.1016/j.cemconres.2010.02.015

[56] Carrico, A., Bogas, J.A., Hawreen, A., Guedes, M. (2018). Durability of multi-walled carbon nanotube reinforced concrete. Const. & Build. Mater., 164, 121-133. https://doi.org/10.1016/j.conbuildmat.2017.12.221

[57] Chaipanich, A., Rianyoi, R., Nochaiya, T. (2017). The effect of carbon nanotubes & silica fume on compressive strength & flexural strength of cement mortar. *Materials today:*

Proceedings, 4, 6065-6071.https://doi.org/10.1016/j.matpr.2017.06.095

[58] Metaxa, Z.S., Gdoutos, M.S.K., Shah, S.P. (2010). Mechanical properties & Nanostructure of cement-based materials reinforced with carbon Nanofibers & Polyvinyl Alcohol (PVA) Microfibers. *American Concrete Institute, ACI Special Publication*, 270SP, 115-126.

[59] Gdoutos, E.E., Konsta-Gdoutos, M.S., Danoglidis, P.A., Shah, S.P. (2016). Advanced cement based nanocomposites reinforced with MWCNTs and CNFs. *Frontiers of Struct. Civil Engineering*, 10, 142-149. https://doi.org/10.1007/s11709-016-0342-1

[60] Sarvandani, M.M., Mahdikhani, M., Aghabarati, H., Fatmehsari, M.H. (2021). Effect of functionalized multi-walled carbon nanotubes on mechanical properties and durability of cement mortars. *J. Build. Engg.*, 41, 102407. https://doi.org/10.1016/j.jobe.2021.102407

[61] Zhang, W., Zeng, W., Zhang, Y., Yang, F., Wu, P., Xu, G., Gao, Y. (2020). Investigating the influence of multi-walled carbon nanotubes on the mechanical and damping properties of ultra-high performance concrete. *Sci. Eng. Compos. Mater.*, 27, 433–444. https://doi.org/10.1515/secm-2020-0046

[62] Fan, J., Li, G., Deng, S., Wang, Z. (2019). Mechanical Properties and Microstructure of Polyvinyl Alcohol (PVA) Modified Cement Mortar. *Applied Sciences*, 9, 2178 https://doi.org/10.3390/app9112178

[63] Ange-Therese A. (2020). Effect of nano-TiO_2 on C-S-H phase distribution within portland cement paste. *J. Materials Science*, 55, 11106-11119. https://doi.org/10.1007/s10853-020-04847-5

[64] Lee, B.Y., Jayapalan, A.R., Kurtis, K.E. (2013). Effects of nano-TiO2 on properties of cement-based materials. *Magazine of Concrete Res.*, 65, 1293–1302. http://doi.org/10.1680/macr.13.00131

[65] Li, H., Zhang, M.H., Ou, J.P. (2006). Abrasion resistance of concrete containing nano-particles for pavement. *Wear*, 260, 1262–1266. https://doi.org/10.1016/j.wear.2005.08.006

[66] Liu, C., Su, X., Wu, Y., Zheng, Z., Yang, B., Luo, Y., Yang, J., Yang, J. (2021). Effect of nano-silica as cementitious materials reducing admixtures on the workability, mechanical properties and durability of concrete. *Nanotechnology Reviews*, 10, 1395–1409 https://doi.org/10.1515/ntrev-2021-0097

[67] Han, B., Li, Z., Zhang, L., Zeng, S., Yu, X., Han, B., Ou, J. (2017). Reactive powder concrete reinforced with nano SiO_2-coated TiO_2. *Const. & Build. Mater.*, 148, 104-112. https://doi.org/10.1016/j.conbuildmat.2017.05.065

[68] Rong, Z., Sun, W., Xiao, H., Jiang, G. (2015). Effects of nano-SiO_2 particles on the mechanical and microstructural properties of ultra-high performance cementitious composites. *Cem. Concr. Com-pos.*, 56, 25-31. https://doi.org/10.1016/j.cemconcomp.2014.11.001

[69] Liu, M., Tan, H., He, X. (2019). Effects of nano-SiO_2 on early strength and microstructure of steam-cured high volume fly ash cement system. *Const. Build. Mater.*, 194, 350-359. https://doi.org/10.1016/j.conbuildmat.2018.10.214

[70] Slosarczyk, A., Kwiecinska, A., Pelszyk, E. (2017). Influence of Selected Metal Oxides in Micro and Nanoscale on the Mechanical and Physical Properties of the Cement Mortars. *Procedia Engineering*, 172, 1031-1038. https://doi.org/10.1016/j.proeng.2017.02.155

[71] Abdulabbas, Z.H., Jasim, A.T., Salih, M.A. (2020). Assessment the Influence of Fe_2O_3 Micro and Nanoparticles on Properties of Concrete. *Key Engg. Mater.*, 870, 29-37. https://doi.org/10.4028/www.scientific.net/KEM.870.29

[72] Largeau, M.A., Mutuku, R., Thuo, J. (2018). Effect of Iron Powder (Fe_2O_3) on Strength, Workability, and Porosity of the Binary Blended Concrete. *Open Journal of Civil Engineering*, 8, 411-425. DOI: 10.4236/ojce.2018.84029

[73] Sikora, P., Horszczaruk, E., Cendrowski, K., Mijowska, E. (2016). The Influence of Nano-Fe_3O_4 on the Microstructure and Mechanical Properties of Cementitious Composites. *Nanoscale Res. Letters*, 11, 182. https://doi.org/10.1186/s11671-016-1401-1

[74] Pan, Z., He, L., Qiu, L., Korayem, A.H., Li, G., Zhu, J.W., Collins, F., Li, D., Duan, W.H., Wang, M.C. (2015). Mechanical properties and microstructure of a graphene oxide–cement composite. *Cement & Concrete Composites*, 58, 140–147. https://doi.org/10.1016/j.cemconcomp.2015.02.001

[75] Wang, Q., Wang, J., Lu, C.X., Liu, B.W., Zhang, K., Li, C-Z. (2015). Influence of graphene oxide additions on the microstructure and mechanical strength of cement. *New Carbon Mater.*, 30, 349-356. https://doi.org/10.1016/S1872-5805(15)60194-9

[76] Li, G.Y., Wang, P.M., Zhao, X. (2005). Mechanical behavior and microstructure of cement composites incorporating surface-treated multi-walled carbon nanotubes. *Carbon*, 43, 1239–1245. https://doi.org/10.1016/j.carbon.2004.12.017

[77] Assi, L., Alsalman, A., Bianco, D., Ziehl, P., Khatib, J.E., Bayat, M., Hussein, F.H. (2021). Multiwall carbon nanotubes (MWCNTs) dispersion & mechanical effects in OPC mortar & paste: A review. *J. Build. Engg.*, 43, 102512. https://doi.org/10.1016/j.jobe.2021.102512

[78] Liu, B., Shi, J., Sun, M., He, Z., Xu, H., Tan, J. (2020). Mechanical and permeability properties of polymer-modified concrete using hydrophobic agent. *J. Building Engineering*, 31, 101337. https://doi.org/10.1016/j.jobe.2020.101337

[79] Yuan, P., Zhang, B., Yang, Y., Jiang, T., Li, J., Qiu, J., He, H. (2023). Application of polymer cement repair mortar in underground engineering: A review. *Case Studies in Construction Materials*, 19, e02555. https://doi.org/10.1016/j.cscm.2023.e02555

[80] Pei, C., Zhu, J.H., Xing, F. (2021). Photocatalytic property of cement mortars coated with graphene/TiO_2 nanocomposites synthesized via sol gel assisted electrospray method. *J. Cleaner Production*, 279, 123590. https://doi.org/10.1016/j.jclepro.2020.123590

[81] Guo, Z., Huang, C., Chen, Y. (2020). Experimental study on photocatalytic degradation eflciency of mixed crystal nano-TiO_2 concrete. *Nanotechnol. Rev.*, 9, 219–229. https://doi.org/10.1515/ntrev-2020-0019

[82] Shankar, A.N., Mandal, P. (2024). Mechanical and Photocatalytic Properties of Cement Composites Containing Metal and Oxide Nanoparticles. *J. of Materi Eng and Perform.*, 33, 3559-3569. https://doi.org/10.1007/s11665-023-08237-1

https://doi.org/10.1007/s11665-023-08237-1

[83] Lucas, S.S., Ferreira, V.M., Barroso-de-Aguiar, J.L. (2013). Incorporation of titanium dioxide nanoparticles in mortars-Influence of microstructure in the hardened state properties and photocatalytic activity. *Cement & Concrete Research*, 43, 112–120. https://doi.org/10.1016/j.cemconres.2012.09.007

[84] Cerro-Prada, E., Garcia-Salgado, S., Quijano, M.A., Varela, F. (2019). Controlled Synthesis and Microstructural Properties of Sol-Gel TiO_2 Nanoparticles for Photocatalytic Cement Composites. *Nanomaterials*, 9, 26. https://doi.org/10.3390/nano9010026

[85] Janus, M., Madraszewski, S., Zajac, K., Kusiak-Nejman, E. (2020). A New Preparation Method of Cement with Photocatalytic Activity. *Materials*, 13, 5540. https://doi.org/10.3390/ma13235540

[86] Wu, L., Pei, X., Mei, M., Li, Z., Lu, S. (2022). Study on Photocatalytic Performance of Ag/TiO_2 Modified Cement Mortar. *Materials,* 15, 4031. https://doi.org/10.3390/ma15114031

[87] Khannyra, S., Mosquera, M.J., Addou, M., Gil, M.L.A. (2021). Cu-TiO_2/SiO_2 photocatalysts for concrete-based building materials: Self-cleaning and air de-pollution performance. *Const. & Build. Mater.*, 313, 125419. https://doi.org/10.21203/rs.3.rs-1389807/v1

[88] He, K., Chen, Y., Mei, M. (2020). Study on influencing factors of photocatalytic performance of CdS/TiO_2 nanocomposite concrete. *Nanotechnol. Rev.*, 9, 1160–1169. https://doi.org/10.1515/ntrev-2020-0074

[89] Janus, M., Zatorska, J., Czyzewski, A., Bubacz, K., Kusiak-Nejmana, E., Morawski, A.W. (2015). Self-cleaning properties of cement plates loaded with N,C-modified TiO_2 photocatalysts. *Appl. Surf. Sci.*, 330, 200–206. https://doi.org/10.1016/j.apsusc.2014.12.113

[90] Geng, Z., Xin, M., Zhu, X., Xu, H., Cheng, X., Wang, D. (2021). A new method for preparing photocatalytic cement-based materials and the investigation on properties and mechanism. *J. of Build. Engg.*, 35, 102080. https://doi.org/10.1016/j.jobe.2020.102080

[91] Klapiszewska, I., Parus, A., Ławniczak, L., Jesionowski, T., Klapiszewski, L., Slosarczyk, A. (2021). Production of antibacterial cement composites containing ZnO/lignin and ZnO–SiO_2/lignin hybrid admixtures. *Cement & Concrete Composites*, 124, 104250. https://doi.org/10.1016/j.cemconcomp.2021.104250

[92] Sikora, P., Cendrowski, K., Markowska-Szczupak, A., Horszczaruk, E., Mijowsk, E. (2017). The effects of silica/titania nanocomposite on the mechanical and bactericidal properties of cement mortars. *Const. & Build. Mater.*, 150, 738–746. https://doi.org/10.1016/j.conbuildmat.2017.06.054

[93] Sikora, P., Augustyniak, A., Cendrowski, K., Nawrotek, P., Mijowska, E. (2018). Antimicrobial activity of Al_2O_3, CuO, Fe_3O_4, and ZnO nanoparticles in scope of their further application in cement-based building materials. *Nanomaterials*, 8, 212. https://doi.org/10.3390/nano8040212

[94] Mori, A.D., Gregorio, E.D., Kao, A.P., Tozzi, G., Barbu, E., Sanghani-Kerai, A., Draheim, R.R., Roldo, M. (2019). Antibacterial PMMA Composite Cements with Tunable Thermal and Mechanical Properties. *ACS Omega*, 4, 19664–19675. https://doi.org/10.1021/acsomega.9b02290

[95] Hegyi, A., Lăzărescu, A.V., Szilagyi, H., Grebenisan, E., Goia, J., Mircea, A. (2021). Influence of TiO_2 Nanoparticles on the Resistance of Cementitious Composite Materials to the Action of Bacteria. *Materials*, 14, 1074. https://doi.org/10.3390/ma14051074

[96] Jedrzejczak, P., Ławniczak, L., Slosarczyk, A., Klapiszewski, L. (2022). Physicomechanical and Antimicrobial Characteristics of Cement Composites with Selected Nano-Sized Oxides and Binary Oxide Systems. *Materials*, 15, 661. https://doi.org/10.3390/ma15020661

[97] Singh, V.P., Sandeep, K., Kushwaha, H.S., Powar, S., Vaish, R. (2018). Photocatalytic, hydrophobic and antimicrobial characteristics of ZnO nano needle embedded cement

composites. *Const. Build. Mater.*, 158, 285–294.
https://doi.org/10.1016/j.conbuildmat.2017.10.035

[98] Pan, H.H., Wang, C.K., Tia, M., Su, Y.M. (2020). Influence of water-to-cement ratio on piezoelectric properties of cement-based composites containing PZT particles. *Const. Build. Mater.*, 239, 117858. https://doi.org/10.1016/j.conbuildmat.2019.117858

[99] Santos, J.A., Sanches, A.O., Akasaki, J.L., Tashima, M.M., Longo, E., Malmonge, J.A. (2020). Influence of PZT insertion on Portland cement curing process and piezoelectric properties of 0–3 cement-based composites by impedance spectroscopy. *Const. Build. Mater.*, 238, 117675. https://doi.org/10.1016/j.conbuildmat.2019.117675

[100] Dang, N., Tao, J., Zeng, Q., Zhao, W. (2021). May the Piezoresistivity of GNP-Modified Cement Mortar Be Related to Its Fractal Structure? *Fractal Fract.*, 5, 148.
https://doi.org/10.3390/fractalfract5040148

[101] Lee, S.J., Kawashima, S., Kim, K.J., Woo, S.K., Won, J.P. (2018). Shrinkage characteristics and strength recovery of nanomaterials-cement composites. *Composite structures*, 202, 559-565. https://doi.org/10.1016/j.compstruct.2018.03.003

[102] Hawreen, A., Bogas, J.A., Dias, A.P.S. (2018). On the mechanical and shrinkage behavior of cement mortars reinforced with carbon nanotubes. *Const. & Build. Mater.*, 168, 459-470. https://doi.org/10.1016/j.conbuildmat.2018.02.146

[103] Chakraborty, S., Mandal, R., Chakraborty, S., Guadagnini, M., Pilakoutas, K. (2021). Chemical attack and corrosion resistance of concrete prepared with electrolyzed water. *J. Mater. Res. & Technol.*, 11, 1193-1205. https://doi.org/10.1016/j.jmrt.2021.01.101

[104] Daniyal, M., Akhtar, S., Azam, A. (2019). Effect of nano-TiO_2 on the properties of cementitious composites under different exposure environments. *J. Mater Res Technol.*, 8, 6158–6172. https://doi.org/10.1016/j.jmrt.2019.10.010

[105] Yousefi, A., Tang, W., Khavarian, M., Fang, C., Wang, S. (2020). Thermal and Mechanical Properties of Cement Mortar Composite Containing Recycled Expanded Glass Aggregate and Nano Titanium Dioxide. *Appl. Sci.*, 10, 2246.
https://doi.org/10.3390/app10072246

[106] Jing, G., Ye, Z., Wu, J., Wang, S., Cheng, X., Strokova, V., Nelyubova, V. (2020). Introducing reduced graphene oxide to enhance the thermal properties of cement composites. *Cement & Concrete Composites*, 109, 103559.
https://doi.org/10.1016/j.cemconcomp.2020.103559

[107] Tian, W., Chai, J., Cao, J. (2023). Cement-based composites modified by graphene oxide nano-materials: porosity and thermal conductivity. *J. Phys.: Conf. Ser.*, 2553, 012003.

10.1088/1742-6596/2553/1/012003

[108] Hu, Y.G., Awol, J.F., Chen, S., Jiang, J.N., Pu, X., Jia, X., Xu, X.Q. (2022). Experimental study of the electrical resistance of graphene oxide-reinforced cement-based composites with notch or rebar. *J Building Engg*, 51, 104331, https://doi.org/10.1016/j.jobe.2022.104331

[109] Lim, S., Mondal, P. (2015). Effects of Nanosilica Addition on Increased Thermal Stability of Cement-Based Composite. *ACI Materials Journal*, 112, 305. DOI:10.14359/51687177

[110] Huo, J., Wang, Z., Guo, H., Wei, Y. (2020). Hydrophobicity Improvement of Cement-Based Materials Incorporated with Ionic Paraffin Emulsions (IPEs). *Materials*, 13, 3230. https://doi.org/10.3390/ma13143230

[111] Baghban, M.H., Holvik, O.K., Hesselberg, E., Javadabadi, M.T. (2018). Cementitious Composites with Low Water Permeability through Internal Hydrophobicity. *Key Engineering Materials*, 779, 37-42. https://doi.org/10.4028/www.scientific.net/KEM.779.37

[112] Tian, L., Qiu, L.C., Liu, Y. (2021). Fabrication of integrally hydrophobic self-compacting rubberized mortar with excellent waterproof ability, corrosion resistance and stable mechanical properties. *Const. Build. Mater*, 304, 124684. https://doi.org/10.1016/j.conbuildmat.2021.124684

[113] Shahbazi, R., Korayem, A.H., Razmjou, A., Duan, W.H., Wang, C.M., Justnes, H. (2020). Integrally hydrophobic cementitious composites made with waste amorphous carbon powder. *Const. & Build. Mater*, 233, 117238. https://doi.org/10.1016/j.conbuildmat.2019.117238

[114] Mundo, R.D., Petrella, A., Notarnicola, M. (2018). Surface and bulk hydrophobic cement composites by tyre rubber addition. *Const. & Build Mater*, 172**,** 176–184. https://doi.org/10.1016/j.conbuildmat.2018.03.233

[115] Chen, C.Y., Shen, Z.Y., Lee, M.T. (2021). On Developing a Hydrophobic Rubberized Cement Paste. *Materials*, 14, 3687. https://doi.org/10.1016/j.conbuildmat.2018.03.233

[116] Dong, W., Li, W., Zhu, X., Sheng, D., Shah, S.P. (2021). Multifunctional cementitious composites with integrated self-sensing and hydrophobic capacities toward smart structural health monitoring. *Cement & Concrete Composites*, 118, 103962. https://doi.org/10.1016/j.cemconcomp.2021.103962

[117] Sharma, S., Kumar, D., Kumar, S., Goyat, M.S., Mandal, P. (2018). Structural and optical properties of Cu incorporated $ZnFe_2O_4$ ferrite nanoparticles prepared by wet chemical route. *Materials Chemistry and Physics*, 212, 292-297

https://doi.org/10.1016/j.matchemphys.2018.03.051

[118] Lassoued, A., Dkhil, B., Gadri, A., Ammar, S. (2017). Control of the shape and size of iron oxide (α-Fe_2O_3) nanoparticles synthesized through the chemical precipitation method. *Results in Physics*, 7, 3007–3015 https://doi.org/10.1016/j.rinp.2017.07.066

[119] Madhu, B.J., Bhagyalakshmi, H., Shruthi, B., Veerabhadraswamy, M. (2021). Structural, AC conductivity, dielectric and catalytic behavior of calcium oxide nanoparticles derived from waste eggshells. *S N Applied Sciences*, 3, 637
https://doi.org/10.1007/s42452-021-04607-3

[120] Meng, S., Ouyang, X., Fu, J., Niu, Y., Ma, Y. (2021). The role of graphene/graphene oxide in cement hydration. *Nanotechnology Reviews*, 10, 768.
https://doi.org/10.1515/ntrev-2021-0055

[121] Jing, G., Wu, J., Lei, T., Wang, S., Strokova, V., Nelyubova, V., Wang, M., Ye, Z. (2020). From graphene oxide to reduced graphene oxide: Enhanced hydration and compressive strength of cement composites. *Construction and Building Materials*, 248, 118699. https://doi.org/10.1016/j.conbuildmat.2020.118699

[122] de Souza, F.B., Shamsaei, E., Crentsil, K.S., Duan, W. (2022). Proposed mechanism for the enhanced microstructure of graphene oxide–Portland cement composites. *Journal of Building Engineering*, 54, 104604. https://doi.org/10.1016/j.jobe.2022.104604

[123] Vaičiukynienė, D., Skipkiūnas, G., Daukšys, M., Sasnauskas, V. (2013). Cement hydration with zeolite-based additive. *Chemija*, 24, 271.

[124] Kashyap, V.S., Agrawal, U., Arora, K., Sancheti, G. (2021). FTIR analysis of nanomodified cement concrete incorporating nano silica and waste marble dust. *IOP Conf. Series: Earth and Environmental Science*, 796, 012022.
DOI: 10.1088/1755-1315/796/1/012022

[125] Lin, C., Wei, W., Hu, Y.H. (2016). Catalytic behavior of graphene oxide for cement hydration process. *Journal of Physics and Chemistry of Solids*, 89, 128.
https://doi.org/10.1016/j.jpcs.2015.11.002

[126] Tararushkin, E.V., Shchelokova, T.N., Kudryavtseva, V.D. (2020). A study of strength fluctuations of Portland cement by FTIR spectroscopy. *IOP Conf. Series: Materials Science and Engineering*, 919, 022017. DOI: 10.1088/1757-899X/919/2/022017

[127] Qureshi, T.S., Panesar, D.K. (2019). Impact of graphene oxide and highly reduced graphene oxide on cement based composites. *Construction and Building Materials*, 206, 71.
https://doi.org/10.1016/j.conbuildmat.2019.01.176

List of Publications

A. Refereed journals

1. **A. N. Shankar** et al, *'Mechanical and photocatalytic properties of cement composites containing metal and oxide nanoparticles'*, Journal of Materials Engineering and Performance, 33 (2024) 3559-3569

2. **A. N. Shankar** et al, *'Experimental investigation of the hydrophobic and modal properties of epoxy nanocomposites reinforced with graphene nanofillers'*, Trans Indian Inst Met 76 (2023) 1313–1319

3. **A. N. Shankar** et al., *'Mechanical and smart properties of cement nanocomposites containing nanomaterials: a brief review',* Open Engineering 14 (2024) 20240043.

4. **A. N. Shankar,** et al, *'Effect of GO/RGO additives on the cement hydration, mechanical, microstructure and antimicrobial properties of OPC-Fe_2O_3 cement paste'*, in review (2024).

thesis-shankar

ORIGINALITY REPORT

10%	7%	7%	2%
SIMILARITY INDEX	INTERNET SOURCES	PUBLICATIONS	STUDENT PAPERS

PRIMARY SOURCES

1	www.researchgate.net Internet Source	1%
2	www.mdpi.com Internet Source	1%
3	dr.ddn.upes.ac.in:8080 Internet Source	1%
4	Submitted to University of Leeds Student Paper	<1%
5	"Handbook of Graphene", Wiley, 2019 Publication	<1%
6	Submitted to University of Petroleum and Energy Studies Student Paper	<1%
7	www2.mdpi.com Internet Source	<1%
8	"Proceedings of SECON 2020", Springer Science and Business Media LLC, 2021 Publication	<1%
9	core.ac.uk	